Q-switched diode lasers

Williams, Kevin

Award date:
1995

Awarding institution:
University of Bath

Q-SWITCHED DIODE LASERS

submitted by Kevin Williams

for the degree of PhD

of the University of Bath

1995

Kevin Williams

ProQuest LLC
789 East Eisenhower Parkway
P.O. Box 1346
Ann Arbor, MI 48106-1346

CONTENTS

Picosecond Optical Pulse Generation.

Carrier Dynamics in Gain-switched Lasers.

Timing Jitter in Forced Q-switching.

SUMMARY

The Q-switched operation semiconductor diode lasers is characterised in detail identifying limits to the powers and stability of the generated pulse trains. The first three introductory chapters highlight the requirements for picosecond optical pulse sources, the physics fundamental to pulse generation in semiconductor lasers, and the range of techniques available. A review of state of the art laser systems and the characterisation available in the literature indicates a dearth of information on stability, pulse control, and upper limits to repetition rates and powers. This work highlights the advantages of Q-switched semiconductor lasers through direct comparison of such parameters with alternative picosecond pulse generation schemes for diode lasers.

The comparison of experiment with theory for gain-switched InGaAsP/InP lasers in chapter 4 shows that nonlinear gain suppression limits pulse powers and leads to significant pulse asymmetry. Indeed contributions from carrier transport quantum well lasers are highlighted for the first time for gain-switched operation. Chapter 5 details the jitter performance of forced Q-switched diode lasers for the first time. A multicontact structure allows saturable absorption to enhance the optical powers while significantly reducing the timing jitter. Subpicosecond (900fs) jitter is measured for Q-switched pulse trains with a 2GHz repetition rate. Chapter 6 compares jitter for a wide range of picosecond pulse techniques. Feedback techniques offering improved stability for reduced system cost are detailed and a novel single chip optoelectronic feedback technique is proposed. To allow enhanced optical powers, chapter 7 details the use of tapered

waveguide structures in overcoming nonlinear gain suppression in Q-switched multicontact Bow-Tie lasers. Record optical powers of up to 6.9W and energies in excess of 100pJ are achieved in a single spatial mode.

ACKNOWLEDGEMENTS

It is a pleasure to acknowledge the supervision of Professor Ian White. Personal financial support for the duration of the work has been provided jointly by the Engineering and Physical Sciences Research Council and BNR Europe Limited through a CASE award.

Collaboration with the optical systems group at BNR Europe has been stimulating and the additional supervision of Richard Epworth is acknowledged. The assistance of the advanced sources group at BNR Europe has also been invaluable. InGaAsP/InP distributed feedback lasers in chapter 4, and multicontact InGaAsP/InP lasers in chapters 5 and 6 were all supplied by BNR Europe at Harlow. The assistance of Dr Martyn Fice with the supply of multicontact lasers to the required configuration has been invaluable. Discussions with Drs Robin Thompson and James Whiteaway at BNR Europe Ltd and Brian Garrett at Northern Telecom, have been invaluable in the understanding of ultrafast dynamics in gain-switched diode lasers. Brian Garrett is particularly thanked for the explanation of and provision of a simplified model for longitudinal mode spatial hole burning in quarter wave phase shifted distributed feedback lasers.

Dr Peter Vasil'ev from the P.N. Lebedev Institute in Moscow has spent fifteen months on leave at the University of Bath during the course of the work. His assistance and encouragement in the development of Q-switched diode lasers at Bath is gratefully acknowledged. Collaboration with the University of St Andrews Department of Physics and Astronomy allowed the use of the Streak camera, low phase noise microwave source and phase noise measurement equipment required for high speed Q-switching work in chapter 5. Dr David

Burns, David Hughes and Professor Wilson Sibbett are thanked for their invaluable part in numerous collaborative experiments and for their helpful comments.

Collaboration with the School of Electrical Engineering at the University of Bath has allowed the development of picosecond pulsed tapered lasers in chapter 7. Dr John Roberts at Sheffield University III-V facility and Dr John Ralston of the Fraunhofer Institute are both acknowledged for supplying wafers used in the fabrication of the lasers. AlGaAs laser fabrication carried out by Trevor Ryan is gratefully acknowledged. Drs Frances Laughton, Richard Penty and Jay Sarma are acknowledged for their intrinsic part in the project.

The optoelectronics group and associated staff and technicians as a whole have been invaluable in providing the equipment, ideas, programs, and support essential to this work.

PUBLICATIONS

"Spectral chirp in long wavelength multiquantum well semiconductor lasers subject to gain switching", I.H. White, P.S. Griffin, K.A. Williams, and J.E.A. Whiteaway, IEE colloquium digest 080, London, UK, 1992.

"Spectral dynamics of long wavelength quantum well distributed feedback lasers under gain switching", I.H. White, P.S. Griffin, K.A. Williams, G.H.B. Thompson, J.E.A. Whiteaway, and B. Garrett, IEEE LEOS International Laser Conference, paper O-4, Takamatsu, Japan, 1992.

"Line-narrowed operation of multiquantum well lasers", K.A. Williams, I.H. White, A. Wonfor, P.S. Griffin, J.E.A. Whiteaway, G.H.B. Thompson and B. Garrett, IEE colloquium digest 057, London, UK, 1993.

"Forced Q-switching of multicontact InGaAsP lasers", D. Burns, K.A. Williams, I.H. White, W. Sibbett, and M.J. Fice, Eleventh UK National Quantum Electronics conference, Belfast, UK, 1993.

"Low jitter picosecond pulses at 1.5 microns from Q-switched multicontact DFB laser", K.A. Williams, P.P. Vasil'ev, I.H. White, D. Burns, W. Sibbett, and M.J. Fice, European conference on optical communications, paper WeP8.4, Montreux, Switzerland, 1993.

"Picosecond pulse generation in multisection diode lasers by gain-switching and Q-switching", I.H. White, K.A. Williams, W. Sibbett, D. Burns, P.P. Vasil'ev, and M.J. Fice, IEE colloquium digest 202, Invited tutorial paper, 1993.

"Enhance energy picosecond pulse generation in multisection diode lasers", I.H. White, K.A. Williams, W. Sibbett, D. Burns, P.P. Vasil'ev and M.J. Fice, LEOS proceedings, Invited paper, San Jose, CA, 1993.

"High energy Q-switched pulse generation using Bow-Tie laser diodes", K.A. Williams, J. Sarma, I.H. White, R.V. Penty, I. Middlemast, T. Ryan, F.R. Laughton, and J.S. Roberts, LEOS proceedings, Postdeadline paper, San Jose, CA, 1993.

"Passively mode-locked Bow-Tie lasers", K.A. Williams, J. Sarma, F.R. Laughton, I.H. White, R.V. Penty, I. Middlemast, T. Ryan, and J.S. Roberts, Semiconductor and integrated optoelectronics conference, Cardiff, UK, 1994.

"Tapered Bow-Tie lasers for high energy Q-switched pulse geenration", K.A. Williams, J. Sarma, I.H. White, R.V. Penty, I. Middlemast, T. Ryan, F.R. Laughton, and J.S. Roberts, CLEO proceedings, paper CTh15, Anaheim, CA, 1994.

"Ultrashort pulse semiconductor lasers with improved timing jitter", D.M. Hughes, D. Burns, W. Sibbet, K.A. Williams, and I.H. White, CLEO proceedings, paper CWN4, Anaheim, CA, 1994.

"High power picosecond pulse generation in multicontact diode lasers using modified Q-switching techniques", I.H. White, K.A. Williams, D.M. Hughes, D. Burns, and W. Sibbett, CLEO Europe proceedings, paper CTuL2, Amsterdam, 1994.

"Passive mode-locking in Bow-Tie lasers", K.A. Williams, I.H. White, F.R. Laughton, J. Sarma, R.V. Penty, I. Middlemast, and T. Ryan, CLEO Europe proceedings, Paper CTuL2, Amsterdam, 1994.

"Jitter in picosecond Q-switched multicontact lasers", K.A. Williams, I.H. White, D. Burns, and W. Sibbett, LEOS proceedings, Boston, MA, 1994.

"Monolithic passive mode-locking in single contact tapered laser", K.A. Williams, H.D. Summers, M.K. Abd., Rahman, J. Mueller, F.R. Laughton, I.H. White, R.V. Penty, Z. Jiang, J. Sarma, I. Middlemast, and J.D. Ralson, LEOS proceedings, 1995.

"Advances in high power short pulse semiconductor lasers", I.H. White, K.A. Williams, F.R. Laughton, R.V. Penty, Z. Jiang, H.D. Summers, and J. Sarma, Twelfth UK Quantum Electronics conference, Invited paper, Southampton, 1995.

"Substantial reduction of dynamic wavelength chirp of 2Gbit/s pseudorandom optical signal using three contact InGaAsP/InP multiquantum well distributed feedback laser", P.S. Griffin, K.A. Williams, I.H. White, and M.J. Fice, Electronics Letters, 28, 2045-2046, 1992.

"Picosecond pulse generation with ultralow jitter in 1.5 micron multicontact MQW lasers using Q-switching", K.A. Williams, D. Burns, I.H. White, W. Sibbett, and M.J. Fice, IEEE Photonics Technology Letters, 4, 867-869, 1993.

"Carrier transport effects in long wavelength multiquantum well lasers under large siganl modulation", K.A. Williams, P.S. Griffin, I.H. White, B. Garrett, J.E.A. Whiteaway, and G.H.B. Thompson, IEEE Journal of Quantum Electronics, 30, 1355-1357, 1994.

"Q-switched Bow-Tie lasers for high energy picosecond pulse generation", K.A. Williams, J. Sarma, F.R., Laughton, I.H. White, R.V. Penty, I. Middlemast, T. Ryan, and J.S. Roberts, Electronics Letters, 30, 320-321, 1994.

"Low jitter Q-switching using optoelectronic feedback", K.A. Williams, I.H. White, D. Burns, and W. Sibbett, Electronics Letters, 30, 1687-1688, 1994.

"Detailed large-signal dynamic modelling of DFB laser structures and comparison with experiment", J.E.A. Whiteaway, A.P. Wright, B. Garrett, G.H.B. Thompson, J.E. Carroll, L.M. Zhang, C.F. Tsang, I.H. White, K.A. Williams, Optical and Quantum Electronics, Invited paper, 26, S817-S842, 1994.

PICOSECOND OPTICAL PULSE TECHNOLOGY

The applications of picosecond pulsed diode lasers are discussed in the context of current experimental systems and future system requirements. Examples from communications, optical signal processing, sensing and environmental measurement are outlined. Important picosecond optical pulse characteristics are highlighted. Tolerances on the pulse shape, beam profile, spectral content and stability are discussed.

1.1 Picosecond Pulsed Semiconductor Lasers.

Semiconductor lasers have largely been developed through the huge investment made to increase the capacity of telecommunication networks [1-5]. Increasing demand from telephone, entertainment channels and computer links have resulted in the widespread implementation of optical fibre in trunk links between telephone exchanges and over long-haul transcontinental and transoceanic distances. It is the potential compactness, efficiency, reliability, ease of integration and low cost of high power diode lasers as compared to other developed laser technologies that has lead to the considerable research interest.

Picosecond optical pulse trains generated by diode lasers find application in both high power and high speed systems. An example high power application for picosecond optical pulses is frequency doubling in nonlinear crystals. A train of picosecond duration optical pulses is enhanced in peak optical power, while the mean power levels remain similar to those achieved under continuous wave (CW) operation. Mode-locking (discussed in chapter 3) is an established picosecond pulse technique used for efficient frequency doubling in nonlinear

crystals. The second harmonic optical power depends instantaneously on the square of the intensity. As a result the pulse like form is expected to significantly improve the conversion efficiency as compared to a CW laser with the same mean intensity [6]. Second harmonic generation (SHG) efficiency does not depend on the fast temporal variation in the optical intensity of the picosecond pulse train however. It is the potential application of picosecond pulsed lasers in high speed systems that is now to be discussed in this chapter.

Applications for picosecond pulsed diode lasers are increasingly evident in areas as varied as ultrahigh speed signal processing, ranging and sensing. The design of lasers for such application depends on a number of system determined pulse characteristics. Control over the pulse profile, duration, peak power, repetition rate, and stability are critical to sampling and communication applications. Tolerances in fibre communication applications are further complicated as the wavelength shift or chirp during the pulse determines the pulse propagation characteristics in fibre. For the pumping of nonlinear components the beam profile limits peak achievable intensity and the absolute wavelength becomes more critical. This chapter identifies key applications for picosecond pulsed semiconductor lasers, and highlights pulse requirements.

1.2 Terahertz Fibre Communication.

Communication systems based on the transmission of a coded sequence of optical picosecond pulses are envisaged at several hundred Gigahertz data-rates [7-8]. With a return-to-zero modulation scheme and a high mark-space ratio, several pulse trains could be optically time division multiplexed with fibre combiners. The electronic drive circuits could thereby be operated in parallel at

commercially available data-rates [7-9]. Sources are therefore required to generate picosecond duration pulses at up to ten Gigahertz.

The data-rate transmission-distance product is limited by optical fibre loss and group velocity dispersion [10]. InGaAsP lasers operating at 1.3 and 1.55 μm have attracted the most attention in this field as the group velocity dispersion and loss minima for conventional silica based fibres are centred at 1.3 and 1.55 μm respectively [11]. The commercial availability of high gain (>30dB) wideband (>THz) Erbium doped fibre amplifiers in the 1.52-1.56μm window results in group velocity dispersion as the key limiting factor to the data-rate transmission-distance product.

A red shift in the optical spectrum, where the trailing edge is longer in wavelength then the leading edge, is characteristic of picosecond pulsed diode lasers. A group velocity dispersion of 17 ps/km/nm at 1.56 μm has been measured for standard 1.31 μm dispersion minimum fibre and this leads to pulse broadening and the loss of information through intersymbol interference [10-11]. Three main approaches have been taken to overcome the broadening. Reducing the wavelength shift during pulse generation is discussed in chapter 3. A second approach modifies the fibre dispersion through a shift in the minimum [11]. Optical fibre spans of alternate sign dispersion can also be cascaded to compensate broadening with a pulse narrowing [10]. Kawanishi and coworkers consider 100Gbit/s transmission over 100km of dispersion shifted fibre [8]. Spans of alternate dispersion-sign fibre prevent pulse distortion. An Erbium doped fibre ring laser mode-locked at a 6.3 GHz generates the train of 3.5ps duration optical pulses. Both optical time division and polarisation multiplexing were used to give the 100 Gbit/s output. Alternative semiconductor mode-locked laser sources are outlined in chapter 3.

1.3 Optical Soliton Communications.

Optical soliton systems using Fourier transform limited[1] picosecond pulses rely on self phase modulation to counterbalance the group velocity dispersion [12-13]. For sufficiently high power pulses the instantaneous refractive index of the fibre is modulated by the guided picosecond optical pulse. As the propagating pulse modifies the fibre refractive index, so the front of the pulse experiences a retardation relative to the rear and a net pulse compression occurs. The stringent spectral purity, spectral stability and timing stability requirements for the $sech^2$ pulse power profiles for soliton propagation have lead to the use of colour centre lasers [13-14] and mode-locked Erbium doped fibre lasers [14], and semiconductor sources [15-17].

Both gain-switched and mode-locked semiconductor laser systems have been considered at 2.4Gbit/s by Mollenauer and coworkers [16]. While transmission distances of 12000km are demonstrated for the mode-locked laser source, pulse train jitter for the gain-switched diode is suggested as leading to observed broadening after 6000km. Gain-switched lasers have however been used in 10Gbit/s transmission experiments over 10000km by Iwatsuki and coworkers [17]. Spectral filtering to eliminate nonlinear chirp and select only the linearly wavelength shifted (chirped) part of the spectrum is however required before subsequent pulse compression. The scheme should also allow reduced jitter gain-switched operation, (as highlighted in chapter 5), enabling the enhanced transmission distance.

---

1 Chapter 3 discusses the spectral properties of picosecond pulsed diode lasers.

1.4 Free Space Communication.

The development of high power semiconductor optical sources is of interest for intersatellite and free space terrestrial links. The ability to collimate and focus high quality beams allows sufficiently low divergence to challenge the more established microwave communication technologies. High optical powers are required to overcome losses through scattering in terrestrial applications and divergence in space communications. A concerted effort to develop integrated high power laser sources using postamplification has resulted [18-20]. Recently discrete [21] and integrated [22] flared-waveguide postamplifier structures have been implemented for power enhancement by Alexander and coworkers and Dzurko and coworkers respectively. Using frequency shift keying, the highest reported power 1W, 1Gb/s coherent modulation is thus achieved with a tapered waveguide amplifier. The small signal 3dB bandwidth of the integrated tapered laser amplifiers so far reported are 2.2GHz [22]. The increasingly active field of waveguide optimisation for high power lasers is considered in chapter 7.

Picosecond pulse techniques such as self Q-switching are unlimited by the electrical bandwidth of the device and are able to generate higher peak optical powers. Vasil'ev and coworkers have assessed the radio frequency (RF) locked self Q-switched operation of nontapered lasers. 1W peak power, 17ps duration pulses have been achieved at 2.6 GHz repetition rates [23]. Vasil'ev has also shown that self Q-switching is possible for frequencies of up to 18GHz with peak pulse powers of Watts [24]. Using the flared amplifier technologies in conjunction with picosecond pulse technologies should enable even higher power levels and repetition rates.

1.5 Optical Sampling.

The operating speeds of the fastest electronic devices and integrated circuits surpass the capabilities of conventional instrumentation such as sampling oscilloscopes. Noninvasive optical probes for integrated circuits, single shot Gigahertz bandwidth sampling oscilloscopes and Gigahertz bandwidth analogue to digital converters are all being developed with picosecond optical pulse technologies.

High temporal resolution, noninvasive probing has been realised by passing a subpicosecond duration optical pulse through the device under test [25-27]. The voltage to be measured and the crystal birefringence are linked through the Pockel effect. This allows voltage fluctuations to be measured on a subpicosecond time scale through the polarisation of a transmitted pulse. Appropriately positioned polarisers before and after the device under test translate the change in polarisation to a change in amplitude. By scanning the delay of the probe pulse relative to the detected signal a time resolved profile with 200fs resolution has been demonstrated. As the scanning of the delay takes longer than the measured event, the measured voltage waveform must be periodic and the measurement must be time averaged.

The ability to capture microwave frequency waveforms in a single shot is increasingly important. Optical sampling offers a means to bridge the gap between current high speed electronic circuits and systems operating at higher sampling rates of up to 16 Giga-samples per second. For example the use of a high speed 1x16 integrated optical switch allows serial-to-parallel demultiplexing to the 1GS/s rates of commercially available sampling circuits [28-31]. The electrical signal to be sampled biases a matrix of Lithium Niobate

optical modulators. This spatial multiplexing allows the parallel processing at a lower sampling rate. The resolution is limited by the achievable pulse duration and the timing and amplitude stability of the pulse train. Stability in picosecond pulsed diode lasers is discussed in chapters 5 and 6.

1.5 Optical Signal Processing.

Pulses of sufficient energy, power, and intensity for optical switches and logical function in semiconductor amplifiers and components have only recently been possible to generate using diode lasers. Nonlinearities used in switching experiments may be categorised as either resonant or nonresonant, depending on whether carrier-photon interactions take place. Switched based on nonresonant nonlinearities require pulse powers of hundreds of Watts [32-33], currently unachievable with semiconductor technology. Nonresonant two photon absorption has however been demonstrated by Tsang and coworkers with a diode laser pump [37]. The InGaAsP waveguide was pumped with 3.5 ps duration, 7W peak power pulses from a Q-switched AlGaAs laser. Higher pump powers are however required to use the nonlinearity for switching applications.

Reduced power optical switches might utilise resonant nonlinearities involving relatively slow carrier interactions. An all optical polarisation rotation switch has been demonstrated by Day and coworkers [34] using a Q-switched multicontact InGaAsP laser [35]. 30ps duration pulses optically amplified to 190pJ, 6.3W are coupled to the InGaAsP waveguide. The optical pulse changes polarisation states with increasing power. Appropriately positioned polarisers translate polarisation switching to a change in amplitude. The recovery time has

been reduced to 18ps with appropriate reverse bias [36].

Picosecond duration pulses also find applications in optical logic. Such functions might find application in the all optical demultiplexing of high data rate communication systems [38-39]. An optical AND gate has been demonstrated by the Schnabel and coworkers using four wave mixing in a semiconductor amplifier [39]. Optical pulse trains generated by a gain-switched and mode-locked laser were combined and fibre-launched into a saturated semiconductor amplifier. When the gain-switched and mode-locked pulses overlap, an output shifted in wavelength by the wavelength separation of the pulse trains was isolated with appropriate optical filters. The mode-locked laser used required fibre amplifiers, indicating a need for higher power integrated picosecond pulse sources.

Optical clock recovery is an increasingly important feature in higher bit rate return-to-zero all-optical (transparent) communication systems [7-8,40]. A clock signal is extracted from the pulse train to synchronise the electronic processing components to the incoming data stream. Variation in the repetition rate of the pulse train is expected, and therefore clock extraction is required to be bit-rate flexible. This in turn has lead to significant interest in self-pulsing diode lasers. While pulsations from 0.5-18GHz have been reported for GaAs lasers, self pulsations in the tens of Gigahertz range are observed for distributed feedback InGaAsP lasers [41-42]. The stability of the self-pulsation limits the error rate.

1.6 Ranging and Sensing.

Lasers offer noncontacting, nondestructive, directional means of ranging and sensing. With proper collimation and appropriate detection, the attenuation of reflected signals can be used for light detection and ranging and environmental analysis through gas detection. Pulsed solid state and gaseous lasers are frequently used in a research environment for such detection and ranging. To achieve the required pulse energies Nd:YLF, Nd:YAG and CO_2 lasers are widely used [43], providing energies from tens of microjoules to Joules at repetition rates of up to a few kilohertz. Broad area Q-switched diode lasers are now being specifically developed for displacement measurement applications. Ten nanojoule pulses have already been used by Volpe and coworkers [44-45] for molten steel level measurement.

1.7 References.

1. CHIARIGLIONE, L., "Generic media coding - Attacking the broadband communication problem from the user side", ECOC'93, Plenary paper MoC0.1, Montreux, 1993.

2. LI, T., "Next-generation lightwave transmission systems", ECOC'93, Plenary paper MoC0.2, Montreux, 1993.

3. SHUMATE, P., "Economic considerations for Fiber-to-the-subscriber", ECOC'93, Invited paper ThC11.1, Montreux, 1993.

4. BLANC, E., REINAUDO, Ch., CHABERT, J.-L., and LEMAIRE V., "Undersea optical transmission systems", Alcatel technical journal, 4, 45-50, 1992.

5. IKEGAMA, T., "Survey of telecommunications: Application of quantum electronics - Progress with fibre communications", IEEE Proceedings, 80, 411-419, 1992.

6. ZERNIKE, F., and MIDWINTER, J.E., Applied Nonlinear Optics, John Wiley and Sons, New York, 111, 1973.

7. KAWANISHI, S., TAKARA, H., KAMATANI, O., and MORIOKA, T., "100Gbit/s 500km optical transmission experiment", Electronics Letters, 31, 737-738, 1995.

8. KAWANISHI, S., TAKARA, H., UCHIYAMA, K., SARUWATARI, M., and KITOH, T., "100Gbit/s, 100km optical transmission with in-line amplification utilizing all-optical multi/demultiplexing and improved PLL timing extraction", ECOC'93, MoC1.5, Montreux, 1993.

9. LEE, W.S., and HADJIFOTIOU, A., "Optical transmission over 140km at 40Gbit/s by optical time division multiplexing / demultiplexing", Electronics Letters, 31, 997-998, 1995.

10. JOPSON, B., and GNAUK, A., "Dispersion compensation for optical fibre systems", IEEE Communications Magazine, 98-102, 1995.

11. AGRAWAL, G.P., Nonlinear Fiber Optics, Academic Press, San Diego, CA, 1989.

12. HASEGAWA, A., and TAPPERT, F., "Transmission of stationary nonlinear optical pulses in dispersive dielectric fibres. I. Anomalous dispersion", Applied Physics Letters, 23, 142-144, 1973.

13. MOLLENAUER, L.F., STOHLEN, R.H., and GORDON, J.P., "Experimental observation of picosecond pulse narrowing and soliton in optical fibres", Physics Review Letters, 1095-1098, 45, 1980.

14. SUZUKI, K., KIMURA, Y., and NAKAZAWA, M., "Subpicosecond soliton amplification and transmission using Er-3+-doped fibres pumped by InGaAsP laser diodes", Optics Letters, 14, 865-867, 1989.

15. TAYLOR, J.R. editor, Optical Soliton - Theory and Experiment, Cambridge University Press, 1992.

16. MOLLENAUER, L.F., NYMAN, B.M., NEUBELT, M.J., RAYBON, G., and EVANGELIDES, S.G., "Demonstration of soliton transmission at 2.4Gbit/s over 12,000km", Electronics Letters, 27, 178-179, 1991.

17. IWATSUKI, K., SUZUKI, K., NISHI, S., and SARUWATARI, M., "Observation 10GBit/s optical soliton over 10,000km using gain-switched DFB-LD pulse source".

18. KOREN, U., JOPSON, R.M., MILLER, B.I., CHIEN, M., YOUNG, M.G., BURRUS, C.A., GILES, C.R., PRESBY, H.M., RAYBON, G., EVANKOW, J.D., TELL, B., and BROWN-GOEBELER, K., "High power laser-amplifier photonic integrated circuit for 1.48μm wavelength operation", Applied Physics Letters, 59, 2351-2353, 1991.

19. WHITEAWAY, J.E.A., THOMPSON, G.H.B., GOODWIN, A.R., and FICE, M.J., "Design of monolithically integrated single frequency laser and booster amplifier", Electronics Letters, 27, 2250-2252, 1991.

20. FICE, M.J., GOODWIN, A.R., THOMPSON, G.H.B., WHITEAWAY, J.E.A., and FICE, M.J., "Realisation of monolithically integrated single frequency laser and booster amplifier", Electronics Letters, 27, 2305-2307, 1991.

21. ALEXANDER, S.B., KINTZER, E.S., LIVAS, J.C., WALPOLE, J.N., WANG, C.A., MISSAGGIA, L.J., and CHINN, S.R., "1Gbit/s coherent optical communication system using a 1W optical power amplifier", Electronics Letters, 29, 114-115, 1993.

22. DZURKO, K.M., PARKE, R., WELCH, D.F., LANG, R.J., "Modulation characteristics of MFA-MOPAs", LEOS'93, paper SCL1.3.

23. VASIL'EV, P.P., WHITE, I.H., BURNS, D., and SIBBETT, W., "High power low-jitter encoded picosecond pulse generation using RF-locked self-Q-switching multicontact GaAs/GaAlAs diode lasers", Electronics Letters, 29, 1593-1594, 1993.

24. VASIL'EV, P.P., "Ultrashort pulse generation in diode lasers", Optical and Quantum Electronics, 801-824, 24, 1992.

25. VALDMANIS, J.A., and MOUROU, G.A., "Sub-picosecond electrooptic sampling: Principles and applications", IEEE Journal of Quantum Electronics, 22, 69-78, 1986.

26. KOLNER, B.H., and BLOOM, D.M., "Electrooptic sampling in GaAs integrated circuits", IEEE Journal of Quantum Electronics, Invited paper, 22, 79-93, 1986.

27. WEINGARTEN, K.J., RODWELL, M.J.W., and BLOOM, D.M., "Picosecond optical sampling of GaAs integrated circuits", IEEE Journal of Quantum Electronics, Invited paper, 24, 198-220, 1988.

28. TAYLOR, H.F., "An optical analogue to digital converter - design and analysis", IEEE Journal of Quantum Electronics", 15, 210-216, 1979.

29. WALKER, R.G., BENNION, I., and CARTER, A.C., "Novel GaAs/AlGaAs guided wave analogue/digital converter", Electronics Letters, 25, 1443-1444, 1989.

30. CARR, A.D., PARSONS, N.J., and AITKEN, A.J.S., "Electro-optically addressable digitiser for 16GS/sec waveform capture", IEE colloquium digest 1994/022, Microwave optoelectronics, paper 7, 1994.

31. BECKER, R.A., WOODWARD, C.E., LEONBERGER, F.J., and WILLIAMSON, R.C., "Wide-band electrooptic guided-wave analog-to-digital converters", Proceedings of the IEEE, 72, 802-819, 1984.

32. TSANG, H.K., SNOW, P.A., DAY, I.E., WHITE, I.H., PENTY, R.V., GRANT, R.S., SU. Z., KENNEDY, G.T., and SIBBETT, W., "All optical modulation with ultrafast recovery at low pump energies in passive InGaAs/InGaAsP multiquantum well waveguides", Applied Physics Letters, 62, 1451-1453, 1993.

33. SNOW, P.A., DAY, I.E., WHITE, I.H., PENTY, R.V., TSANG, H.K., GRANT, R.S., SU, Z., SIBBETT, W., SOOLE, J., LEBLANC, H.P., GOZDZ, A.S., ANDREADAKIS, N.C., and CANEAU, C., "Demonstration of polarisation rotation gate in GaAs/AlGaAs multiquantum well waveguides", Electronics Letters, 28, 2346-2348, 1992.

34. DAY, I.E., SNOW, P.A., JIANG, Z., PENTY, R.V., WHITE, I.H., DAVIES, D.A.O., FISHER, M.A., and ADAMS, M.J., "Low power all optical polarisation gate switch in a passive InGaAsP MQW waveguide at 1.53μm", Electronics Letters, 30, 1050-1051, 1994.

35. VASIL'EV, P.P., WHITE, I.H., and FICE, M.J., "Narrow line high power picosecond pulse generation in a multicontact distributed feedback laser using modified Q-switching", Electronics Letters, 29, 561-563, 1993.

36. SNOW, P.A., DAY, I.E., PENTY, R.V., WHITE, I.H., GRANT, R.S., KENNEDY, G.T., and SIBBETT, W., "Bias dependant recovery time of all-optical resonant nonlinearity in InGaAs/InGaAsP QW waveguide", proceedings IQEC, paper QMB7, 1994.

37. TSANG., H.K., VASIL'EV, P.P., WHITE, I.H., PENTY, R.V., and AITCHISON, J.S., "First demonstration of two photon absorption in a semiconductor waveguide pumped by a diode laser", Electronics Letters, 29, 1660-1661, 1993.

38. PATRICK, D.M., ELLIS, A.D., and SPIRIT, D.M., "Bit-rate flexible all-optical de-multiplexing using a nonlinear optical loop mirror", proceedings ECOC, Paper TuC6.2, Montreux, 1993.

39. SCHNABEL, R., PIEPER, W., LUDWIG, R., and WEBER, H.G., "All-optical AND gate using femtosecond nonlinear gain dynamics in semiconductor laser amplifiers", proceedings ECOC, paper TuC5.3, Montreux, 1993.

40. BARNSLEY, P.E., WICKES, H.J., WICKEND, G.E., and SPIRIT, D.M., "All-optical clock recovery from 5Gb/s RZ data using a self-pulsating diode laser", IEEE Photonics Technology Letters, 3, 942-945, 1991.

41. MARCENAC, D.D., CARROLL, J.E., "Comparison of self-pulsation mechanisms in DFB laser diodes", LEOS'94, paper SL8.5, Boston, 1984.

42. VASIL'EV, P.P., and WHITE, I.H., "Large-signal dynamics of ultrafast single-mode self-pulsations in 1.5 micron phase-shifted DFB MQW triple contact diode lasers", to be presented at CLEO'95.

43. See for example IEEE Transactions on Geoscience and Remote Sensing special issue on Remote sensing of the atmosphere, 31 (1), January 1993.

44. KOMPA, G., "Optical short-range radar for level control measurement", IEE Proceedings part H, 131, 159-164, 1984.

45. VOLPE, F.P., GORFINKEL, V., SOLA, J., and KOMPA, G., "140-W/40-ps single optical pulses for laser sensor application", proceedings CLEO'94, Paper CWC4, 1994.

PHYSICS OF SEMICONDUCTOR LASERS

Physical processes key to the picosecond pulsed operation of semiconductor diode lasers and example laser designs are reviewed. Comparisons between bulk and quantum well active layers, and AlGaAs/GaAs and InGaAsP/InP material systems are made. Commonly used laser cavity designs are compared. Rate equations are finally introduced to summarise the key processes qualitatively.

2.1 Outline.

The history, design and operation of diode lasers is well documented [1-5]. The widespread edge emitting AlGaAs/GaAs and InGaAsP/InP laser technologies are considered here as much of the published work on picosecond pulsed diode lasers is confined to such laser materials. The layer structure is first described for an example AlGaAs/GaAs double heterostructure laser. Radiative and nonradiative recombination mechanisms are outlined prior to a discussion of stimulated emission and absorption. The density of states function and state occupational probability are discussed for bulk and quantum well lasers to describe differences in the gain spectra. The advantages of incorporating quantum wells in the active layer are thus outlined. Refractive index and gain are coupled through the linewidth enhancement factor to describe the wavelength deviation or chirp noted for modulated lasers.

Resonator structures, waveguides and confinement mechanisms recurrent throughout the work are described. Distributed feedback and Fabry-Perot resonators are described outlining the mode discriminatory mechanisms. The

implementation of feedback gratings and the use of phase shifts to ensure single frequency operation is discussed. Processes key to picosecond pulsed diode lasers are finally summarised through the coupled differential photon and carrier density rate equations. Lumped equations are given along with inherent assumptions and limitations. A summary of the parameters appearing throughout the chapter is finally included.

2.2 Material Systems.

The diode structures most commonly used in semiconductor lasers employ double heterostructures as illustrated for the bulk GaAs example in figure 2.1. The material composition and dopants used in the grown layers determine the confinement of the optical field and charge carriers, refractive index, band gap, recombination rates and conductivity. The central intrinsic (nominally undoped) layer in the schematic provides the active region. The recombination of electrons and holes here results in radiation with a rotational frequency ω equal to the quotient of the transition energy and Planck's constant $E/\hbar$. Direct gap semiconductor alloys are required for efficient radiative transitions. Cladding the active layer with AlGaAs layers of lower refractive index results in a high level of optical confinement perpendicular to the active layer. The higher bandgap energy of these cladding layers also confines electrons and holes to the intrinsic region. While high doping levels in the cladding layers will increase the conductance and therefore the device modulation bandwidth while reducing resistive heating, an intrinsic active layer is required to reduce the number of scattering sites and thereby reduce optical loss. Additional highly doped layers of semiconductor ensure good ohmic contact to the metal contacts.

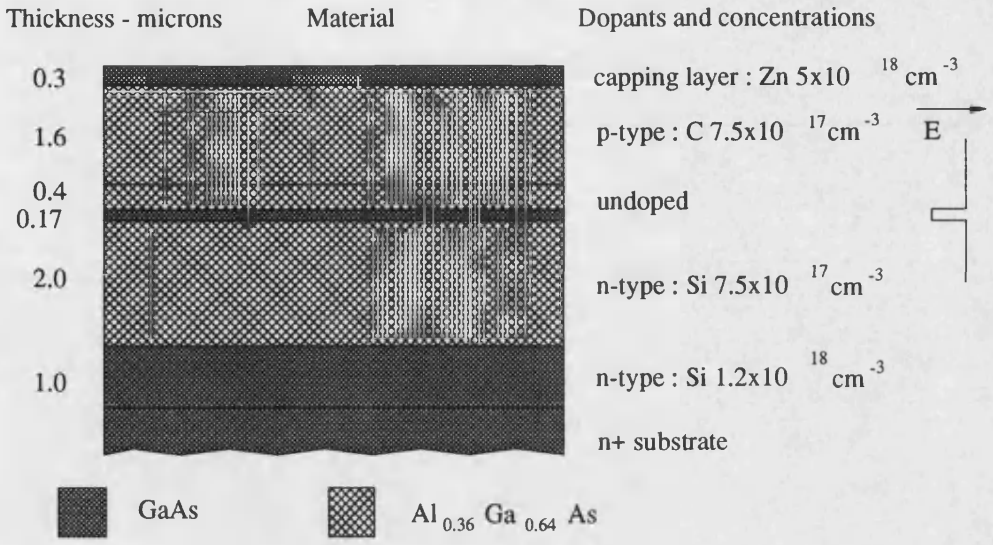

Figure 2.1 : Example layers for a bulk GaAs laser with typical dimensions, material composition, and doping levels [7].

While the bulk laser shown above has an active layer a few hundreds of nanometres in thickness, quantum confinement is commonly implemented in the more advanced high performance lasers. Here potential or quantum wells of a few nanometres width form the active layer. The well thickness is of the order of the electron de Broglie wavelength, (the quotient of Plank's constant and electron momentum h/p), leading to carrier confinement to discrete energy levels of which the lowest will be used for radiative lasing transitions. The quantum well dimensions define the energy bands and therefore the lasing wavelength [5,6]. Through improved carrier confinement both in spatial terms and in terms of the energy levels, a number of advantages have been cited for quantum well lasers including differential gain and bandwidth enhancement, and spectral linewidth broadening factor and threshold current reduction [5,6,8]. The origins of the improvements are best appreciated through the modifications to the density of states function described in 2.4.

Radiative and nonradiative electron hole recombination are readily quantified through carrier density dependent carrier lifetimes. Lattice and surface defects lead to a carrier density dependent recombination characterised by the coefficient A. Auger recombination becomes significant in narrower band gap InGaAsP lasers [5]. The energy released from the recombination of two carriers excites a third carrier to a higher energy level. As this is a three carrier process, a cubic relation to the carrier density is assumed for the CN^3 term. The excited carrier relaxes through phonon emission. The radiative spontaneous recombination rate is characterised by the coefficient B and a square law carrier dependency as both a hole and an electron is required for such recombination. Stimulated emission and absorption are described with an optical gain Γg acting on the photon density P. The internal quantum efficiency of the laser is therefore readily quantified by the ratio of radiative to nonradiative processes. To determine the probabilities for photon stimulated emission and absorption and therefore the optical gain requires information on the photon energy and the energy distribution of the carriers. This is discussed in terms of the density of states function and state occupancy in the following section 2.3.

2.3 Carrier Distribution.

The density of states function for the active layer is required to describe the gain dependence on carrier density and wavelength. While a quantum well active layer may be characterised with a step-like density of states, a bulk active layer laser has a parabolic relationship between density of states and energy as illustrated in figure 2.2. The distribution of states is estimated by integrating the over the electron energy surface with respect to k space. Together with a

knowledge of the energy dependence on wave vector k, a square law increase in possible electron states with increase in energy level is induced [1-5]. For energy E and conduction band effective mass m_c, a simplified density of states function $\rho_c(E)$ for the conduction band can take the form [5]:

$$\rho_c(E) = 4\pi\left(\frac{2m_c}{h^2}\right)^{3/2} E^{1/2} \qquad 2.1$$

Fermi-Dirac statistics describe the occupation of states in thermal equilibrium in terms of a Fermi energy F_c. The temperature T dependent occupation factor $f_c(E)$ for the conduction band is given in equation 2.2. The relation is similar for holes in the valence bands [5].

$$f_c(E) = \left\{\exp\left(\frac{E-F_c}{kT}\right)+1\right\}^{-1} \qquad 2.2$$

The occupied states deduced from the possible states and occupational probability is illustrated schematically in figure 2.2. The gain spectrum is determined from this carrier distribution and it is therefore desirable to confine the carriers to a small energy range to allow higher peak gain. Conservation of momentum, and therefore the wave number k, also limits the possible transitions to between states of similar momentum as illustrated in figure 2.3, as the photons have negligible momentum themselves. Some broadening does however occur as carrier carrier scattering occurs on a 100fs time scale. Recently vacated states are filled rapidly by carriers scattered from states previously unaffected by the transition [9-10]. Scattering and crystal imperfections results in a continuum of electronic states.

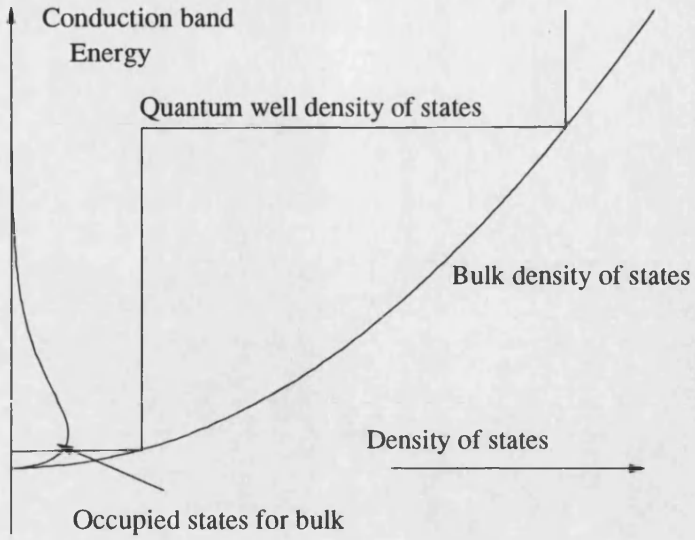

Figure 2.2 : Schematic for the density of states functions for bulk and quantum well lasers. The occupied states determined by the product of the density of states function and the occupational probability in equation 2.2 is included for a bulk laser.

In quantum well lasers, the kinetic energy of the confined carriers for motion normal to the wells is further quantized. This results in a step-like density of states function also illustrated in figure 2.2 [5,6]. The energies at which the steps occur are defined by the barrier and well dimensions. As a result of a more abrupt change in the density of states function at the lower energy states, a greater proportion of carriers are confined in the lower energy bands. This leads to an enhanced differential gain around the transparency and therefore normal operating conditions [8].

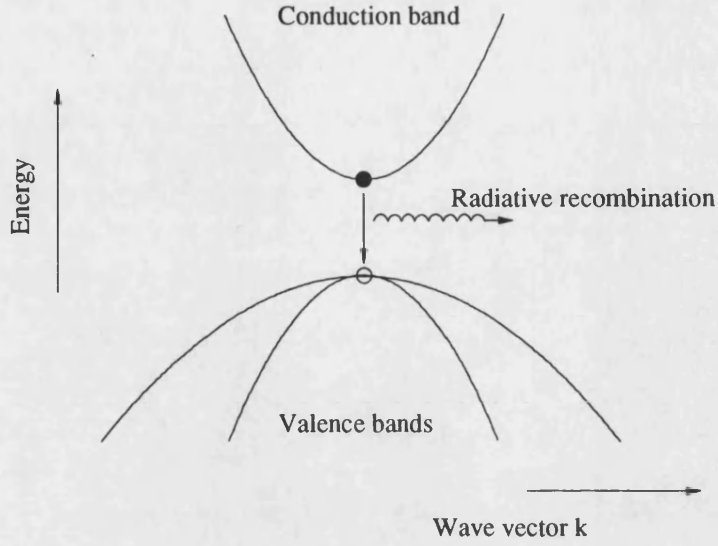

Figure 2.3 : Radiative recombination in a diode laser with the energy - wave number (E - k) diagram. Transitions occur between states of similar k.

2.4 Gain Spectrum.

From the density of states and occupancy functions the gain and absorption may be calculated as a function of wavelength and carrier density [11]. Figure 2.4 shows the gain spectrum for a bulk GaAs laser for increasing current densities. As increasing numbers of carriers populate the states, (starting with the lower energy states), the gain spectrum broadens, and the absorption edge moves to higher energies and therefore shorter wavelengths. A band-gap shrinkage due to Coulombic interaction leads to some renormalisation [9-10]. The gain spectrum is typically be tens of nanometers in width. The peak shifts to shorter wavelength as the average carrier energy level increases.

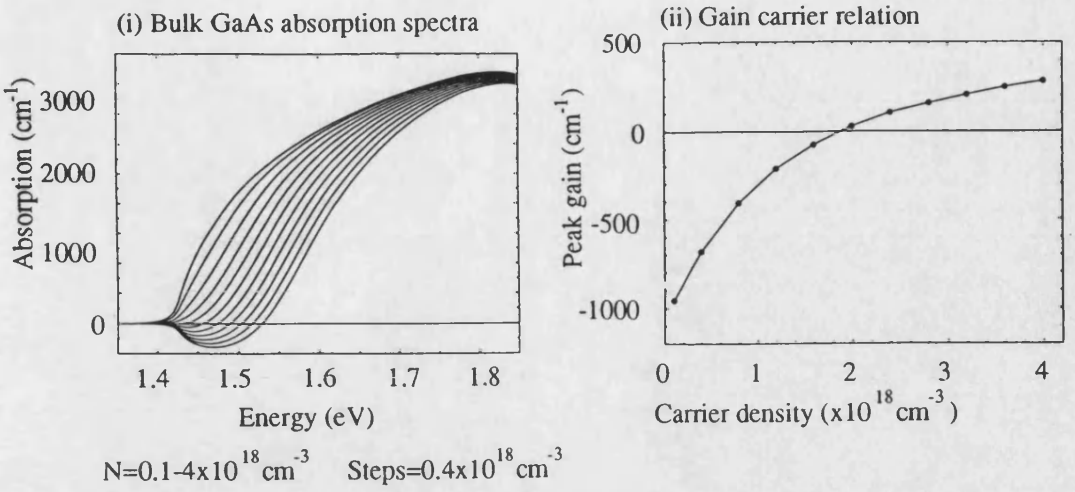

Figure 2.4 : (i) Gain spectra for a bulk GaAs laser with varied carrier concentrations. (ii) Gain as a function of the carrier concentration as determined at the gain peak showing a reduction in differential gain with increasing carrier density [9].

The gain as a function of carrier concentration is also shown in figure 2.4 to indicate the relation between gain and carrier concentration for a the peak emission energy $\hbar\omega$. Under normal laser operation the carrier concentration is pinned at just above transparency as stimulated emission depletes carriers. This corresponds to approximately 2×10^{18} cm^{-3} in figure 2.4. Optical losses through scattering in the waveguide and facet emission lead to the pinning occuring above transparency. The gain carrier density relation can usually assumed to be linear at this operating point and is approximated by the constant dg/dn. The reduction in differential gain at higher carrier densities is expected to be of significance in lasers operated at high carrier concentrations. As a result of the step like density of states function, the reduction in differential gain at higher carrier densities can be enhanced for quantum well lasers. Indeed, logarithmic

fits are often used to describe gain in quantum well lasers [12]. Both the carrier concentration N, and photon density P are assumed to define the optical gain Γg [5].

$$\Gamma g = \Gamma v_g \frac{dg}{dN}\left(\frac{N-N_o}{1+\varepsilon P}\right) \qquad 2.3$$

Here the structure dependant optical confinement factor Γ describes the overlap of the optical field with the active layer, g is the material gain, and dg/dn is a linear approximation to figure 2.4 (ii) above transparency. Multiplying the gain by the group velocity term v_g gives a stimulated emission rate. The widely implemented photon dependant nonlinear gain suppression term $(1+\varepsilon P)$ is included for completeness. Contributions to ε are the subject of chapter 4 where carrier transport effects in quantum well lasers are also discussed.

Intrinsically related to variation in carrier concentration is the active layer refractive index. As noted from figure 2.4, a small increase in carrier density shifts the gain peak as the energy bands are filled. The band-filling causes the emission wavelength to shift towards the blue. The wavelength shift or chirp may be described through a linear carrier dependent modulation of the cavity refractive index often quantified by a constant $d\mu_r/dN$. As wavelength chirp limits device performance in fibre based systems, much work has addressed quantifying the chirp in a structure dependant manner leading to the defining of the linewidth enhancement factor α_H [11-12].

$$\alpha_H = -\frac{4\pi}{\lambda_o}\frac{d\mu_r/dN}{dg/dN} \qquad 2.4$$

The linewidth enhancement factor, or antiguiding parameter is structure dependant with values ranging from 6 to 2.5 for bulk and lattice matched quantum well InGaAsP Fabry-Perot lasers [13]. The enhanced differential gain

in quantum well lasers is responsible for the reduction observed.

2.5 Resonator Design.

The cleaved facets in Fabry-Perot lasers provide 30% intensity reflection sufficient to generate tens of milliwatts of CW optical power. The spatial and spectral profiles of the optical field are intrinsically related to the cavity design and as such resonator design is increasingly application orientated. As many commercial semiconductor lasers will be fibre coupled, a single transverse spatial mode is desirable. Mode control is also necessary for improving the light current linearity [14-15] and therefore amplitude modulation response. Waveguiding can be achieved through gain or refractive index variation. Gain-guiding restricts current injection to the active region. Patterned insulating oxide layers underneath the metallisation [16] or high resistivity proton bombarded areas [17-18] have been used extensively. The transverse mode in gain-guided lasers is determined by the distribution of optical gain along the junction plane which in turn is determined by the injected carrier distribution. Carrier induced refractive index reduction leads to antiguiding and self-focussing effects and an often unacceptably nonlinear light current relation however. Weakly index guided lasers include laterally stepped p-side contact layer to form a ridge [19-21] or rib [14, 22-23] waveguide. For the more readily processed ridge waveguide, the p-side of the laser is etched after the wafer has been grown. Buried heterostructures [15, 24-28] are used for stronger index guiding.

The diode laser emits in the form of an elliptical spot. The spatial distribution of the emitted light near the diode facet is called the near field

pattern. The angular intensity distribution far from the laser is known as the far field pattern. Without a sufficiently narrow active layer and waveguide for appropriate optical confinement, several spatial modes may be excited in the laser, and the resulting near and far field patterns are formed by a superposition of them. For a single vertical mode, the active layer thickness is a few hundred nanometres resulting in the emitted beam diffracting in free space to spread into a total angle of around 45 degrees [3]. In the junction plane, where the waveguide width is a few microns in width, the reduced divergence leads to the undesirable astigmatism. The transverse mode profile is well characterised through the near field intensity pattern. Imaging the near field onto a camera with a microscope objective readily show the intensity distribution at the facet indicating the number of excited lateral modes.

Longitudinal mode patterns are also of concern to fibre based systems and for Fabry-Perot lasers multimode operation is the norm. Successive cavity length defined longitudinal modes contain an extra half wavelength with the intermode spacing being defined:

$$\delta\lambda = \frac{\lambda_o^2}{2n_r L} = \frac{\lambda_o^2}{c\tau_{rt}} \qquad 2.5$$

The round trip time τ_{rt} is defined by the cavity length and therefore is related to the intermode spacing. The parameter is of particular interest in the assessment of picosecond pulsed lasers as is highlighted in chapter 3. For a 300μm GaAs laser, the modal separation of 1nm, leads to tens of modes in the gain spectrum. The high levels of spontaneous emission coupling into the modes across the gain spectrum support the modes more or less indiscriminately at threshold. The forward and backward travelling optical fields build up in an exponential manner travelling down the cavity, leading to an enhancement of

the modes nearer the gain peak relative to the side modes. Spatial and spectral hole burning, (discussed in chapter 4), suppress the higher intensity modes however to allow some energy to remain in side modes.

Cavity designs for single moded operation are discussed by Buus in [11]. The commercially widespread distributed feedback laser is of interest as a result of its availability, compactness and lack of external optical components. An example structure is given in figure 2.5 for a ridge waveguide distributed feedback laser similar to those considered in subsequent gain-switching experiments. Schematic mode profiles indicate the roles the different composition layers play in defining a single transverse and lateral spatial mode.

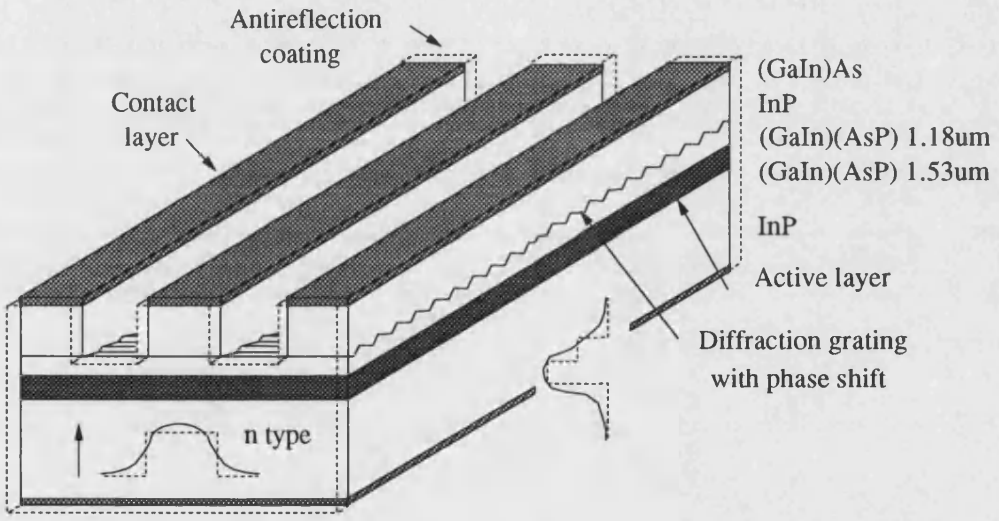

Figure 2.5: Schematic for a ridge waveguide InGaAsP distributed feedback laser.

A Bragg grating can be created by electron-beam lithography above the active layers. Subsequent overgrowth modulates the refractive index along the length of the laser to provide a Bragg reflector. Backward Bragg scattering

provides coupling between the forward and backward propagating waves. Antireflection coatings are applied to reduce facet reflections to typically less than 0.1% and therefore suppress Fabry-Perot modes. For laser operation the grating may be considered in terms of its transmission, and to allow oscillation in the centre of the reflector stop band a quarter wavelength phase shift may be introduced to the grating to allow forward and backward travelling waves to add in phase [3-4,29-33]. Work investigating the optimum position of the phase shift indicates either a centrally positioned $\lambda/4$ or two $\lambda/8$ phase shifts placed towards the facets are optimum for stable single mode operation [32]. The Bragg reflector stopband is typically around ten nanometres in width with a coupling strength cavity length product κL of 1-4 defined by the depth of the grating etch.

2.6 Rate Equations.

The dynamic performance may be formalised in terms of carrier and photon rate equations. The carrier density is increased by $\eta J/ed$, for injected current density ηJ reaching the active layer. e is the electron charge and d the active layer depth. The carrier density N is reduced through the spontaneous and stimulated recombination terms outlined in 2.2 and 2.4:

$$\frac{dN}{dt} = \frac{\eta J}{ed} - AN - BN^2 - CN^3 - v_g \frac{dg}{dN}\left(\frac{N-N_o}{1+\varepsilon P}\right)P \qquad 2.6$$

$$\frac{dP}{dt} = \Gamma\beta BN^2 + \Gamma v_g \frac{dg}{dN}\left(\frac{N-N_o}{1+\varepsilon P}\right)P - \frac{P}{\tau_p} \qquad 2.7$$

The spontaneous radiative recombination term included in the photon density equation is scaled by β to describe the spectral overlap of the spontaneous emission with the longitudinal modes resulting from stimulated emission. The

optical confinement factor Γ describes the spatial overlap of the optical mode with the active region. The photon density P is increased through the coupled spontaneous emission and stimulated emission, and is depleted through waveguide loss and loss at the facets through the photon lifetime. In a Fabry-Perot laser the losses can be characterised with the lifetime τ_p :

$$\tau_p^{-1} = v_g\{\ln(1/R^2)/2L + \alpha_i\} \qquad 2.8$$

Losses at the facet depend on the logarithm of the facet reflectivity R as the optical intensity will increase exponentially along the length L of the cavity. Both facet and waveguide losses (α_i) are assumed to be lumped. Such a lumped approximation is only expected to remain valid if the carrier and photon population changes are small on the round trip time scale. Carrier and photon densities are also assumed to be spatially nonvariant. The rate equations are used extensively in a dynamic analysis in chapter 4, where the picosecond dynamics of bulk and quantum well lasers are compared for distributed feedback lasers with varied grating structure. Table 2.1 provides a summary of the parameters used.

A	Surface and defect carrier recombination rate	s^{-1}
B	Spontaneous carrier recombination rate	cm^3s^{-1}
C	Auger recombination rate	cm^6s^{-1}
d	Depth of the active layer	cm
dg/dN	Differential gain	cm^2
$d\mu/dN$	Refractive index dependence on carrier density	cm^{-3}
e	Electronic charge	C
E_g	Band gap energy $\hbar\omega$	eV
h	Planck's constant	Js
$\hbar$	Planck's constant divided by 2π	Js
J	Current density injected into laser	Acm^{-2}
k	Wave vector $2\pi/\lambda_o$	cm^{-1}
k	Boltzmann's constant	J/K
L	Cavity length	cm
m_c	Effective mass of carriers in conduction band	
N	Charge carrier density	cm^{-3}
N_o	Charge carrier density at transparency	cm^{-3}
P	Photon density	cm^{-3}
R	Facet reflectivity	
t	Time	s
T	Absolute temperature	K
α	Linewidth enhancement factor	
α_i	Intrinsic optical waveguide losses	cm^{-1}
β	Spontaneous emission coupling factor	
η	Current injection efficiency	
η_i	Internal quantum efficiency	
Γ	Optical confinement factor	
λ_o	Emission wavelength	cm
v_g	Group velocity in the active layer	cms^{-1}
τ_p	Photon lifetime	s

Table 2.1 : Symbols used recurringly through the text.

2.7 References.

1. CASEY, H.C and PANISH, M.B., Heterostructure Lasers, Orlando, Academic Press, 1978.

2. KRESSEL, H and BUTLER, J.K., Semiconductor Lasers and Heterojunction LEDs, New York, Academic Press, 1977.

3. THOMPSON, G.H.B., Physics of Semiconductor Laser Devices, Chichester, John Wiley and Sons, 1980.

4. PETERMANN, K., Laser Diode Modulation and Noise, Dordrecht, Kluwer Academic Publishers, 1988.

5. AGRAWAL, G.P. and DUTTA, N.K., Long-Wavelength Semiconductor Lasers, Van Nostrand Reinhold, New York, 1986.

6. KATZ, A., editor, Indium Phosphide and related materials : Processing, devices and technology, Chapter 11, Artech House, Boston, 1992.

7. ROBERTS, J.S., Example bulk active layer GaAs/AlGaAs wafer structure as grown at SERC III-V facility, University of Sheffield.

8. ARAKAWA, Y., and YARIV, A., "Theory of gain, modulation response, and spectral linewidth in AlGaAs quantum well lasers", IEEE Journal of Quantum Electronics, 21, 1666-1674, 1985.

9. ZIELINSKI, E., SCHWEIZER, H., HAUSSER, S., STUBER, R., PILKUHN, M.H., and WEIMANN, "Systematics of laser operation in GaAs/AlGaAs multiquantum well heterostructures", IEEE Journal of Quantum Electronics, 23, 969-976, 1987.

10. BLOOD, P., COLAK, S., and KUCHARSKA, A.I., "Influence of broadening and high injection effects on GaAs/AlGaAs quantum well lasers", IEEE Journal of Quantum Electronics, 24, 1593-1604, 1988.

11. REES, P., SUMMERS, H.D., and BLOOD, P., "Gain-current calculations for bulk GaInP lasers including many-body effects", Applied Physics Letters, 59, 3521-3523, 1991.

9. SUMMERS, H.D., University of Bath, Gain dependance on carrier density in GaAs/AlGaAs calculations.

10. GREENE, P.D., WHITEAWAY, J.E.A., HENSHALL, G.D., GLEW, R.W., LOWNEY, C.M., BHUMBRA, B., and MOULE, D.J., "Optimisation and comparison of InP-based quantum well

lasers incorporating InGaAlAs and InGaAsP alloys", International symposium on GaAs and related compounds, Jersey, 1990, Institute of Physics conference series number 112, chapter 8, 555-560.

11. BUUS, J., Single frequency semiconductor lasers, 1990.

12. OSINSKI, M., and BUUS, J., "Linewidth broadening factor in semiconductor lasers - an overview", IEEE Journal of Quantum Electronics, 23, 9-29, 1987.

13. GRIFFIN, P.S., WHITE, I.H., WHITEAWAY, J.E.A., "Low linewidth enhancement factor for InGaAsP and InGaAlAs multiple quantum well lasers", Optical and Quantum Electronics, 23, 1031-1035, 1991.

14. AIKI, K., NAKAMURA, M., KURODA, T., and UMEDA, J., "Channeled substrate planar structure (AlGa)As injection lasers", Applied Physics Letters, 30, 649-651, 1977.

15. DUTTA, N.K., WILT, D.P., BESOMI, P., DAUTREMONT-SMITH W.C., WRIGHT, P.D., and NELSON, R.J., "Improved linearity and kink criteria for 1.3 μm InGaAsP-InP channeled substrate buried heterostructure lasers", Applied Physics Letters, 44, 483-485, 1984.

16. DYMENT, J.C., "Hermite-Gaussian mode patterns in GaAs injection lasers", Applied Physics Letters, 10, 84-86, 1967.

17. DYMENT, J.C., D'ASARO, L.A., NORTH, J.C., MILLER, B.I., and RIPPER, J.E., "Proton-bombardment formation of stripe geometry heterostructure lasers for 300K CW operation", Proceedings IEEE, 60, 726-728, 1972.

18. HENSHALL, G.D., THOMPSON, G.H.B., WHITEAWAY, J.E.A., SELWAY, P.R., and BROOMFIELD, M., "Deep proton-isolated lasers and proton range data for InP and GaSb", IEE Journal Solid State and Electron Devices, 3, 1-5, 1979.

19. KAMINOV, I.P., STULTZ, L.W., KO, J.S., DENTAI, A.G., NAHORY, R.E., DEWINTER, J.C., and HARTMAN, R.L., "Low threshold InGaAsP ridge waveguide lasers at 1.3 μm", IEEE Journal of Quantum Electronics, 19, 1312-1319, 1983.

20. TSANG, W.T., and LOGAN, R.A., "A new high power narrow beam transverse mode stabilized semiconductor laser at 1.5 μm : the heteroepitaxial ridge-overgrown laser", Applied Physics Letters, 45, 1025-1027, 1984.

21. TEMKIN, H., LOGAN, R.A., PANISH, M.B., and VAN DER ZIEL, J.P., "$\lambda = 1.5$ μm InGaAsP ridge lasers grown by gas source molecular beam epitaxy", Applied Physics Letters, 45, 330-332, 1984.

22. LEE, T.P., BURRUS, C.A., MILLER, B.I., and LOGAN, R.A, "$Al_xGa_{1-x}As$ double heterostructure rib-waveguide injection laser", IEEE Journal of Quantum Electronics, 11, 432-435, 1975.

23. KAWAGUCHI, H., and KAWAKAMI, T., "Transverse mode control in an injection laser by a strip loaded waveguide", IEEE Journal of Quantum Electronics, 13, 556-560, 1977.

24. HIROA, M., DOI, A., TSUJI, S., NAKAMURA, M., and AIKA, K., "Fabrication and characterisation of narrow stripe InGaAsP/InP buried heterostructure lasers", Journal of Applied Physics, 51, 4539-4540, 1980.

25. MITO, I., KITAMURA, M., KOBAYASHI, K., MURATA, S., SEKI, M., ODAGIRI, Y., NISHIMOTO, H., YAMAGUCHI, M., AND KOBAYASHI, K., "InGaAsP double channel planar buried heterostructure laser diode (DC-PBH LD) with effective current confinement", Journal of Lightwave Technology, 1, 195-202, 1983.

26. MITO, I., KITAMURA, M., KAEDE, K., ODAGIRI, SEKI, M., SUGIMOTO, and KOBAYASHI, K., "InGaAsP planar buried heterostructure laser diode (PBH LD) with very low threshold current", Electronics Letters, 18, 2-3, 1982.

27. NELSON, R.J., WRIGHT, P.D., BARNES, P.A., BROWN, R.L., CELLA, T., and SOBERS, R.G., "High output power InGaAsP ($\lambda = 1.3$ μm) strip buried heterostructure lasers", Applied Physics Letters, 36, 358-360, 1980.

28. ISHIKAWA, H., IMAI, H., TANAHASHI, T., NISHITANI, Y., TAKUSAGAWA, M., and TAKAHEI, K., "V-grooved substrate buried heterostructure InGaAsP/InP lasers", Electronics Letters, 17, 465-466, 1981.

29. HAUS, H.A., Waves and fields in optoelectronics, chapter 8, Prentice-Hall.

30. SEKARTEDJO, K., EDA, N., FURUYA, K., SUEMATSU, Y., KOYAMA, F., and TANBUN-EK, T., "1.5 μm phase-shifted DFB lasers for single mode operation", Electronics Letters, 20, 80-81, 1984.

31. WHITEAWAY, J.E.A., THOMPSON, G.H.B., COLLAR, A.J., and ARMISTEAD, C.J., "The design and assessment of $\lambda/4$ phase shifted DFB laser structures", IEEE Journal of Quantum Electronics, 25, 1261-1279, 1989.

32. WHITEAWAY, J.E.A., GARRETT, B., THOMPSON, G.H.B., COLLAR, A.J., ARMISTEAD, A.J., and FICE, M.J., "The static and dynamic characteristics of single and multiple phase shifted DFB laser structures", IEEE Journal of Quantum Electronics, 28, 1277-1293, 1992.

33. KINOSHITA, J.-I., and MATSUMOTO, K., "Yield analysis of SLM DFB lasers with an axially flattened internal field", IEEE Journal of Quantum Electronics, 25, 1324-1332, 1989.

PICOSECOND OPTICAL PULSE GENERATION

An overview of picosecond pulse techniques is given in the context of state of the art systems and established theory. Gain-switching, Q-switching and mode-locking are all considered and compared. Measurement techniques and their limitations are highlighted.

3.1 Outline.

Gain-switching, Q-switching and mode-locking are established techniques enabling picosecond and subpicosecond pulse generation in semiconductor diode lasers. A survey of recently published work for GaAs/AlGaAs and InGaAsP/InP highlights the advantages and the limitations of the techniques. Gain-switching is shown to be the simplest technique for generating tens of picosecond duration pulses. The optical spectrum will be chirped through high carrier depletion, and as a result, compensatory techniques for Fourier limited pulse generation are considered. The enhancement in optical power through saturable absorption is demonstrated in the review of work on Q-switching. Both active and passive schemes are considered, with an emphasis on the multicontact structures as used throughout subsequent chapters. Active, passive and colliding pulse mode-locking are considered along with the benefits of external cavities and wavelength selective grating cavities. Finally a review of experimental techniques is made to highlight the limitations of temporal and spectral measurement techniques used throughout subsequent work.

3.2 Mechanisms for Picosecond Pulse Generation.

Picosecond pulsations result from rapid spatial and temporal changes in the laser cavity gain. The potential limits to pulse repetition rates can be quantified at several levels. The electrical modulation response is primarily defined by the diode junction capacitance and the bond wire inductance to allow bandwidths of typically a few Gigahertz. Bandwidths of up to tens of Gigahertz are feasible in lasers optimised for broad band small signal modulation. An upper limit to direct modulation rates is therefore established. Modulation at rates above the electrical bandwidth and unlimited by the carrier lifetime is achieved through localised saturable absorption in Q-switching and mode-locking. Either the introduction of localised impurities or an electric field to sweep out charge carriers from part of the active layer allows enhanced absorption. The p-side metalisation is often segmented to electrically isolate regions of gain from regions of loss. The application of a reverse bias to a loss contact allows subnanosecond carrier sweep out to enhance mode-locked and Q-switched operation.

The bandwidth theorem sets a minimum pulse duration equal to the reciprocal of the gain bandwidth. With tens of nanometres gain bandwidth, tens of femtosecond duration pulses should therefore ultimately be feasible. A recent literature survey however indicates that durations of a few hundred femtoseconds are the lowest achieved for some fifteen years in semiconductor diode lasers [1]. Experimentally achievable pulse durations are limited by the modulation scheme, material and structure used.

3.3 Gain-switching.

The simplest of the pulse generation techniques optimises the optical turn on transient. A high gain condition is achieved before pulse turn-on by driving the laser with subnanosecond high current pulses from a comb generator [2], avalanche transistor pulse generator [3] or using large signal microwave modulation [4-6]. Carrier densities are observed to increase to around 1.3 times the transparency level with a correspondingly enhanced gain before optical turn-on for the InGaAsP lasers simulated in chapter 4. With the photon and carrier populations coupled through rate equations, such modulation results in a rapid increase in the photon population and subsequent switch in the gain through the subsequently enhanced carrier depletion. The prospect of ensuing relaxation oscillations is reduced if the generated optical pulse sufficiently depletes the carrier population and the (subnanosecond duration) electrical pulses are sufficiently short. The change in carrier density does however lead to a large refractive index modulation and a red shift in the lasing wavelength. This in turn will lead to duration bandwidth products approximately five times greater than the Fourier limit for single mode lasers [7-10]. A dependence of pulse duration and pulse energy on the differential gain, carrier and photon lifetimes and the transferred charge lead to a requirement for high gain short cavity lasers [10-11]. A larger cavity allows higher carrier injection to the active layer before pulse turn on and therefore higher optical pulse energies. Longer pulse durations result from the increased cavity length dependant photon lifetime and no significant peak power improvement results.

3.4 Fourier Limited Gain-Switching.

The degree of spectral broadening or chirp may be reduced [12] and peak powers may be enhanced from around 10mW to 25mW [13] by spatially nonuniform current injection. The scheme proposed by Lourtioz and coworkers [12] to generate Fourier-transform limited pulses through a chirp compensating phase section is illustrated in figure 3.1. By adjusting the delay of the compensating RF to the phase section, the chirp can either be broadened or narrowed to the limit of $\Delta\nu\Delta\tau = 0.35$.

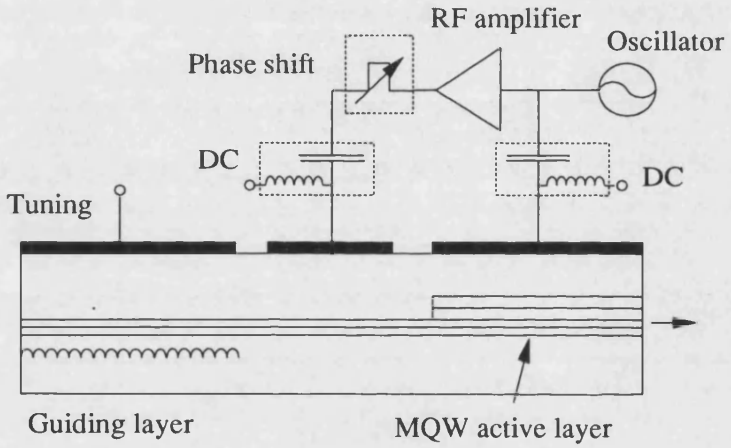

Figure 3.1 : A scheme for the generation of transform limited gain-switched pulse generation as demonstrated by Lourtioz and coworkers [12].

Pulse durations of 100-200ps at 1-2GHz modulation rates are generated with unspecified optical powers. The bias conditions used do however indicate that the laser is biased very close to threshold with low modulation powers (7dBm and 17dBm to the gain and phase sections respectively) indicating low refractive index perturbation and reduced chirp. A compromise between peak powers and spectral broadening is inherent in picosecond pulsed lasers.

Spectral filtering allows near transform limited pulse generation through the use of semiconductor amplifiers [14], diffraction gratings [15-16] and pulse compression in optical fibre [15-19]. The chirp is compensated for using a medium with an opposite sign of dispersion which leads to pulse width compression. The intrinsically red-shifted spectrum of a picosecond pulsed diode laser will experience a relative retardation of the shorter wavelength components at the leading edge of the pulse in anomalous dispersion fibre, a grating cavity or combinations thereof [20].

3.5 Q-switching.

Through the introduction of a localised intracavity saturable absorber, a low Q cavity hold off stimulated emission and allow only negligible carrier depletion of the population inversion. Significantly higher carrier levels with 4.5 times the transparency level prior to pulse turn on is predicted by Vasil'ev for InGaAsP lasers [21]. Switching the cavity to a high Q resonator will allow the stimulated emission to rapidly build up to deplete the population until either the cavity gain is switched or the loss recovers.

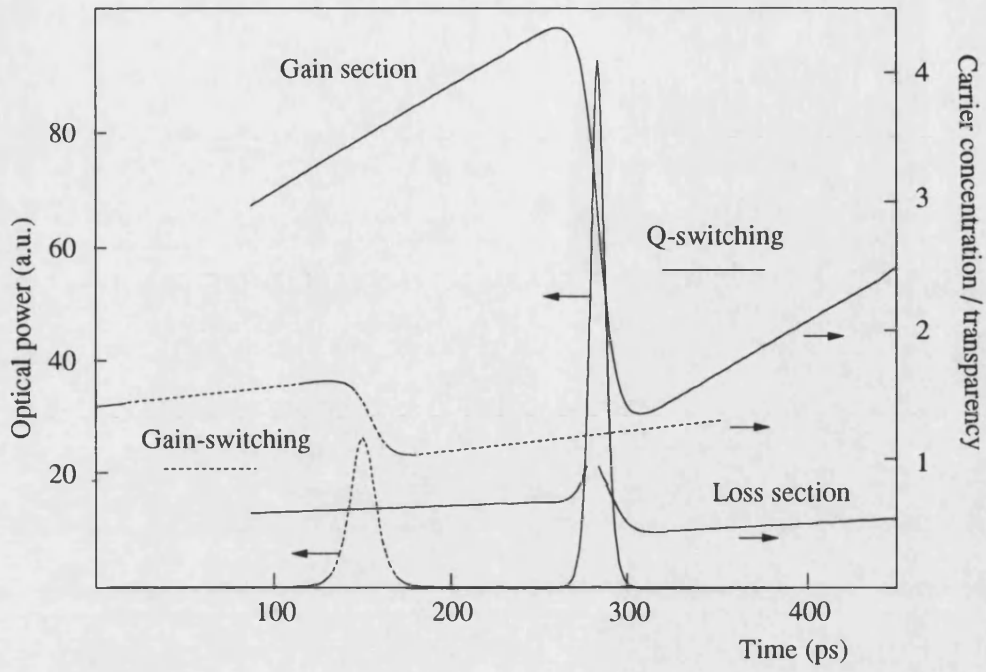

Figure 3.2 : Comparison of carrier dynamics and optical intensity variation during (i) gain-switching and (ii) Q-switching.

A schematic comparison is made in figure 3.2, showing variation in the carrier density and optical power during gain and Q-switching. The carrier densities in both the gain and loss section are given for the Q-switched example. Pulse turn on is now initiated by reduced absorption in the loss section. The enhanced pulse powers and reduced durations of the optical pulses result from enhanced carrier levels as a result of the delayed pulse turn on.

For a passively Q-switched laser, the irradiated absorber experiences the excitation of carriers to higher energy states and a resultant shift in the absorption edge until the material is bleached. With the significantly higher differential gain in the loss regime (below transparency) indicated in chapter 2, a significantly reduced perturbation of the carrier concentration in the loss section switches the gain of the cavity by four times more than expected for gain-switching. It has

been shown that for the passive generation of Q-switched pulse trains the differential absorption should be greater than the differential gain and that the gain section carrier lifetime such be greater than the carrier lifetime in the absorber section [22-24]. This is conveniently achieved in diode lasers using proton bombardment of the facets [25-26], or with a segmented electrode multicontact structures [27-40]. A centrally positioned absorber is recommended by Vasil'ev to increase the rate of excited carriers transfering from the loss to the amplifying sections [35]. Transferred carriers should be recycled to take part in the stimulated emission rather than vanish through spontaneous recombination. The upper limit of pulse repetition frequency would not be limited by the absorber spontaneous recombination lifetime but by the population transportation rate. The Q-switching efficiency would increase by the extra pumping of the carrier drift from the absorber.

A linear self-pulsation repetition rate dependence on gain section current is also noticed in the theoretical work of Vasil'ev [21]. A reverse biased absorber is modelled by assuming a differential absorption eight to ten times greater than the differential gain and a 50-100ps spontaneous recombination time in the absorber. Such modelling allows 2-10ps duration pulses for 50-500ps recombination times. Pulses of 10ps duration with 200-700mW peak power have been generated by Q-switched InGaAsP lasers at pulse generator limited 140MHz rates [29]. Self-Q-switching has also been observed in aged lasers [42] and as a result of dark line defects [43].

For an actively Q-switched diode laser, the loss section will be electrically modulated to define a nonrecovery time dependant repetition rate. A survey of Q-switched GaAs lasers is made to indicating wide variation in structures, powers, and modulation rates.

Rate	Q-switching scheme	FWHM	Power
500Hz	Optically Q-switched broad area laser [36]	21ps	6W
kHz	Transverse mode switched broad area laser (Single heterostructure) [37]	40ps	140W
40MHz	Passive Q-switching in a grating cavity (Discrete absorber) [38]	20ps	0.75W
400MHz	Passive Q-switched broad area laser [39]	40ps	7.5W
1.5GHz	Actively Q-switched broad area laser (Quantum well) [40]	24ps	1.3W
2.5GHz	Radio frequency locked self Q-switching [41]	17ps	1W
18GHz	Self Q-switching (multilobe far field) [35]	5ps	10W

Table 3.1 : Comparison of state of the art Q-switched GaAs lasers. While data for InGaAsP is scarce, details are given in chapter 5.

Q-switching is established as a technique for generating high power high energy pulses, and as such much work has been carried out on broad area lasers with the highest reported powers (140W) for large optical volume single heterojunction lasers. This often results in multiple transverse mode operation and unstable near and far field patterns. It is also noted that the quantum well broad area laser shows significantly reduced peak powers relative to the bulk broad area lasers.

High frequency pulsations have also been observed recently in distributed feedback lasers. Both single and multimode pulsations have been observed at modulation rates from 1-10GHz [44], 30GHz [45], 12-60 and 80GHz [46]. Electrical repetition rate tuning is not consistently observed however and modulation has not so far been shown to be complete.

3.6 Mode-locking.

While unlocked modes randomly related in phase result in small irregular irradiance fluctuations on a steady DC optical level, locked modes initiate an optical pulse to circulate back and forth inside the laser cavity. A mode-locked laser therefore emits pulses separated by a time equal to the round trip time of the laser cavity. The phase relation may be enforced by modulating loss or gain in the laser cavity at a frequency equal to the intermode frequency separation. This corresponds to the reciprocal of the round trip time as shown in figure 3.3.

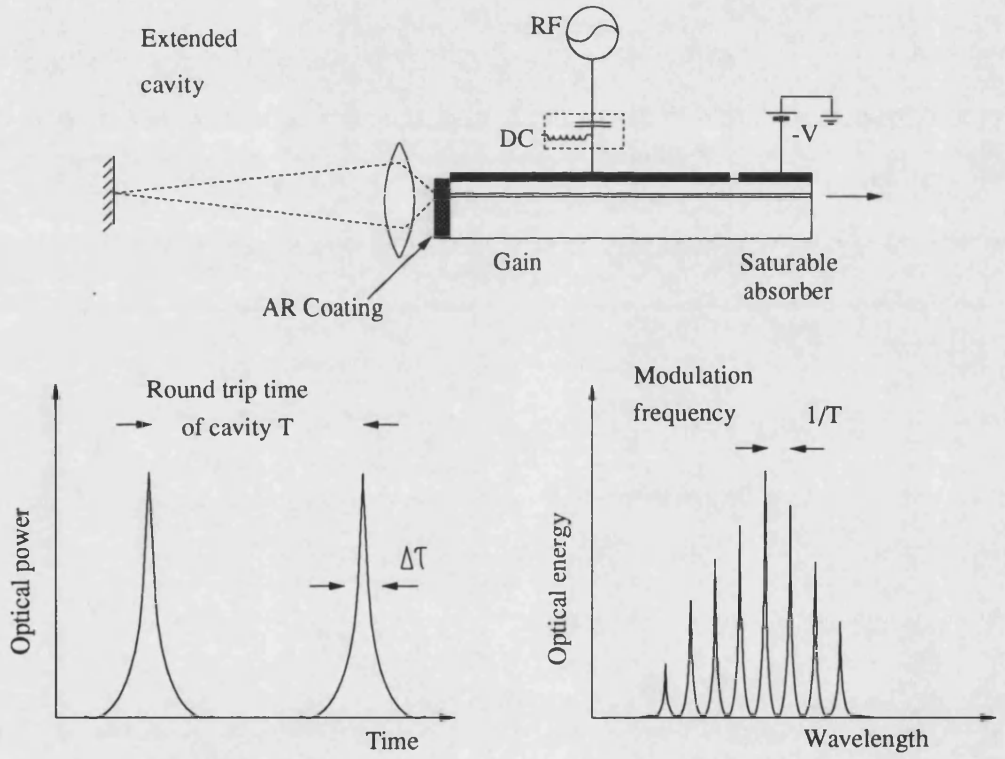

Figure 3.3: Mode-locking in an external cavity. Schematic spectra and pulse profiles are included for clarification.

Under steady state operation an optical pulse arrives at the gain section slightly after the peak of the current pulse. The leading portion of the pulse receives a small amount of amplification as the electrical pulse has just increased the segment gain. The middle portion receives the largest amount of gain. The trailing edge of the pulse receives reduced amplification as the earlier portions of the pulse deplete the gain. The output pulse is therefore shortened on successive round trips to become much narrower than the electrical current pulses. The final optical pulse width is achieved when the gain modulation section's pulse shortening is counterbalanced by cavity dispersion. Extended cavities are required for actively mode-locked lasers to allow modulation at electrically achievable frequencies. For GaAs lasers mode-locked at 200MHz in a external grating cavity, 15ps duration, 1W peak power pulses are reported by Bessonov [47]. Active mode-locked lasers with single gain elements in extended cavities are known to be very susceptible to multiple pulse formation [48-49]. The undesirable secondary pulsations are initiated by reflections from imperfect antireflection coatings on the diode laser facet. The reflected pulse is then amplified because the main pulse does not fully deplete the gain and the current drive to the segment may still be creating new carriers. Multiple pulse formation for reflectivities as low as 10^{-5} have been suggested by Schell and coworkers [49]. A saturable absorber section as illustrated in figure 3.2 can be used for single pulse operation at the higher bias levels. 2.8ps duration, 25mW peak power pulses are thus obtained by Derickson and coworkers [50-51]. Such hybrids of active and passive mode-locking schemes can be implemented with ion implantation at the emitting facet. Pulse widths are reduced from 45ps to 8ps at 1GHz modulation frequency by including saturable absorption in work by Schell and coworkers [52]. The requirement for complex cavities has also been removed

through the used of fibre mirror and grating schemes at Bell laboratories [53-54].

Purely passive schemes using either a saturably absorbing section [55-58] or bombarded facets [59] are required for ultrashort pulses at the higher repetition rates. When the pulse enters the highly attenuating absorber section, the leading edge is absorbed and excitons result, reducing the attenuation for the following part of the pulse. Efficient carrier sweepout resets the absorption for improved mode-locked operation. Pulsation at repetition rates unlimited by the laser parasitics and damping mechanisms are achieved.

For a centrally placed absorber, the passively mode-locked laser can simultaneously support two counter-rotating pulses in the cavity. Known as colliding pulse mode-locking [60-63], the pulses collide in the absorber to doubly saturate for further pulse narrowing, while occupying different regions of gain. This results in shorter duration pulses at half the round trip time. A comparison of state of the art mode-locked InGaAsP lasers is given to identify the roles of the schemes.

Rate (GHz)	Cavity and scheme	Duration (ps)	Power (mW)	dvdτ
2	Active with fibre cavity			
	Comb generator [52]	4.8 [1]	56 (0.54)	-
	Radio frequency [64]	7.7 [2]	39 (0.6)	0.56
2.5	Hybrid fibre grating cavity	23	137 (7.8)	0.88
	HR/AR coated laser [54]			
4.4	Active monolithic [65]	9	95 (4)	15.6
5	Active grating cavity [66]	10	2 (0.1)	0.36
20	Active fibre cavity	5 [1]	18 (1.8)	0.44
	HR/AR coated laser [68]			
40	Active monolithic [67]	3.8 [3]	-	1.4
40	CPM monolithic [63]	1.1 [1]	1 (0.05)	0.34
80	CPM monolithic [64]	1.28 [2]	5 (0.5)	0.34
104	Ion bombarded facets [59]	0.64 [2]	20 (1.3)	0.51
1540	Passive DBR laser [69]	0.26 [3]	40	0.52

Table 3.2 : State of the art mode-locking in ($\lambda = 1.5\mu m$) InGaAsP lasers. HR/AR coatings indicate emission from an anti reflection coated facet, with high reflectivity coatings at the often inaccessible second facet.

Repetition rate in Gigahertz, pulse duration in picoseconds, peak and average power levels in milliwatts.

Where pulse profiles have been assumed or measured:

[1] Single sided exponential profile.

[2] $sech^2$ profile.

[3] Gaussian profile.

3.7 Picosecond Pulse Characterisation.

The preceding discussion identifies significant variations in pulse profile, duration, power and optical spectrum for different pulse generation techniques and material systems. To fully characterise such picosecond optical pulses a combination of measurement techniques is often required. While Fabry-Perot interferometers, diffraction grating spectrometers, streak cameras and sampling oscilloscopes are able to give much detail [1], there is a requirement for field correlations to characterise pulses too short in duration to be properly characterised. It is noted for example that the ability of a picosecond pulse to fully illuminate a grating at any given time is limited by its duration. A 1ps duration pulse will occupy only 0.3mm in space. It is for this reason that is of interest to consider the coherence function of ultrashort optical pulses with a Michelson interferometer. Here the envelope function of the interference fringes is measured as the pulse train is split into two beams which are recombined having passed through a fixed and adjustable optical delay. This autocorrelation function may be Fourier transformed to obtain the spectral width.

The Michelson interferometer is key also in ultrashort pulse measurement when square law detection allows a second order intensity correlation to be made [70-71]. The recombined beams are now mixed in a nonlinear crystal such as $LiIO_3$ to generate a level of frequency doubled light proportional to the square of the average overlapped input light. The fundamental is blocked with appropriate optical edge filters and the second harmonic of the recombined beam is recorded as a function of the variable delay with a photomultiplier tube and appropriate amplifiers. The sum of the two nonmixed beams gives a background level to which the envelope function will be normalised. Around

zero delay where overlap is complete the second harmonic light detected is double the background intensity. The recorded function is proportional to $\int |(E(t)+E(t-\tau))^2|^2 dt$. For variable delay time τ, $E(t)+E(t-\tau)$ is the electrical field of the light entering the frequency doubling crystal. From such information, and for a pulse profile determined from a high bandwidth oscilloscope, the duration may be determined from the autocorrelation half width. Scaling factors are now tabulated for commonly generated pulse profiles.

$I(t)$	$\Delta\tau/\Delta t$	$\Delta t\Delta\nu$
$\exp\left\{-\frac{(4\ln 2)t^2}{\Delta t^2}\right\}$	$\sqrt{2}$	0.441
$sech^2\left\{\frac{1.76t}{\Delta t}\right\}$	1.55	0.315
$\exp\left\{-\frac{ln2\,t}{\Delta t}\right\}(t\geq 0)$	2	0.11

Table 3.3 : Example pulse profiles with durations at full width half maximum for second order autocorrelations and the theoretical time bandwidth products. Commonly encountered Gaussian, $sech^2$ and single sided exponential profiles are given.

Interference fringes are averaged out for a sufficiently fast scan and low bandwidth detector. Coherent pulses generated under complete mode-locked operation will peak at three times the background level. Incoherent pulses generated under gain and Q-switching peak at twice the background level. At

the laser cavity round trip time spacing.

Streak cameras offer a means of direct time resolved intensity measurement with picosecond and subpicoseond resolution. Generally speaking the Streak camera also converts information about ultrashort pulses from the time domain to the spatial domain. While the camera may be run in a single shot mode, synchroscan mode operates frequencies around 100MHz and is particularly suited to lasers pulsing in the hundreds Megahertz regime. The laser pulses to be measured are projected onto the camera slit, and the slit in turn is imaged on the photocathode of the streak tube. The photoelectrons are accelerated by an electrostatic field between the photocathode and the mesh electrode. A high power radio frequency voltage is applied to plates at the sides to sweep the photoelectrons at high speed in a direction perpendicular to the slit. After multiplication by a microchannel plate, the electrons incident on a phosphor screen form an intensity dependant image. The spatial deflection is now a measure of time. This information is readily transfered to a plotter or computer.

3.8 References.

1. VASIL'EV, P.P., Ultrafast diode lasers : Principles and applications, Artech House, 1995.

2. LIN, C., LIU, P.L., DAMEN, T.C., EILENBERGER, D.J., and HARTMAN, R.L., "Simple picosecond pulse generation scheme with injection lasers", Electronics Letters, 16, 600-602, 1980.

3. BIMBERG, D., KETTERER, K., SCHÖLL, H.E., and VOLLMER, H.P., "Generation of 4ps light pulses from directly modulated V-groove lasers", Electronics Letters, 20, 343-345, 1984.

4. ITO, H., YOKOYAMA, H., MURATA, S., and INABA, H., "Picosecond optical pulse generation from an RF modulated AlGaAs DH diode laser", Electronics Letters, 15, 738-740, 1979.

5. AUYEUNG, J., "Picosecond optical pulse generation at gigahertz rates by direct modulation of a semiconductor laser", Applied Physics Letters, 38, 308-310, 1981.

6. TORPHAMMER, P.T., and ENG, S.T., "Picosecond pulse generation in semiconductor lasers using resonant oscillation", Electronics Letters, 16, 587-589, 1980.

7. KOCH, T.L., and BOWERS, J.E., "Nature of wavelength chirping in directly modulated semiconductor lasers", Electronics Letters, 20, 1038-1040, 1984.

8. BUUS, J., "Dynamic line broadening of semiconductor lasers modulated at high frequencies", Electronics Letters, 21, 129-131, 1985.

9. CARROLL, J.E., WHITE, I.H., and GALLAGHER, D.F.G., "Dependance of chirp in injection lasers on temporal optical pulse shape", IEE Proceedings part J, 132, 34-37, 1985.

10. LIN, C., and BOWERS, J.E., "Measurement of 1.3 and 1.5 μm gain-switched semiconductor pulses with picosecond IR streak camera and a high speed InGaAsa PIN photodiode", Electronics Letters, 21, 1200-1201, 1985.

11. DOWNEY, P.M., BOWERS, J.E., TUCKER, R.S., and AGYEKUM, E., "Picosecond dynamics of a gain-switched InGaAsP laser", IEEE Journal of Quantum Electronics, 23, 1039-1047, 1987.

12. LOURTIOUZ, J.-M., CHUSSEAU, L., BRUN, E., HAMAIDE, J.-P., LESTERLIN, D., and LEBLOND, "Fourier-transform limited pulses from gain-switched distributed Bragg reflector laser using simultaneous modulation of the gain and phase sections", Electronics Letters, 28, 1499-1500, 1992.

13. WHITE, I.H., GRIFFIN, P.S., FICE, M.J., and WHITEAWAY, J.E.A., "Line narrowed picosecond optical pulse generation using a three contact InGaAsP/InP multiquantum well distributed feedback laser under gain-switching", Electronics Letters, 28, 1257-1258, 1992.

14. SUNDERSAN, H., and WICKENS, G.E., "Very high amplitude, minimal chirp optical pulse generation at 1.55um using multicontact DFBs and an Erbium doped fibre amplifier", Electronics Letters, 26, 725-727, 1990.

15. LIU, H.F., OSHIBA, S., OGAWA, Y., and KAWAI, Y., "Method of generating nearly transform-limited pulses from gain-switched distributed-feedback laser diodes and its application to soliton tranmission", Optics Letters, 17, 64-66, 1992.

16. IWATSUKI, K., SUZUKI, K., and NISHI, S., "Generation of transform limited gain-switched DFB-LD pulses <6ps with linear fibre compression and spectral window", Electronics Letters, 27, 1981-1982, 1991.

17. CHUSSEAU, L., XIE, J.-M., DUVILLARET, L., LOURTIOZ, J.-M., ACCARD, A., and HEBERT, J.-P., "Bandwidth-limited 0.3W picosecond pulses (4ps) from a 1.53 μm microwave modulated DFB laser with fibre compression", Electronics Letters, 26, 1085-1086, 1990.

18. TAKADA, A., SUGIE, T., and SARUWATARI, M., "Transform limted 5.6ps optical pulse generation at 12GHz repetition rate from gain-switched distributed feedback laser diode by employing pulse compression technique", Electronics Letters, 22, 1347-1348, 1986.

19. SCHELL, M., HUHSE, D., and, BIMBERG, D., "Picosecond pulse generation with a 1.55μm tunable twin guide laser using blue-chirp compression", Applied Physics Letters, 64, 1923-1925, 1994.

20. AGRAWAL, G.P., Nonlinear Fiber Optics, Chapter 5, Academic Press, San Diego, CA, 1989.

21. VASIL'EV, P.P., "High power high frequency picosecond pulse generation by passively Q-switched 1.55 μm diode lasers", IEEE Journal of Quantum Electronics, 29, 1687-1692, 1993.

22. DIXON, R.W., and JOYCE, W.B., "A possible model for sustained oscillations (pulsations) in AlGaAs DH lasers", IEEE Journal of Quantum Electronics, 15, 470-475, 1979.

23. UENO, M, and LANG, R., "Conditions for self-sustained pulsation and bistability in semiconductor lasers", Journal of Applied Physics, 58, 1689-1692, 1985.

24. VAN DER ZIEL, J.P., TSANG, W.T., LOGAN, R.A., and AUGUSTYNIAK, W.M., "Pulsating output of seperate confinement heterostructure buried optical guide lasers due to the deliberate introduction of saturable loss", Applied Physics Letters, 39, 377-378, 1981.

25. VOLKOV, L.A., GURIEV, A.L., DANIL'CHENKO, V.G., DERYAGIN, A.G., KUKSENKOV, D.V., KUCHINSKII, V.I., PORTNOI, E.L., and SMIRNITSKII, V.B., "Generation and detection of picosecond optical pulses in InGaAsP/InP lasers (λ=1.5-1.6μm) with passive Q-switching", Soviet Technology Letters, 1989, 15, 497-498.

26. LEE, T.P., and ROLDAN, R.H.R., "Repetitively Q-switched light pulses from GaAs injection lasers with tandem double section stripe geometry", IEEE Journal of Quantum Electronics, 339-352, 1970.

27. KITAYAMA, K., and WANG, S., "A new Q-switching method by intracavity phase modulation in a semiconductor laser", Applied Physics Letters, 1984, 44, 571-537.

28. TSANG, D.Z., WALPOLE, J.N., LIAU, Z.L., GROVES, S.H., and DIADIUK, V., "Q-switching of low-threshold buried heterostructure diode lasers at 10GHz", Applied Physics Letters, 45, 205-207, 1984.

29. VASIL'EV, P.P., WHITE, I.H., and FICE, M.J., "Narrow line high power picosecond pulse generation in a multicontact distributed feedback laser using modified Q switching", Electronics Letters, 29, 561-563, 1993.

30. WILLIAMS, K.A., BURNS, D., WHITE, I.H., SIBBETT, W., and FICE, M.J., " Picosecond pulse generation with ultralow jitter in 1.5μm multicontact MQW lasers using Q-switching", IEEE Photonics Technology Letters, 5, 867-869, 1993.

31. ARAKAWA, Y., LARRSON, A., PASLASKI, J., and YARIV, A., "Active Q-switching in a GaAs/AlGaAs multiquantum well laser with an intracavity monlithic loss modulator", Applied Physics Letters, 48, 561-563, 1986.

32. ITO, H., ONODERA, N., GEN-EI, K., and INABA, H., "Self Q-switched picosecond optical pulse generation with tandem type AlGaAs TJS laser", Electronics Letters, 17, 15-17, 1981.

33. TSUKADA, T., and TANG, C.L., "Q-switching of semiconductor lasers ", IEEE Journal of Quantum Electronics, 13, 37-43, 1977.

34. TSANG, D.Z., and WALPOLE, J.N., "Q-switched semiconductor diode lasers", IEEE Journal of Quantum Electronics, 19, 145-156, 1983.

35. VASIL'EV, P.P., "Picosecond injection laser : a new technique for ultrafast Q-switching", IEEE Journal of Quantum Electronics, 24, 2386-2391, 1988.

36. THEDREZ, B.J., SADDOW, S.E., LIU, Y.Q., WOOD, C., WILSON, R., and LEE, C.H., "Experimental and theoretical investigation of large output power Q-switched AlGaAs semiconductor lasers", IEEE Photonics Technology Letters, 5, 19-22, 1993.

37. VOLPE, F.P., GORFINKEL, V., SOLA, J., KOMPA, G., "140W, 40ps single optical pulses for laser sensor application", proceedings CLEO, paper CWC4, 1994

38. BOUCHOULE, S., STELMAKH, N., CAVELIER, M., and LOURTIOZ, J.M., "Highly attenuating external cavity for picosecond tunable pulse generation from gain/Q-switched laser diodes", IEEE Journal Quantum Electronics, 29, 1594-1699, 1993.

39. GAVRILOVIC, P., STELMAKH, N., ZARRABI, J.H., and BEYEA, D.M., "High energy CW Q-switched operation of multicontact semiconductor laser", Electronics Letters, 31, 1154-1155, 1995.

40. O'GORMANN, J., LEVEL, A.F.J., and HOBSON, W.S., "High power switching of multielectrode broad area lasers", Electronics Letters, 27, 13-15, 1991.

41. VASIL'EV, P.P., WHITE, I.H., BURNS, D., and SIBBETT, W., "High power low jitter encoded picosecond pulse generation using an RF-locked self Q-switched multicontact GaAs/GaAlAs diode laser", Electronics Letters, 29, 1594-1595, 1993.

42. PAOLI, T.L., "Changes in the optical properties of CW (AlGa)As junction lasers during accelerated aging", IEEE Journal of Quantum Electronics, 13, 351-357, 1977.

43. YANG, E.S., MCMULLIN, P.G., SMITH, A.W., BLUM, J., and SHIH, K.K., "Degradation induced microwave oscillations in double heterostructure injection lasers", Applied Physics Letters, 24, 324-327, 1974.

44. MARCENAC, D.D., and CARROLL, J.E., "Comparison of self-pulsation mechanisms in DFB laser diodes", proceedings LEOS, paper SL8.5, 1994.

45. VASIL'EV, P.P., and WHITE, I.H., "Large-signal dynamics of ultrafast single mode self-pulsations in 1.5 micron phase shifted DFB MQW triple contact diode lasers", proceedings CLEO, 1995.

46. FEISTE, U., MÖHRLE, M., SARTORIUS, B., HÖRER, J., and LÖFFLER, R., "12GHz to 64GHz continuous frequency tuning in self-pulsing 1.55 μm quantum well DFB lasers", International Semiconductor Laser Conference, Paper Th2.3, Hawaii, 1994.

47. BESSONOV, Y.L., BOGATOV, A.P., VASIL'EV, P.P., MOROZOV, V.N., and SERGEEV, A.B., "Generation of picosecond pulses in an injection laser with an external selective resonator", Soviet Journal of Quantum Electronics, 12, 1510-1512, 1982.

48. BOWERS, J.E., MORTON, P.A., MAR, A., CORZINE, S.W., "Actively mode-locked semiconductor lasers", IEEE Journal of Quantum Electronics, 25, 1426-1439, 1989.

49. SCHELL, M., WEBER, A., SCHOL, E., and BIMBERG, D., "Fundamental limits of subpicosecond pulse generation by active mode-locking of semiconductor lasers : The spectral gain width and the facet reflectivities", IEEE Journal of Quantum Electronics", 27, 1661-1668, 1991.

50. DERICKSON, D.J., HELKLEY, R.J., MAR, A., KARIN, J.R., BOWERS, J.E., and THORNTON, R.L., "Suppression of multiple pulse formation in external cavity mode-locked semiconductor lasers using interwaveguide saturable absorbers", IEEE Photonic Technology Letters, 4, 333-335, 1992.

51. DERICKSON, D.J., HELKEY, R.J., MAR, A., KARIN, J.R., WASSERBAUER, J.G., and BOWERS, J.E., "Short pulse generation using multisegment mode-locked semiconductor lasers", IEEE Journal of Quantum Electronics, 28, 2186-2202, 1992.

52. SCHELL, M., WEBER, A.G., and BIMBERG, D., "Sub-Picosecond Pulse Generation at 1.3 μm by Hybrid mode locking", International Semiconductor Laser Conference, Paper N-4, Takamatsu, 1992.

53. EISENSTEIN, G., TUCKER, R.S., KOROTKY, S.K., KOREN, U., VESELKA, J.J., STULZ, L.W., JOPSON, R.M., and HALL, K.L., "Active mode-locking of an InGaAsP 1.55μm laser in a fibre resonator with an integrated single-mode-fibre output port", Electronics Letters, 173-175, 21, 1985.

54. MORTON, P.A., MIZRAHI, V., TANBUN-EK, T., LOGAN, R.A., LEMAIRE, P., ERDOGAN, T., SCIORTINO, P.F., SERGENT, A.M., and WECHT, K.W., "High-power mode-locked hybrid pulse source using two-section laser diodes", Optics Letters, 19, 725-727, 1994.

55. SANDERS, S., ENG, L., and YARIV, A., "Passive mode-locking of monolithic InGaAs/AlGaAs double quantum well lasers at 42GHz repetition rate", 1990, 26, 1087-1089.

56. SANDERS, S., YARIV, A., PASLASKI, J., UNGAR, J.E., and ZAREM, H.A., "Passive mode-locking of a two section multiple quantum well laser at harmonics of the cavity round-trip frequency", Applied Physics Letters, 1991, 58, 681-683.

57. MAY, P.G., and BIERBAUM, M., "Monolithic mode locking of long cavity GaAs-AlGaAs semiconductor lasers", IEEE Photonics Technology Letters, 3, 296-298, 1991.

58. VASIL'EV, P.P., and SERGEEV, A.B., "Generation of bandwidth limited 2 ps pulses with 100GHz repetition rate from multisegmented injection laser", Electronics Letters, 25, 1049-1050, 1989.

59. DERYAGIN, A.G., KUKSENKOV, D.V., KUCHINSKII, V.I., PORTNOI, E.L., and KHRUSHCHEV, I.Yu., "Generation of 110GHz train of subpicosecond pulses in 1.535μm spectral region by passively modelocked InGaAsP/InP laser diodes", Electronics Letters, 30, 309-311, 1994.

60. AGRAWAL, G.P., and OLSSON, N.A., "Self phase modulation and spectral broadening of optical pulses in semiconductor laser amlpifiers", IEEE Journal of Quantum Electronics, 25, 2297-2306, 1989.

61. VASIL'EV, P.P., MOROZOV, V.N., POPOV, Y.M., and SERGEEV, A.B., "Subpicosecond pulse generation by a tandem-type AlGaAs DH Laser with colliding pulse mode locking", IEEE Joural of Quantum Electronics, 22, 149-151, 1986.

62. CHEN, Y.K., WU, M.C., TANBUN-EK, T., LOGAN, R.A., and CHIN, M.A., "Subpicosecond monolithic colliding-pulse mode-locked multiple quantum well lasers", Applied Physics Letters, 58, 1253-1255, 1991.

63. CHEN, Y.K., and WU, M.C., "Monolithic colliding pulse mode-locked quantum well lasers", IEEE Journal of Quantum Electronics, 28, 2176-2185, 1992.

64. EISENSTEIN, G., TUCKER, R.S., KOREN, U., and KOROTKY, S.K., "Active mode-locking characteristics of InGaAsP single mode fibre composite cavity lasers", IEEE Journal of Quantum Electronics, 22, 142-148, 1986.

65. RAYBON, G., HANSEN, P.B., KOREN, U., MILLER, B.I., YOUNG, M.G., NEWKIRK, M., IANNONE, P.P, BURRUS, C.A., CENTANNI, J.C., and ZIRNGIBL, M., "Two contact 1cm long monolithic extended cavity actively mode-locked at 4.4GHz", Electronics Letters, 28, 2220-2221, 1992.

66. BIRD, D.M., FATAH, R.M., COX, M.K., CONSTANTINE, P.D., REGNAULT, J.C., and CAMERON, K.H., "Miniature packaged actively mode-locked semiconductor laser with tunable 20ps transform limited pulses", Electronics Letters, 26, 207-208, 1990.

67. TUCKER, R.S., KOROTKY, S.K., EISENSTEIN, G., KOREN, U., STULZ, L.W., and VESELKA, J.J., "20GHz active mode-locking of a 1.55 μm InGaAsP laser", Electronics Letters, 21, 239-240, 1985.

68. TUCKER, R.S., KOREN, U., RAYBON, G., BURRUS, C.A., MILLER, B.I., KOCH, T.L., and EISENSTEIN, G., "40GHz active mode-locking in a 1.5 μm monolithic extended cavity laser", Electronics Letters, 25, 621-622, 1989.

69. ARAHIRA, S., OSHIBA, S., MATSUI, Y., KUNI, T., and OGAWA, Y., "Terahertz rate optical pulse generation from a passively mode-locked semiconductor laser diode", Optics Letters, 19, 834-836, 1994.

70. SHAPIRO, S.L., Ultrashort light pulses, Topics in Applied Physics, Springer Verlag, Berlin, 1976.

71. DIELS, J-C. M., FONTAINE, J.J., MCMICHAEL, I.C., and SIMONI, F., "Control and measurement of ultrashort pulse shapes (in amplitude and phase) with femtosecond accuracy", Applied Optics, 24, 1270-1282, 1985.

CARRIER DYNAMICS IN GAIN-SWITCHED LASERS

Gain suppression in picosecond pulsed diode lasers is widely known to limit peak powers, distort picosecond pulse profiles and limit the minimum pulse durations. Using lumped rate equation modelling to interpret the temporal dynamics and the spectral performance of gain-switched InGaAsP lasers, physical effects known to lead to gain suppression are identified and isolated. The role of carrier transport in quantum well lasers is discussed for the first time for large signal modulation. Spatial hole burning is described by spatially resolving carriers along the length of the cavity.

4.1 Outline.

Gain-switching readily generates tens of picosecond duration pulses at flexible repetition rates. However, significant temporal and spectral profile variations are noted with electrical drive. Such variation is used here to allow insight into picosecond laser dynamics. Considering the time averaged spectra of gain-switched pulses allows an assessment of the perturbations to the refractive index and measurement of the linewidth broadening factor. In this work the major contributions to gain suppression experienced at high photon density and high carrier levels are investigated through a comparative study of experiment and theory.

Distributed feedback InGaAsP lasers are of widespread commercial interest and are therefore considered in this study. The first laser considered has a bulk active layer and a two $\lambda/8$ phase shifted distributed feedback

grating[1]. The contributions to gain suppression common to bulk and quantum well lasers as well as to lasers with spatially nonuniform carrier densities and fields are therefore described. These comprise spectral hole burning, transverse mode spatial hole burning and carrier heating effects, which are known to contribute to the nonlinear gain suppression term ε.

Quantum well distributed feedback lasers[2,3] are observed to exhibit enhanced damping under gain-switched operation. Carrier transport across the confinement layers and capture from the barrier layers into the wells is known to describe anomalous damping under small signal modulation. For the first time, carrier transport is now modelled to describe large signal modulation. A lumped rate equation model including both gain suppression and carrier transport describes the pulse temporal and spectral dependence on electrical bias well.

Longitudinal carrier inhomogeneity experienced under spatial hole burning is known to suppress the gain further. Comparing a $\lambda/4$ phase shifted distributed feedback laser[3] with a two $\lambda/8$ phase shifted grating ably demonstrates the role of spatial hole burning. Simulating the $\lambda/4$ phase shifted quantum well laser considered experimentally, requires the carriers to be spatially resolved into three longitudinal sections. As the carrier density differential changes little during picosecond pulse generation, spatial hole burning is shown to be a relatively weak effect relative to carrier transport.

4.2 Theory.

Three rate equation models have been developed to describe the distributed feedback lasers in sections 4.4, 4.5 and 4.6 respectively. The first is a

lumped parameter rate equation model which assumed that the carrier density and the field is spatially nonvariant. The second model introduces a rate equation for carriers in the barriers and in the waveguides to describe carrier transport effects in quantum well lasers. The third and final model spatially resolves the cavity into one central and two end sections. The symmetry is appropriate to describe longitudinal mode spatial hole burning in quarter wave phase shifted distributed feedback lasers.

The rate equations introduced as 2.6 and 2.7 are solved using a Runge Kutta algorithm implemented in C++ on a personal computer. A 0.2ps time step allows stable simulation of the gain-switched pulses. As starting conditions, the carrier density is set to transparency, and the photon density is set to zero. The 1GHz gain-switched pulse train starts from spontaneous emission. As experimental measurements are time averaged, the simulation stabilises for ten periods. The intensity profile is then recorded for the final period. Only one longitudinal mode is assumed to oscillate. At each time step, the change in refractive index is calculated. Equation 2.4 gives the linear coefficient describing the refractive index dependance on carrier density. From the refractive index and the instantaneous intensity, the pulse energy can be spectrally resolved, and a time averaged spectrum is generated over one period. The time averaged spectrum is then convolved with a Gaussian function with a width corresponding to the resolution of the Fabry-Perot interferometer used in the experiments. It is the time averaged spectrum and the time resolved intensity profiles that are compared with experimental measurements.

4.3 Experiment.

Measurements are made on a range of three single contact InGaAsP/InP ($\lambda = 1.5$ μm) bulk and lattice-matched multiple quantum well, $\lambda/4$ and two $\lambda/8$ phase shifted distributed feedback lasers. The quantum well lasers comprise five 6.5nm InGaAs wells. Bulk laser active layers are 0.18 μm in thickness. Lasers are between 350-400 μm in length with 3.5 μm ridge waveguides. Coupling coefficient device length products are between 1.5 and 3. The multiple phase shifted devices have two $\lambda/8$ phase shifts which are spaced 245 μm apart giving nominal coupling coefficients of 70cm^{-1}. The second order gratings are created using electron beam lithography. The distributed feedback lasers are antireflection coated.

The lasers are gain-switched to generate picosecond optical pulses by applying 15dBm, 1GHz RF electrical modulation superimposed on a DC forward bias. Figure 4.1 shows a schematic for the experimental arrangement. A 47Ω series resistance provides impedance matching. The DC forward bias is varied for values around threshold, which are typically 25mA. The cavity carrier density at optical pulse turn on and the pulse turn on time relative to the modulation are therefore varied. The laser temperature is kept constant with a thermoelectric cooler to 19°C ± 0.1°C. The spectral output of the lasers is measured using a both a monochromator and Fabry-Perot interferometer to give 0.1 Angstroms resolution. The optical pulses are monitored using a high speed lightwave converter with a 12GHz digital storage oscilloscope.

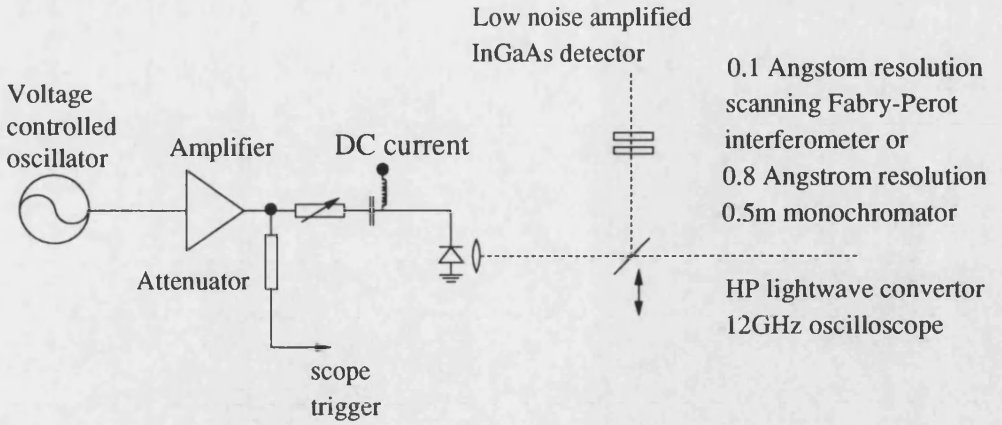

Figure 4.1 : Schematic diagram for the experimental arrangement to characterise gain-switched distributed feedback lasers.

Initial comparisons between a multiquantum well laser[2] and bulk active layer laser[1] in figure 4.2 indicate an enhanced level of damping in the relaxation oscillation. The RF power levels are the same for the six conditions shown in figure 4.2. The DC current is however increased for the bulk laser (left) and the quantum well laser (right) for the traces below. As the DC bias is increased, the gain-switched pulses from the bulk laser start to ring, whereas the pulses from the quantum well laser have a heavily damped tail. Important spectral differences highlight the increased nonlinearity for quantum well lasers. Typically the bulk devices generate smooth spectra at low optical powers but are subject to relaxation oscillations for high DC bias and therefore multipeaked spectra. The multiquantum well devices exhibit significantly larger longer wavelength spectral peaks which will be shown to be characteristic of a slow pulse fall time in figure 4.3.

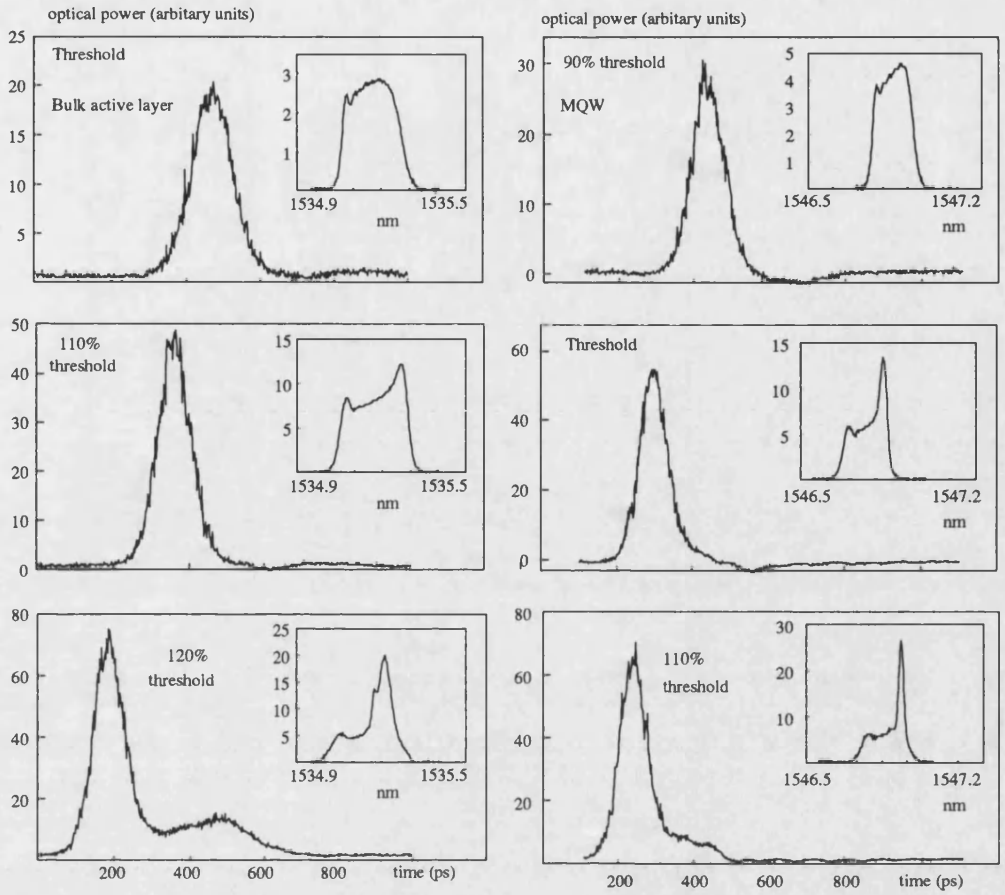

Figure 4.2 : A comparison of the temporal and spectral performance of gain-switched bulk and multiquantum well active layer distributed feedback lasers, indicating increased gain saturation in quantum well structures though increased longer wavelength peaks and reduced relaxation oscillations.

4.4 Nonlinear Gain Suppression.

To determine the mechanisms dominating the spectral output of the bulk and multiquantum well laser diodes, three different numerical simulations are used. Firstly a conventional lumped, single mode rate equation analysis has been implemented to model and account for the experimentally observed spectra in bulk multiple phase shift distributed feedback lasers. With pulse durations well in excess of the cavity round trip time, a lumped parameter model is expected to give good agreement between experiment and theory.

The carrier dependent refractive index changes account for spectral chirp, with the model also assuming nonlinear gain suppression. Gain-switching is shown schematically in figure 4.3, to indicate time resolved carrier depletion and the associated time-averaged spectrum. Shorter wavelength emission occurs as the device starts to oscillate. As the carriers deplete, the effective refractive index of the cavity is reduced and hence wavelength increase. The slowing down of the change in carrier depletion as the first gain-switched pulse turns off causes the longer wavelength spectral peak. Emission due to any following relaxation oscillation occurs at wavelengths between these two extremes, as seen in the multipeaked spectra in figure 4.2. Bandwidth limitations and photodetector ringing in the measurement system have not been accounted for in simulation, leading to minor discrepancies in temporal performance. A spectral resolution of 0.1Å is included however to allow direct comparison of theoretical and experimental optical spectra.

Material parameters used in the simulation are either taken from published work or have been directly measured [1] and are tabulated below. The linewidth enhancement factor and the absolute wavelength are both fitted

to give the observed spectral agreement. The rate equation formalism introduced in chapter 2 is used. A linear approximation for the gain is used for both bulk and quantum well modelling.

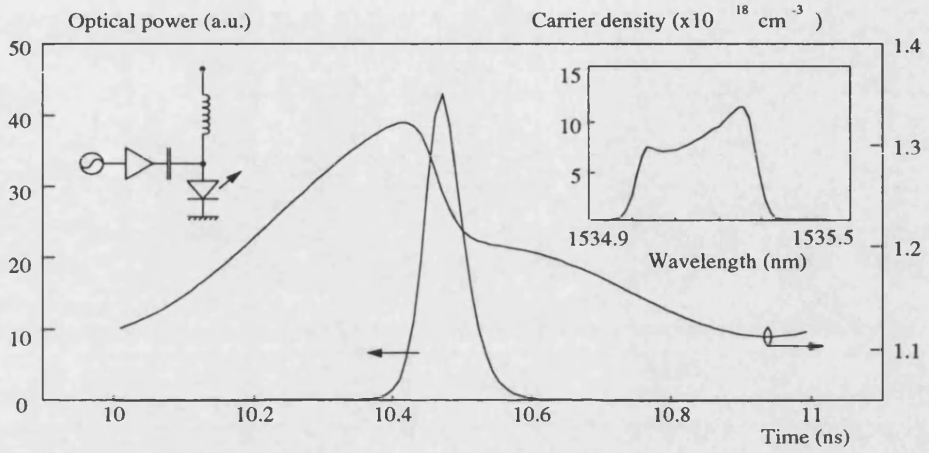

Figure 4.3 : Simulation of gain-switching in a bulk multiple phase shift distributed feedback laser, showing reducing carrier levels during pulse generation with the time averaged red shifted optical spectrum.

Monomolecular carrier recombination rate	A	10^{8}	s^{-1}
Bimolecular recombination coefficient	B	10^{-10}	$cm^{3}s^{-1}$
Auger recombination coefficient	C	$1.3x10^{-28}$	$cm^{6}s^{-1}$
Optical confinement factor	Γ	0.35	
Linewidth enhancement factor	α_H	6	
Differential gain	dg/dn	$3x10^{-16}$	cm^{2}
Gain suppression or nonlinear gain factor	ε	10^{-17}	cm^{3}
Optical scattering loss in waveguide	α_i	40	cm^{-1}
Spontaneous emission coupling factor	β	10^{-4}	
Carrier concentration at transparency	N_o	$1.1.10^{-18}$	cm^{-3}
Current injection efficiency	η_i	0.6	

Table 4.1 : Material parameters assumed in the simulation of bulk InGaAsP gain-switched lasers.

The nonlinear gain suppression term ε is used widely in rate equation analyses to describe the experimentally observed, reduced laser modulation bandwidth [4-5]. The major contributions to ε are spectral hole burning under enhanced optical fields and carrier heating and carrier carrier scattering at enhanced carrier concentrations.

Spectral hole burning results from a localised suppression in the gain spectrum due to stimulated emission. The dips in the gain spectrum occur at discrete energy levels as a result of the enhanced electron hole recombination leading to an intensity dependent gain suppression. The dips are broadened through carrier carrier scattering on a subpicosecond time scale [5-10] and the finite time taken for hot injected carriers to relax [11].

Under high field conditions, carrier carrier scattering effects also lead to a broadening of the gain spectrum at the expense of peak gain, leading to an injection rate dependent contribution to the nonlinear gain suppression term ε [4-5,12-13]. Through electron phonon interactions the carriers relax on a picosecond time scale leading to an additional carrier bottle neck under high depletion conditions [9,13-14].

In a lumped rate equation model where the carrier and intensity variations transversely in the plane of the junction are not explicitly described, the gain suppression is further enhanced through transverse mode spatial hole burning. Such effects depend on the degree of current spreading and carrier diffusion in the plane of the active layer [15-16]. Current spreading and carrier diffusion are approximated through a current injection efficiency. Fluctuations in the transverse mode profile are not considered explicitly in this model and any gain suppression is accounted for through ε. A two $\lambda/8$ phase shifted grating distributed feedback laser with its relatively the uniform optical field

distribution is considered first as longitudinal mode spatial hole burning is expected to be negligible [2-3]. A bulk active layer avoids nonlinearities inherent to the quantum well lasers, as described in the following section.

Implementing the model leads to good agreement with theory and experiment for an increasing DC bias current for both temporal profiles and time-averaged spectra in figure 4.4. While symmetric pulses are readily generated with linearly red-shifted spectra for 1GHz modulation on a threshold DC level, asymmetry is noted in both the pulse and spectral profiles at higher DC levels. Modelling shows that gain suppression results in a damped tail as carriers are not fully depleted by the gain-switched pulse. Reduced fluctuations in the carrier density at the tail of the pulse lead to enhanced energy longer wavelength peaks.

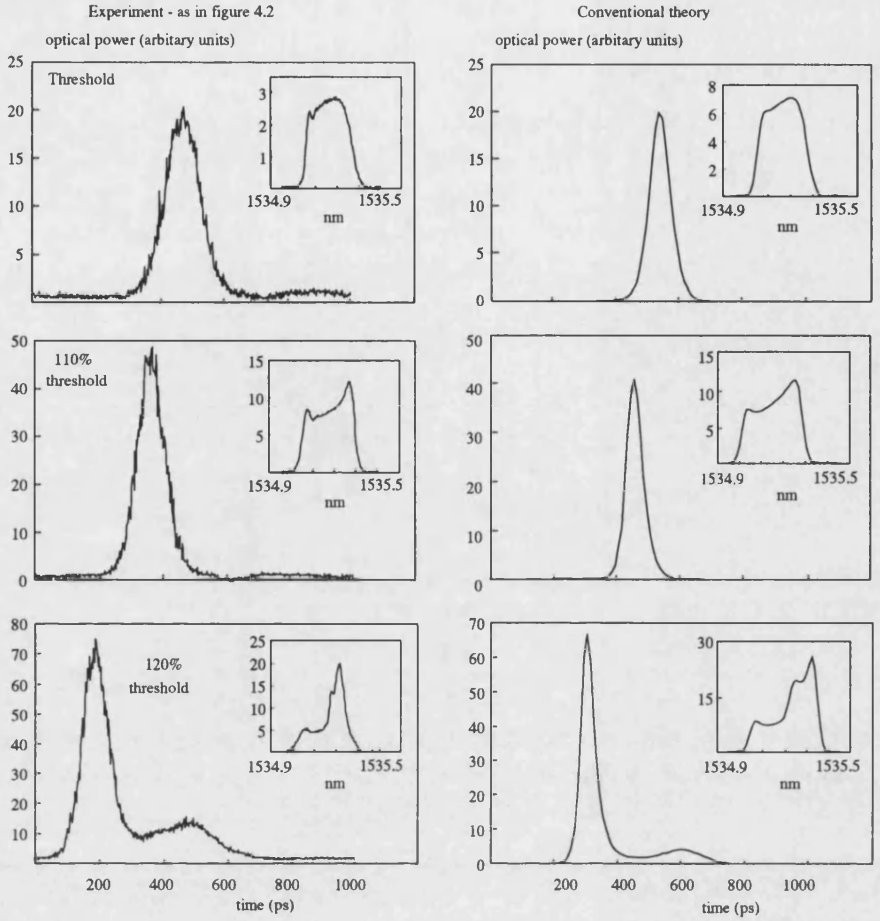

Figure 4.4 : Comparison of experiment gain-switched performance with simulation for varied DC bias current and 15dBm, 1GHz RF power in bulk multiple phase shift distributed feedback lasers. Temporal performance with spectra inset. Bias conditions for the simulation match those for experiment.

4.5 Carrier Transport in Quantum Well Lasers.

The enhanced differential gain achieved in quantum well structures has lead to predictions of superior modulation bandwidths compared to bulk active layer lasers [16-17]. For some time however the maximum reported bandwidths for quantum well lasers [18-19] have been smaller than those for bulk InGaAs lasers [20-21]. The anomalous damping results from an enhanced nonlinearity observed in the gain for both small and large signal modulation [22-24]. Experimental work on the picosecond gain dynamics in semiconductor amplifiers indicates that the modulation bandwidth is limited by carrier transport perpendicular to the junction plane [25-26] and has stimulated much research into laser dynamics [27-36]. Indeed, small signal modulation is not convincingly described using the conventional two energy level rate equation model without using inexplicably large values for nonlinear gain suppression term ε. Carrier transport models are now established for the small signal modulation of quantum well lasers [32-33]. This work implements the small signal theory for gain-switched quantum well lasers to confirm the importance of carrier transport in large signal modulation.

A schematic band structure for a five quantum well laser is shown in figure 4.4 to show three processes important to carrier transport. Carriers injected into the confinement layers will diffuse towards the wells [37-38]. The coupling of carriers from the bulk confinement layers to the quantum wells is described by a local quantum mechanical capture. As the capture time is significantly smaller than the diffusion time, the terms are combined to give a net capture time [27,39]. Thermionic emission of carriers out of the wells maintains a thermal equilibrium.

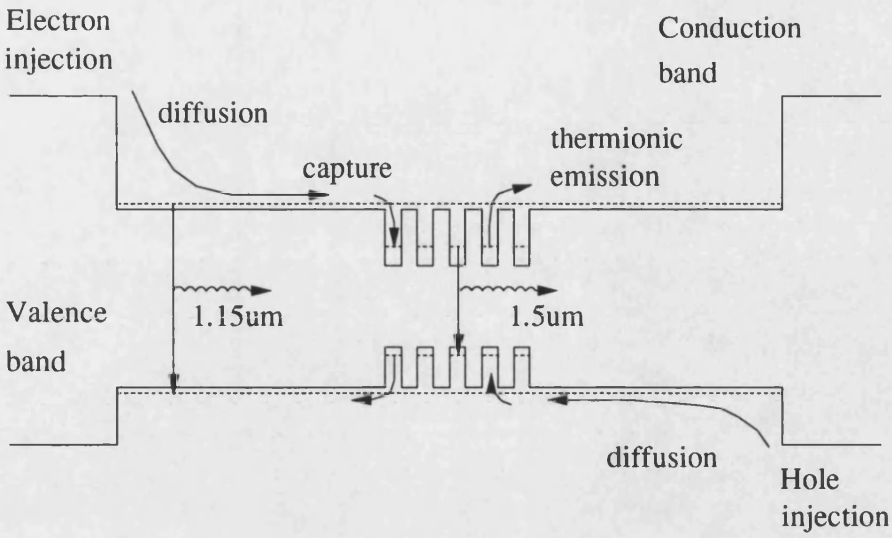

Figure 4.5 : Schematic for carrier transport processes in a multiquantum well laser.

The capture process is assumed to be dominated by diffusion across the confinement layers and will be dominated by the slower hole mobility. For the diffusion constant D and confinement layer thickness L the capture time τ_{cap} may be determined [31-32] :

$$\tau_{cap} = \frac{L^2}{4D} \qquad 4.1$$

Thermionic emission out of the wells is readily defined by the well and barrier dimensions. For a well width L_w, carrier effective mass m^* and barrier height E_b the thermionic emission rate τ_e is defined [33] :

$$\tau_e = L_w \sqrt{\frac{2\pi m^*}{kT}} \exp\left(\frac{E_b}{kT}\right) \qquad 4.2$$

The diffusion dominated capture time of 40ps best described the experimental data and is in agreement with published work for similar structures. Thermionic emission out of the wells allows carriers to populate the

waveguide and barrier layers and is characterised by the structure dependent time constant τ_e=80ps. Again, the thermionic emission time constant is fitted to acheive good experimental agreement. The rate equations have been modified to account for the interactions between carriers in the waveguide and well regions with each other and with the photon density. Now the injected current modulates the waveguide carrier density :

$$\frac{dN_b}{dt} = \frac{J}{qd_b} + \frac{N_w}{\tau_e}\frac{V_w}{V_b} - \frac{N_b}{\tau_c} \qquad 4.3$$

The subscripts b and w denote the barrier or confinement layers and wells respectively. The waveguide carrier density is directly modulated by the injected current, with the right hand term determining the interplay of carriers between the waveguide and wells. Because the equation considers carrier densities, the volume ratio V_w/V_b is introduced to keep consistency in carrier numbers flowing between the two regions. The rate of change of well carrier density is now formulated in terms of well carrier densities, leading to:

$$\frac{dN_w}{dt} = \frac{N_b}{\tau_c}\frac{V_b}{V_w} - \frac{N_w}{\tau_e} - v_g GP - \frac{N_w}{\tau_s} \qquad 4.4$$

The photon rate equation remains as for the conventional two energy level model. Measurements indicate that spontaneous emission from the waveguide is negligible and has been duly neglected [34].

The additional rate equation therefore takes carrier transport effects explicitly into account to allow for the presence of carriers in the confinement region and accounting for a damping mechanism particularly suitable for the structures. The model uses the same amount of nonlinear gain as considered for bulk active layers ($\varepsilon = 10^{-17}$cm^3). The differential gain now becomes 6×10^{-16}cm^2 and a value of 2.9 is used for the linewidth broadening factor.

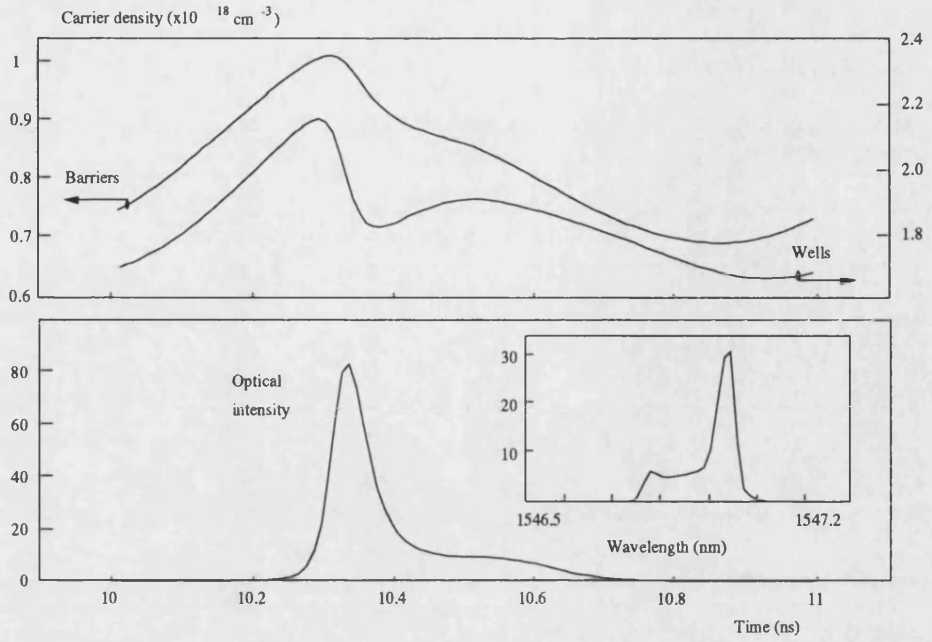

Figure 4.6 : Time resolved carrier density in the barriers and in the wells for a gain-switched quantum well laser. The time resolved intensity profile and time averaged spectrum is also given below. The population of the barriers restricts the flow of carriers into the wells to suppress peak powers, and prolongs the turns off time leading to enhanced tail formation.

Implementing this model allows the accurate simulation of both peak power and relaxation oscillation suppression as observed temporally and implied spectrally. The increase in longer wavelength peak with DC bias current results from the increasingly damped well carrier population as seen in figure 4.6. The capture mechanism causes an effective damping of the well carrier density and therefore gain dynamics. Relaxation oscillation is suppressed leading to reduced peak output powers, enhanced tails, and therefore larger spectral peaks in the quantum well laser gain-switched

spectra. Experimental pulse profiles and optical spectra are given in the left hand column of figure 4.7 for an increase in DC current. Temporal and spectral performance is simulated using both the two energy level rate equations (right hand column) and a three energy level carrier transport model (centre). The bulk value of nonlinear gain is used for the carrier transport model. Good agreement is observed in terms of peak powers and relaxation oscillation frequencies for temporal profiles in the case of the three energy level model in the centre column of figure 4.7. Discrepancies arise from the measurement system resolution. For a linewidth broadening factor $\alpha_H = 2.9$ good agreement is also achieved in terms of spectral broadening and the proportions of energy in the longer wavelength peaks for increasing bias. Without considering carrier transport effects however, relaxation oscillations are underdamped at higher DC bias conditions, leading to substructure in the spectra. Some agreement can however be achieved without the carrier transport model by using a higher nonlinear gain term $\varepsilon = 5\text{x}10^{-17}\text{cm}^3$ as shown in the right hand column of figure 4.7.

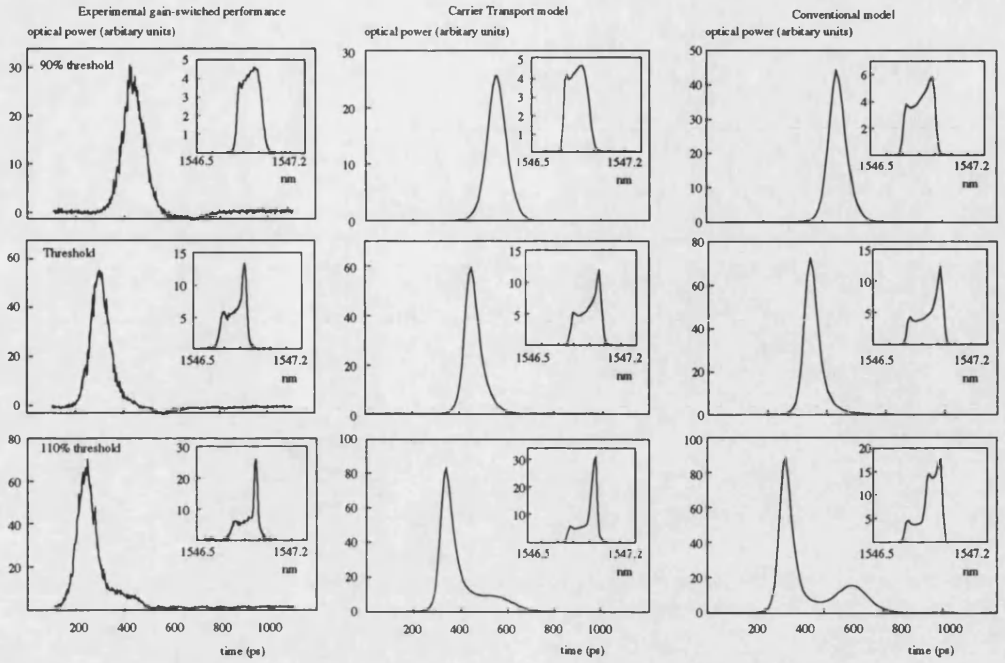

Figure 4.7 : Comparison of experimental gain-switched performance (left) with carrier transport and $\varepsilon=10^{-17}$ (centre) and two rate equation model and $\varepsilon=5\times10^{-17}$ (right) simulation for two $\lambda/8$ phase shift multiquantum well lasers.

The build up of carriers in the confinement region also leads to a carrier influence on the effective cavity refractive index through a free electron plasma. Emissions at the bandgap of the confining layers have been observed, confirming the presence of barrier carriers [28-29]. A resultant spectral broadening under small signal modulation has also been noted [24]. Refractive index modulation is therefore modelled using this additional effect. The right hand term in equation 4.5 accounts for a carrier plasma in the waveguide modulating the refractive index of the cavity.

$$\mu = \mu_o + \Gamma_w \frac{d\mu}{dN_w} N_w + \Gamma_b \frac{d\mu}{dN_b} N_b \qquad 4.5$$

The optical confinement within the waveguide and barrier layers Γ_b is significantly greater than the confinement within the wells Γ_w, and significant broadening resulting from the barrier carrier population has been noted for small signal modulation. Changes in the carrier levels in the barrier layers are noted to be sufficiently small however in the pulse forming time frame, and therefore effects are not as significant as for small signal modulation [31].

4.6 Longitudinal mode spatial hole burning.

In the modelling of quarter wave shifted distributed feedback lasers, the cavity has been divided into one central and two end sections. This allows the uniformly pumped device to have a longitudinally varying carrier concentration and gain, to describe the nonuniform carrier density and mode intensity experienced in spatial hole burning [40] in a more explicit manner. Two carrier rate equations are solved for both the barriers and wells. Terms in the well rate equations including photon density P are modified by a hole burning dependent term [41] derived from more detailed small signal analysis [40]. While the empirical relations themselves provide little physical insight, the modelling is done to demonstrate that longitudinal hole burning may be modelled in a similar fashion for small and large signal alike, that the effects are reasonably limited under gain-switched operation, and to confirm the rate equations implemented for quantum well lasers. While the carrier rate equations are solved separately, the photon generation and lifetime will depend on the carrier distribution. A lumped photon density is still assumed, but now accepts contributions from both sections.

Under high power RF modulation however, the difference in sections' carrier levels remains relatively steady, indicating that spatial hole burning is a relatively weak effect here. The simulated and experimental spectra compared in figure 4.8 show slightly higher spectral peaks as compared with the multiple phase shifted devices for the similar bias conditions, indicating the effect longitudinal spatial hole burning has on damping relaxation oscillation. Agreement is achieved from DC biases below to well above the threshold of 17mA, with the theory describing damping of the oscillations and spectral

performance well.

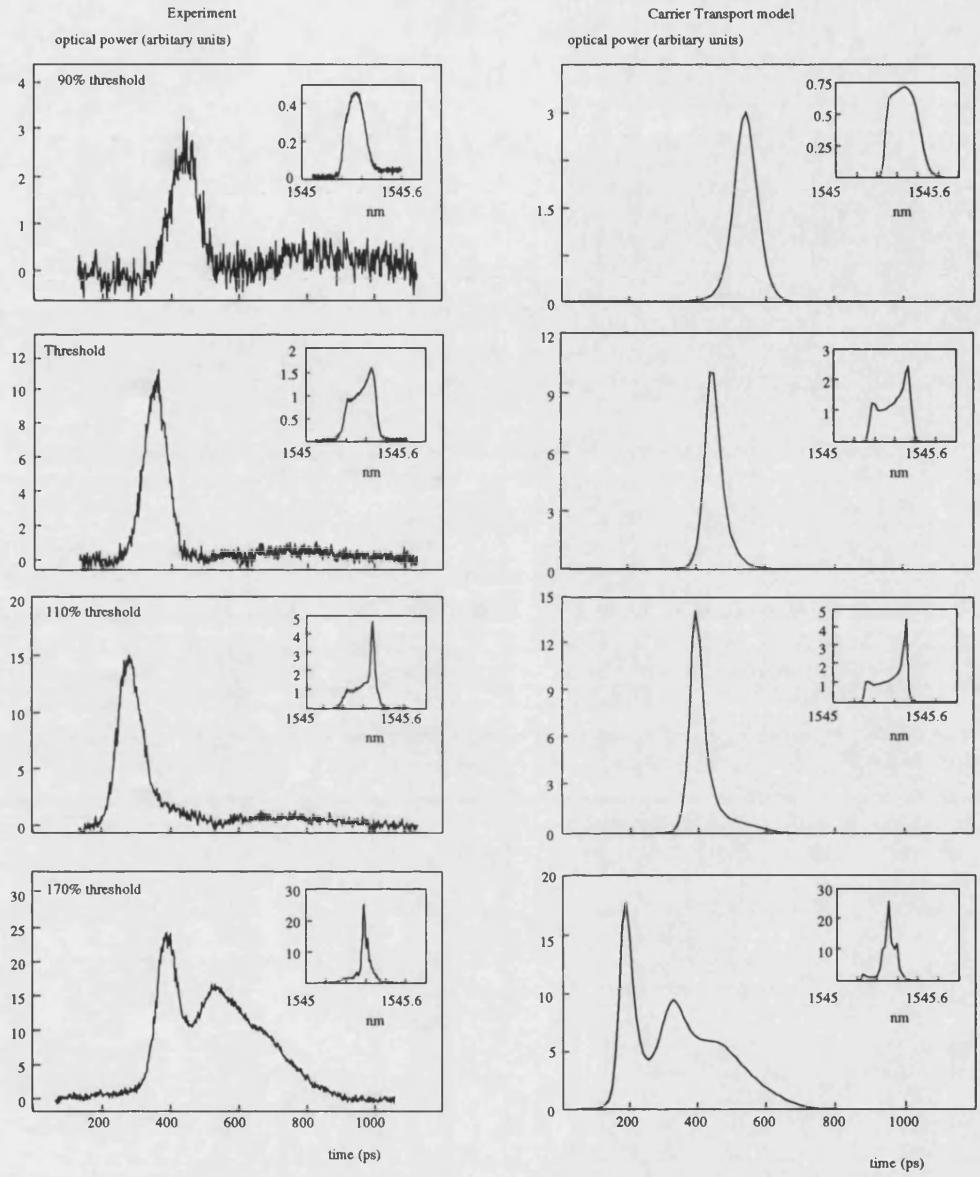

Figure 4.8 : Comparison of experimental gain-switched performance with simulation for varied DC bias current and 15dBm RF power in quarter wave shift multiquantum well distributed feedback lasers. Temporal performance with spectra inset.

4.7. Conclusions.

Through a study of three different laser structrues, carrier transport and longitudinal mode spatial hole-burning have been isolated from carrier heating, carrier carrier scattering, and spectral hole-burning. Such gain nonlinearity has been shown to limit peak acheivable powers, broaden the pulses, and lead to a pronounced asymmetry in the optical spectrum. The importance of carrier transport effects has been hihglighted through this assessment.

Damping due to carrier transport has been shown to be characterised by two time constants, carrier diffusion (40ps), and thermionic emission (80ps). These time constants are in good agreement with the published work on small signal simulation. Without the carrier transport model, the nonlinear gain coefficient must be enhanced to $5x10^{-17}cm^3$ to for any agreement between experiment and theory. Agreement is however limited, and the nonlinear gain parameter is unable to give any physical insight into device limitations.

4.8 References.

1. WHITEAWAY, J.E.A., WRIGHT, A.P., GARRETT, B., THOMPSON, G.H.B., CARROLL, J.E., ZHANG, L.M., TSANG, C.F., WHITE, I.H., and WILLIAMS, K.A., "Detailed large-signal dynamic modelling of DFB laser structures and comparison with experiment", Optical and Quantum Electronics, 26, S817-S842, 1994.

2. KINOSHITA, J.I., and MATSUMOTO, K., "Yield analysis of SLM DFB lasers with an axially flattened internal field", IEEE Journal of Quantum Electronics, 25, 1324-1332, 1989.

3. WHITEAWAY, J.E.A., GARRETT, B., THOMPSON, G.H.B., COLLAR, A.J., ARMISTEAD, C.J., and FICE, M.J., "The static and dynamic characteristics of single and multiple phase shifted DFB laser structures", IEEE Journal of Quantum Electronics, 28, 1277-1293, 1992.

4. BOWERS, J.E., KOCH, T.L., HEMENWAY, B.R., WILT, D.P., BRIDGES, T.J., and BURKHARDT, E.G., "High frequency modulation of 1.52 μm vapour-phase transported InGaAsP laser", Electronics Letters, 21, 297-299, 1985.

5. AGRAWAL, G.P., "Modulation bandwidth of high power single-mode semiconductor lasers : Effect of intraband gain saturation", Applied Physics Letters, 48, 613-615, 1986.

6. YAMADA, M., ISHIGURO, H., and NAGATO, H., "Estimation of the intraband relaxation time in undoped AlGaAs injection laser", Japanese Journal of Applied Physics, 19, 135-142, 1980.

7. ISHIKAWA, H., IMAI, H., TANAHASHI, J., and TAKUSAGAWA, M., "Longitudinal mode behaviour of transverse mode stabilized InGaAsP/InP double heterostructure laser", Applied Physics Letters, 38, 962-964, 1981.

8. YAMANISHI, M., SUEMUNE, I., NONONURA, K., and MIKOSHIBA, N., "Hole burnings observed at high energy tails in spontaneous emission spectra from 1.3 μm InGaAsP/InP double heterostructure lasers", Japanese Journal of Applied Physics, 21, L240-L242, 1982.

9. WILLATZEN, M., USKOV, A., MORK, J., OLESON, H., TROMBERG, B., and JANHO, A.P., "Nonlinear gain suppression in semiconductor lasers due to carrier heating", IEEE Photonics Technology Letters, 3, 606-609, 1991.

10 BLOOD, P., COLAK, S., and KUCHARSKA, A.I., "Influence of broadening and high injection effects on GaAs/AlGaAs quantum well lasers", IEEE Journal of Quantum Electronics, 23, 969-976, 1987.

11. GOMATAM, B., DEFONZO, A.P., "Theory of hot carrier effects on the nonlinear gain in GaAs-AlGaAs lasers and amplifiers", IEEE Journal of Quantum Electronics, 26, 1689-1704, 1990.

12. ADAMS, M.J., and OSINSKI, M., "Influence of spectral hole-burning on quaternary laser transients", Electronics Letters, 19, 628-628, 1983.

13. FRANKENBERGER, R., and SCHIMPE, R., "Origin of nonlinear gain in index-guided InGaAsP laser diodes", Applied Physics Letters, 60, 2720-2722, 1992.

14. WILLATZEN, M., TAKAHASHI, T., and ARAKAWA, Y., "Nonlinear gain effects due to carrier heating and spectral hole burning in strained quantum well lasers", IEEE Photonics Technology Letters, 4, 682-684, 1992.

15. THOMPSON, G.H.B., Physics of Semiconductor Laser Devices, Wiley, Chichester, 1980.

16. TUCKER, R.S., and POPE, D.J., "Circuit modeling of the effect of diffusion on damping in a narrow-stripe semiconductor laser", IEEE Journal of Quantum Electronics, 19, 1179-1183, 1983.

17. ARAKAWA, Y., and YARIV, A., "Theory of gain, modulation response, and spectral linewidth in AlGaAs quantum well lasers", IEEE Journal of Quantum Electronics, 21, 1666-1674, 1985.

18. SUEMUNE, I., COLDREN, L.A., YAMANISHI, M., and NAKAMURA, M., "Extremely wide modulation bandwidth in a low threshold current strained quantum well laser", Applied Physics Letters, 53, 1378-1380, 1988.

19. HIRAYAMA, Y., MORINGA, M., SUZUKI, N., and NAKAMURA, M., "Extremely reduced nonlinear K-factor in high-speed strained layer multiquantum well DFB lasers", Electronics Letters, 27, 875-876, 1991.

20. LEALMAN, L.F., BAGLEY, M., COOPER, D.M., FLETCHER, N., HARLO, M., PERRIN, S.D., WALLING, R.H., and WESTBROOK, L.D., "Wide bandwidth multiple quantum well 1.55 μm lasers", Electronics Letters, 27, 1191-1193, 1991.

20. BOWERS, J.E., KOREN, U., MILLER, B.I., SOCHOLICH, C., and JAN, W.Y., "High speed polymide-based semi-insulating planar buried heterostructure", Electronics Letters, 23, 1263-1265, 1987.

21. MELAND, E., HOLMSTROM, R., SCHLAFER, J., LAUER, R.B., and POWAZINIK, W., "Extremely high frequency (24 GHz) InGaAsP diode lasers with excellent modulation frequency", Electronics Letters, 26, 1827-1829, 1990.

22. SHARFIN, W.F., SCHLAFER, J., RIDEOUT, W., ELMAN, B., LAUER, R.B., LACOURSE, J., and CRAWFORD, F.D., "Anomalously high damping in strained InGaAs-GaAs single quantum well laser", IEEE Photonics Technology Letters, 3, 193-195, 1991.

23. TATHAM, M.C., LEALMAN, I.F., SELTZER, C.P., WESTBROOK, L.D., and COOPER, D.M., "Resonance frequency, damping and differential gain in 1.5 μ m multiple quantum well lasers", IEEE Journal of Quantum Electronics, 28, 408-414, 1992.

24. SOGAWA, T., and ARAKAWA, Y., "Picosecond lasing dynamics of gain-switched quantum well lasers and its dependance on quantum well structures", IEEE Journal of Quantum Electronics, 27, 1648-1654, 1991.

25. EISENSTEIN, G., WIESENFELD, J.M., WEGENER, M., SUCHA, G., CHEMLA, D.S., WEISS, S., RAYBON, G., and KOREN, U., "Ultrafast gain dynamics in 1.5 μm multiple quantum well optical amplifiers", Applied Physics Letters, 58, 158-160, 1991.

26. WEISS, S., WEISENFELD, J.M., CHELMA, D.S., RAYBON, G., SUCHA, G., WEGENER, M., EISENSTEIN, G., BURRUS, C.A., DENTAI, A.G., KOREN, U., MILLER, B.I., TEMKIN, H., LOGAN, R.A., and TANBUN-EK, T., "Carrier capture times in 1.5 μm multiple quantum well optical amplifiers", Applied Physics Letters, 60, 9-11, 1992.

27. SHARFIN, W.F., RIDEOUT, W., KOTELES, E., SCHLAFER, J., ELMAN, B., VASSELL, M., CRAWFORD, D., BENOIT, J., BROSSON, P., and FERNIER, B., "Effect of carrier transport on modulation bandwidth of quantum well lasers", proceedings ECOC, Paper TuA4-4, Paris, 1991.

28. RIDEOUT, W., SHARFIN, W.F., KOTELES, E.S., VASSELL, M.O., and ELMAN, B., "Well-Barrier Hole Burning in Quantum Well Lasers", IEEE Photonics Technology Letters, 3, 784-786, 1991.

29. NAGARAJAN, R., FUKUSHIMA, T., ISHIKAWA, M., BOWERS, J.E., GEELS, R.S., and COLDREN, L.A., "Transport limits in High Speed Quantum-Well Lasers: Experiment and Theory", IEEE Photonics Technology Letters, 4, 121-123, 1992.

30. GRABMAIER, A., HANGLEITER, A., SCHÖFTHALER, M., KAZMIERSKI, C., BLEZ, M., and OUGAZZADEN, A., "Carrier transport limited bandwidth of 1.55 μm quantum well lasers", proceedings ECOC, paper MoB3.4, Berlin, 1992.

31. WRIGHT, A.P., GARRETT, B., THOMPSON, G.H.B., and WHITEAWAY, J.E.A., "Influence of carrier transport on wavelength chirp of InGaAs/InGaAsP MQW laser", Electronics Letters, 26, 1911-1913, 1992.

32. ISHIKAWA, M., NAGARAJAN, R., FUKUSHIMA, T., WASSERBAUER, J.G., and BOWERS, J.E., "Long wavelength high speed semiconductor lasers with carrier transport effects", IEEE Journal of Quantum Electronics, 28, 2230-2241, 1992.

33. NAGARJAN, R., ISHIKAWA, M., FUKUSHIMA, T., GEELS, R.S., and BOWERS, J.E., "High speed quantum well lasers and carrier transport effects", IEEE Journal of Quantum Electronics, 28, 408-414, 1992.

34. SHARFIN, W.F., RIDEOUT, W., and VASSELL, M.O., "The effect of well-barrier hole burning on the dynamic response of quantum well lasers", proceedings SPIE 1634, 104-109, 1992.

35. NAGARAJAN, R., ISHIKAWA, M., FUKUSHIMA, T., GEELS, R.S., and BOWERS, J.E., "Carrier transport effects in high speed quantum-well lasers", proceedings SPIE 1634, 119-126, 1992.

36. GARRETT, B., THOMPSON, G.H.B., WRIGHT, A.P., QUINLAN, S., WHITEAWAY, J.E.A., RASHID, A., WHITE, I.H., "Chirp and dynamics of multiple quantum well, multiple phase jump distributed feedback lasers", ECOC, paper TuP1.4, Berlin, 1992.

37. EISENSTEIN, G., WIESENFELD, J.M., WEGENER, M., SUCHA, G., CHEMLA, D.S., WEISS, S., "Ultrafast gain dynamics in 1.5 μm multiple quantum well optical amplifiers", Applied Physics Letters, 58, 158-160, 1991.

38. MORIN, S., DEVEAUD, B., CLEROT, F., FUJIWARA, K., MITSUNAGA, K., "Capture of photoexcited carriers in a single quantum well with different confinement structures", IEEE Journal of Quantum Electronics, 27, 1669-1675, 1991.

39. NAGARAJAN, R., FUKUSHIMA, T., CORZINE, S.W., BOWERS, J.E., "Effects of carrier transport on high-speed quantum well lasers", Applied Physics Letters, 59, 158-160, 1991.

40. WHITEAWAY, J.E.A., THOMPSON, G.H.B., COLLAR, A.J., and ARMISTEAD, C.J., "The design and assessment of λ/4 phase-shifted DFB laser structures", IEEE Journal of Quantum Electronics, 25, 1261-1279, 1989.

41. GARRETT, B., Details on an approximate solution to longitudinal mode spatial hole burning in a λ/4 phase shifted distributed feedback laser, private communication.

TIMING JITTER IN FORCED Q-SWITCHING

The stability of actively Q-switched multicontact lasers is assessed in detail for the first time. Picosecond pulses are generated with improved repetition rate flexibility and enhanced pulse energies over mode-locking. Reduced timing jitter and enhanced peak powers are achieved when compared to gain-switching.

5.1 Outline.

An assessment of the pulse train noise performance is carried out for forced Q-switched diode lasers for the first time. Simultaneous measurement of pulse profile, energy and spectral performance identifies optimum electrical bias conditions. Forced Q-switching is demonstrated to allow superior picosecond pulse generation with high optical peak powers of up to 100mW and 350mW at Gigahertz repetition rates in InGaAsP and GaAs lasers respectively. Subpicosecond (0.9ps) timing jitter is measured for InGaAsP multiquantum well Fabry-Perot lasers operating at 2GHz repetition rates. Increased microwave modulation power levels and frequency are both noted to improve timing jitter. An optimum modulation power level is however observed and a degradation in the noise performance is noted with increased levels of reverse bias on the absorber contact. Increased current to the gain sections enhances pulse energies and leads to reduced jitter, although ultimately nonlinear gain suppression results in pulse asymmetry and tail formation.

With improved levels of spontaneous coupling into the lasing modes, Fabry-Perot lasers are noted to offer reduced timing jitter when compared with

distributed feedback lasers. Differences between bulk and quantum well lasers are noted in terms of gain suppression for InGaAsP and GaAs lasers. Peak powers are limited, pulse durations broadened and relaxation oscillations are damped. GaAs lasers generate pulse energies three times as high as for the InGaAsP devices in 20ps duration, 350mW peak power pulses. Optimum timing jitter is 3ps and significantly larger than for InGaAsP lasers. Amplitude noise characterising fluctuations in the pulse intensity profile is enhanced as a result of the reduced nonlinear gain suppression. This in turn is expected to couple through to phase noise as a result of perturbations to the carrier density dependant refractive index.

Optical feedback and seeding techniques allow significant improvements in spectral and temporal profiles. By seeding a gain-switched laser with light from a second single frequency CW diode laser, the timing jitter is reduced from 22ps to 2.5ps. The highly symmetric pulses are transform limited. Such spectral narrowing is not observed for seeded Q-switched lasers. Q-switched operation in an external grating cavity is however considered. The tuning characteristics and the spectral narrowing is investigated. It is observed however, that for near transform limited pulse generation, the linear chirp characteristic of highly symmetric Q-switched pulses should be appropriate for high levels of pulse compression with appropriate dispersion sign fibre as detailed in chapter 1. It is therefore more realistic to generate high power pulses with a linear spectral chirp with a high degree of pulse profile symmetry.

5.2 Noise in Picosecond Pulsed Laser Diodes.

As potential applications for high repetition rate picosecond pulses are explored, it becomes increasingly apparent that pulse to pulse amplitude and repetition rate fluctuations limit performance in diode lasers. The stability of gain-switching in diode lasers is well documented [1-7]. The noise initiated pulsation from spontaneous emission leads to a random turn-on time described hereon as timing jitter. As the spontaneous emission levels in a gain-switched laser increase with increasing current the timing jitter reduces. Figure 5.1 illustrates such jitter reduction with bias for one monomode distributed feedback laser and one multimode Fabry-Perot laser as measured in a study by Weber and coworkers [5]. Reduced levels of spontaneous coupling into just one lasing mode lead to the increased jitter for the distributed feedback laser.

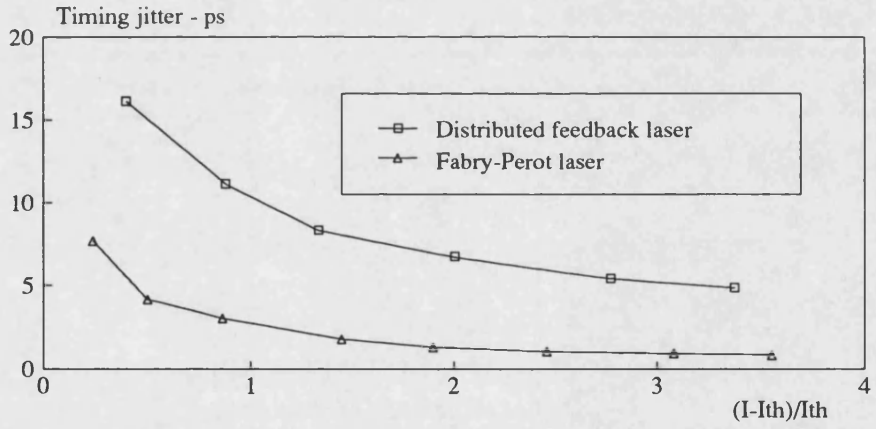

Figure 5.1 : Timing jitter in single mode and multimode gain-switched lasers for varied bias conditions. After Weber and coworkers [5].

In the work by Weber and coworkers, the laser is biased with 10ns electrical pulses at 50kHz. No data is given on the pulse profile, although a tail is likely with such high current long duration electrical pulses. Pulse shape is expected to degrade for lasers biased high above threshold, as observed for the gain-switching work in chapter 4. It is therefore instructive to simultaneously consider the timing jitter and pulse temporal and spectral performance.

Such pulse profile limitations have been overcome for gain-switched distributed feedback lasers in a study by Jinno [6]. The lasers are DC biased at three to four times threshold with a superimposed 5GHz microwave modulation. The pulses are subsequently filtered to remove the nonlinear chirp and the linearly chirped pulse is compressed to ensure a tail free pulse profile. Subpicosecond jitter is therefore allowed without pulse distortion. Timing jitter is plotted as a function of the bias conditions in figure 5.2.

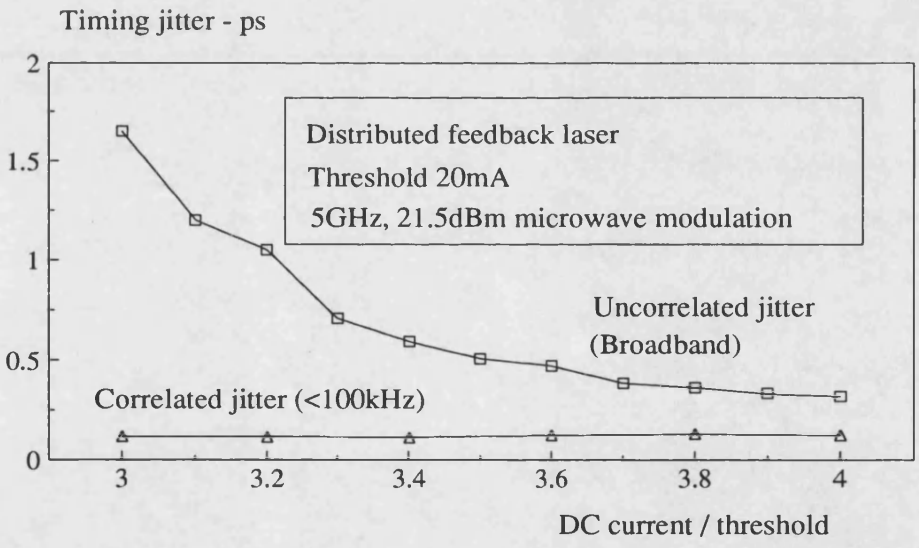

Figure 5.2 : Timing jitter for gain-switched distributed feedback lasers at 5GHz after filtering and compression. After Jinno [6].

The picosecond pulse train with down to 0.5ps jitter at 5GHz is tail-free irrespective of bias condition as the nonlinear chirp characteristic of pulse tails is removed with a 1nm width optical bandpass filter. The pulse compression itself is not expected to effect the measured timing jitter [7], as the wavelength at pulse turn on is not expected to change. The implication that timing jitter is lower at the higher repetition rates warrants a more through experimental investigation.

Two different measurement schemes are used in the work by Weber and coworkers [5] and Jinno [6]. While Weber and coworkers implement a direct time domain assessment using a digital sampling oscilloscope in a multichannel analyser configuration, Jinno considers phase noise in the frequency domain, and subsequently Fourier transforms to the time domain [9]. The indirect measurement approach used by Jinno is more attractive in that it is neither bandwidth limiting nor trigger dependant [10]. The spectral technique also allows discrimination between low level jitter correlated to the electrical drive, and laser dependant jitter uncorrelated to the drive. Figure 5.2 indicates that while uncorrelated jitter may be reduced through an increase in DC bias current, correlated jitter is largely bias independent.

5.3 Timing Jitter Calculation in the Frequency Domain.

The availability of wide bandwidth electrical spectrum analysers with low resolution bandwidth and large dynamic range has allowed the calculation of jitter using data from the frequency domain to become widespread. It is instructive therefore to consider timing jitter in the frequency domain as a variation in the repetition rate. Such fluctuation is characterised by phase noise

bands at the fundamental and its harmonics in the photocurrent microwave spectrum of an illuminated wide bandwidth photodetector. An schematic for the microwave spectrum is given in figure 5.3.

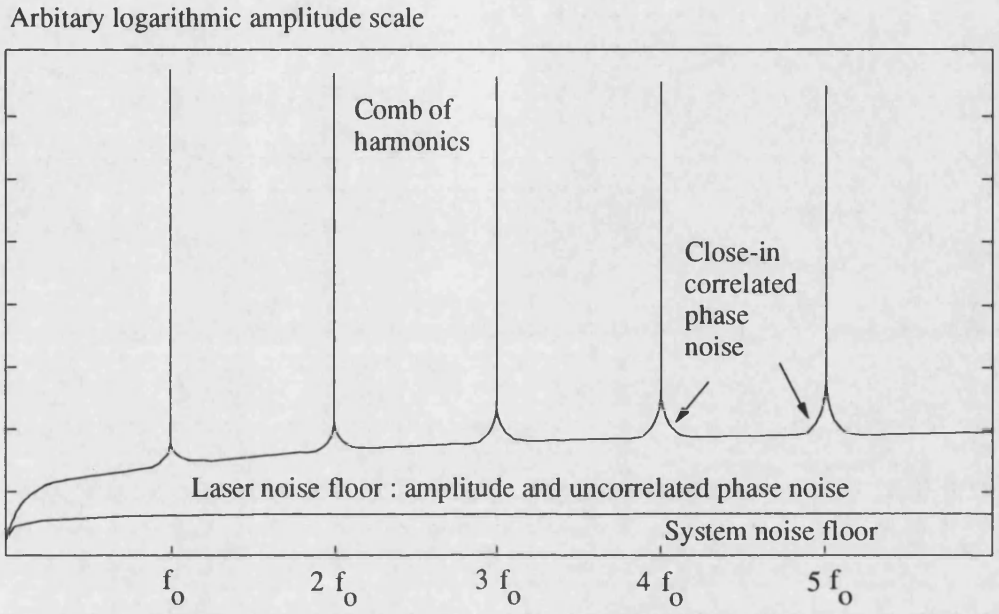

Figure 5.3 : Schematic for the microwave spectrum of an optical pulse train showing the noise distribution as would be measured on a spectrum analyser. Close-in correlated phase noise is present at the fundamental f_o and each harmonic n, increasing in magnitude by n^2. Uncorrelated jitter also increases with n^2, but is uniformly distributed with the nonvariant amplitude noise.

In the generalised context of microwave sources where no discrete electrical phase changes are anticipated, fluctuations are correlated to the nominal carrier frequency. The resulting cumulative build up of jitter over several modulation periods results in higher levels of long term jitter. When considered in the

reciprocal frequency domain this leads to higher levels of phase noise close in to the combs which rapidly fall off with increased frequency offset from the combs. Picosecond pulsed laser diodes therefore mimic this electrical output directly as well as adding their own noise as shown in figure 5.3. Additional to the correlated jitter there is a broadband noise uncorrelated to the modulation resulting from the random spontaneous emission dependant turn on time.

An infinitely long train of Gaussian pulses $P(t)$ with amplitude and phase noise is described in equation 5.1. A power level of P_o, pulse duration σ_t and period T are used with pulse intensity and timing fluctuations being described through the noise terms $N(t)$ and $J(t)$ respectively. The root mean square timing jitter σ_j represents the standard deviation of $J(t)$ [14].

$$P(t) = P_o(1+N(t))T\sum_{n=-\infty}^{n=+\infty}\frac{1}{\sqrt{2\pi}\sigma_t}\exp\left\{-\frac{t-nT-J(t)^2}{2\sigma_t^2}\right\} \qquad 5.1$$

The power spectral density can be approximated with the Fourier transform of $P(t)$ taken as far as the second order in $n\omega_o^2\sigma_j$:

$$\begin{aligned} S(\omega) = P_{ave}^2 e^{-\omega^2\sigma_t^2}\sum_{n=+\infty}^{n=-\infty} & (1-n^2\omega_o^2\sigma_j^2)2\pi\delta(\omega-n\omega_o)+ \\ & (1-n^2\omega_o^2\sigma_j^2)S_n(\omega-n\omega_o)+ \\ & n^2\omega_o^2 S_j(\omega-n\omega_o) \end{aligned} \qquad 5.2$$

The three components of the spectral intensity function represent firstly the sequence of delta functions harmonically related to the modulation frequency of the pulse train, secondly the amplitude noise between the delta functions, and finally the phase noise sidebands around the delta functions. The phase noise is noted to increase with the square of the harmonic number n. As such the phase noise is readily extracted if amplitude noise and system noise floor are assumed nonvariant across the considered frequency range. Noise sidebands

at a harmonic are subtracted from the fundamental frequency sidebands to give the phase noise sidebands L_j as a function of offset frequency f as illustrated in figure 5.5 for a forced Q-switched distributed feedback laser (laser number [5]).

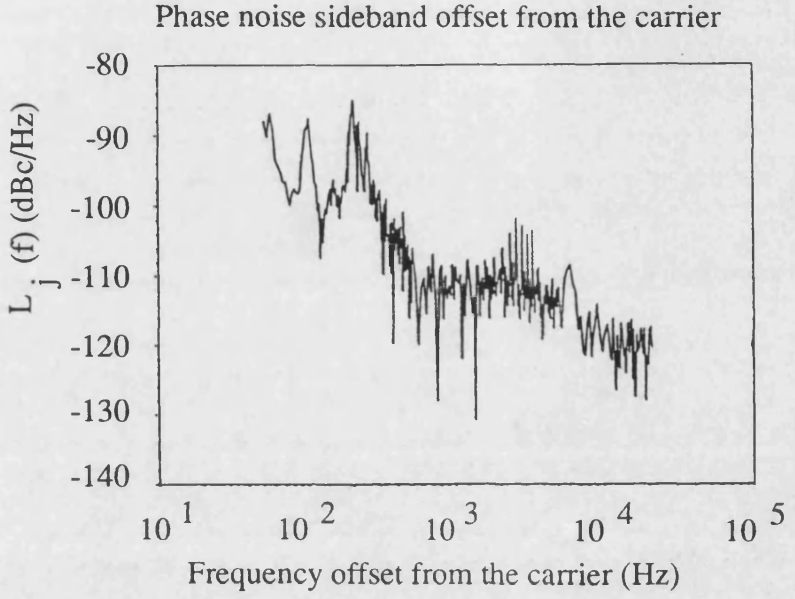

Figure 5.4 : Phase noise sidebands indicating close in correlated timing jitter. Above 10kHz the phase noise sidebands decrease sufficiently to be buried in the measurement system noise floor. Values of correlated noise in higher bands are insignificant.

Using a spectrum analyser, such a measurement is carried out by considering the power in the sidebands relative to the carrier in both the fundamental and one harmonic in a 1Hz bandwidth. Linearising and subtracting

the noise side bands at the fundamental from the noise sidebands at the harmonic gives the phase noise sideband $L_j(f)$ in figure 5.4 in decibels below the carrier level in a one Hertz bandwidth (dBc/Hz) :

$$L_j(f) = 10\log_{10}\left\{10^{\frac{L_n(f)}{10}} - 10^{\frac{L_1(f)}{10}}\right\} \qquad 5.3$$

The correlated timing jitter is measured by integrating over the measured frequency offset limits f_l to f_h, and is often in quoted decade bands:

$$\sigma_j(f_l,f_h) = \frac{1}{\sqrt{2}\pi f_o}\sqrt{\int_{f_l}^{f_h}\frac{10^{\frac{L_j(f)}{10}}df}{n^2-1}} \qquad 5.4$$

As each harmonic band has a given intensity, an increase in the phase noise results in a decreased peak level for the delta function and an effective change in the noise level relative to the carrier. This leads to overestimation of jitter for highly unstable pulse trains. For the short pulsed operation of diode lasers, it is widely reported that correlated timing jitter follows the electrical source closely for mode-locking [8,11-15], gain-switching [15-17] and Q-switching [17-18].

Jitter uncorrelated to the modulation can have a more considerable contribution to the total timing jitter however in gain-switching as indicated for the distributed feedback laser in figure 5.2. Uncorrelated phase noise does not vary significantly with frequency offset although it increases with absolute frequency in a manner described for correlated jitter and as shown schematically in figure 5.3. The discrimination between correlated and uncorrelated jitter is useful in terms of identifying noise sources and inevitable in terms of experimental measurement. Uncorrelated jitter is particularly significant in lasers where pulse turn-on relies solely on the build up of spontaneous emission. As no pulse to pulse phase memory is retained discrete phase changes result in

the wideband noise. The measurement and calculation of uncorrelated jitter remains the same as for correlated jitter [9] although now the complete spectrum is considered with a larger measurement system resolution bandwidth.

5.4 Diagnostics and Experiment.

The measurements made in this chapter were all made at the Department of Physics and Astronomy at the University of St Andrews. The author is very grateful for the assistance received during the experiments, which were carried during a number of visits throughout the course of this work. The use of the synchroscan streak camera system for the high temporal resolution pulse profile measurements, the high dynamic range, low resolution bandwidth electrical spectrum analyser and the low phase noise microwave source available at St Andrews have been invaluable.

The experimental arrangement is summarised schematically in figure 5.5. A low phase noise MG3633A Anritsu synthesized signal generator (-140dBc at 20kHz offset) is used to drive the lasers and the Streak camera. In the synchroscan Streak camera used, the sweeping voltage to the deflector plates has a sinusoidal form. The use of resonant circuits in the camera to generate the high voltage needed for the plates also requires that the detected signal be locked to a harmonic of 80MHz. Optical pulse trains at 650MHz and 1300MHz repetition rates are therefore assessed with the Streak camera. A temporal resolution is measured to be 5ps, by removing the modulation and measuring the full width at half maximum of the static image. Details on the operation of Streak cameras are given in section 3.7.

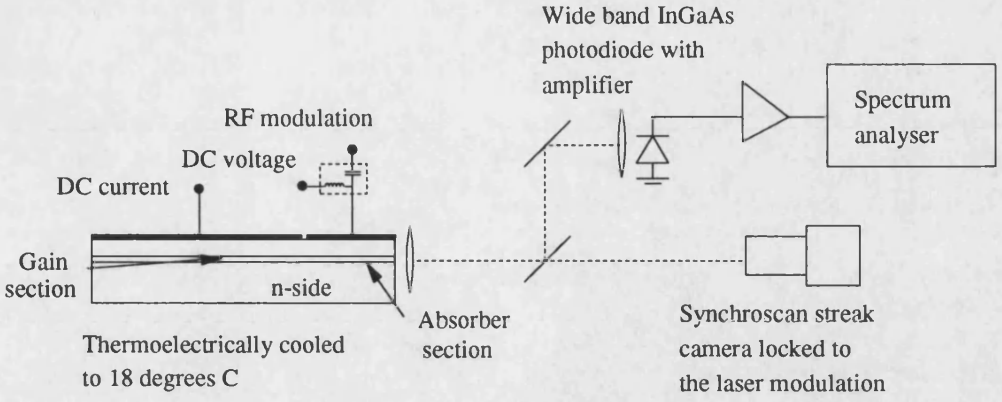

Figure 5.5: The experimental arrangment for the temporal characterisation of Q-switched optical pulse trains.

The timing jitter is calculated from phase noise measurements using a photodetector and electrical spectrum analyser configuration. The InGaAs PIN photodetector has a 8GHz bandwidth and the resultant electrical power spectrum is assessed using an HP70001A spectrum analyser. The need for preamplification to the spectrum analyser limits the overall system detection bandwidth to 4.2GHz. Care is taken to avoid contributions from the system noise floor by firstly amplifying the detected optical signal, and when necessary, by deconvolving the noise floor. A variable optical attenuator prevents saturation at the photodetector. Using a sampling oscilloscope to monitor pulse profile, the phase noise is also measured for 1900MHz modulation allowing assessment of jitter as a function of repetition rate. A scanning Fabry-Perot interferometer and monochromator enable full characterisation of the optical spectrum. Lasers are thermoelectrically cooled to 20°C ± 0.1°C.

The forced Q-switching of multicontact structures involves the application of a strong forward DC bias to the longer gain section. A subthreshold bias with low phase noise high power microwave signal is applied to the shorter absorber

section. Low phase noise content in the microwave signal is essential for low correlated jitter performance. A 47Ω surface mount resistor provides impedance matching. Introducing a directional coupler into the drive circuit indicates that reflections from the load were 13dB below the input power level under the conditions considered.

5.5 Electrical Bias Optimisation for Bulk InGaAsP Laser.

For optimum low jitter Q-switched operation in multisection lasers a temporal and spectral characterisation is simultaneously carried out to determine acceptable operating ranges. A bulk active layer InGaAsP distributed feedback laser with a 200μm absorber in a 400μm cavity is initially assessed and the monomode operation allows comprehensive spectral assessment. The laser[4] is described in further detail in appendix A. The performance is characterised for a variety of bias conditions in terms of pulse duration, energy and jitter. Figure 5.5 shows pulse profile dependence on gain section DC current. A forward bias of 1V is applied to the absorber along with 28dBm, 1300MHz microwave modulation. For gain bias close to the 30mA threshold symmetric tail free pulses are readily generated. At twice threshold however a tail begins to form. Spectra indicate increasing levels of nonlinear chirp associated with tail formation. Nonlinear gain suppression prevents sufficient gain depletion during the front of the Q-switched picosecond pulse. No relaxation oscillations are observed in the damped tails.

The dependence of pulse parameters such as duration, energy, and timing jitter on gain section DC bias conditions are outlined in figure 5.6. The correlated timing jitter has been shown to be bias independent and negligible using the

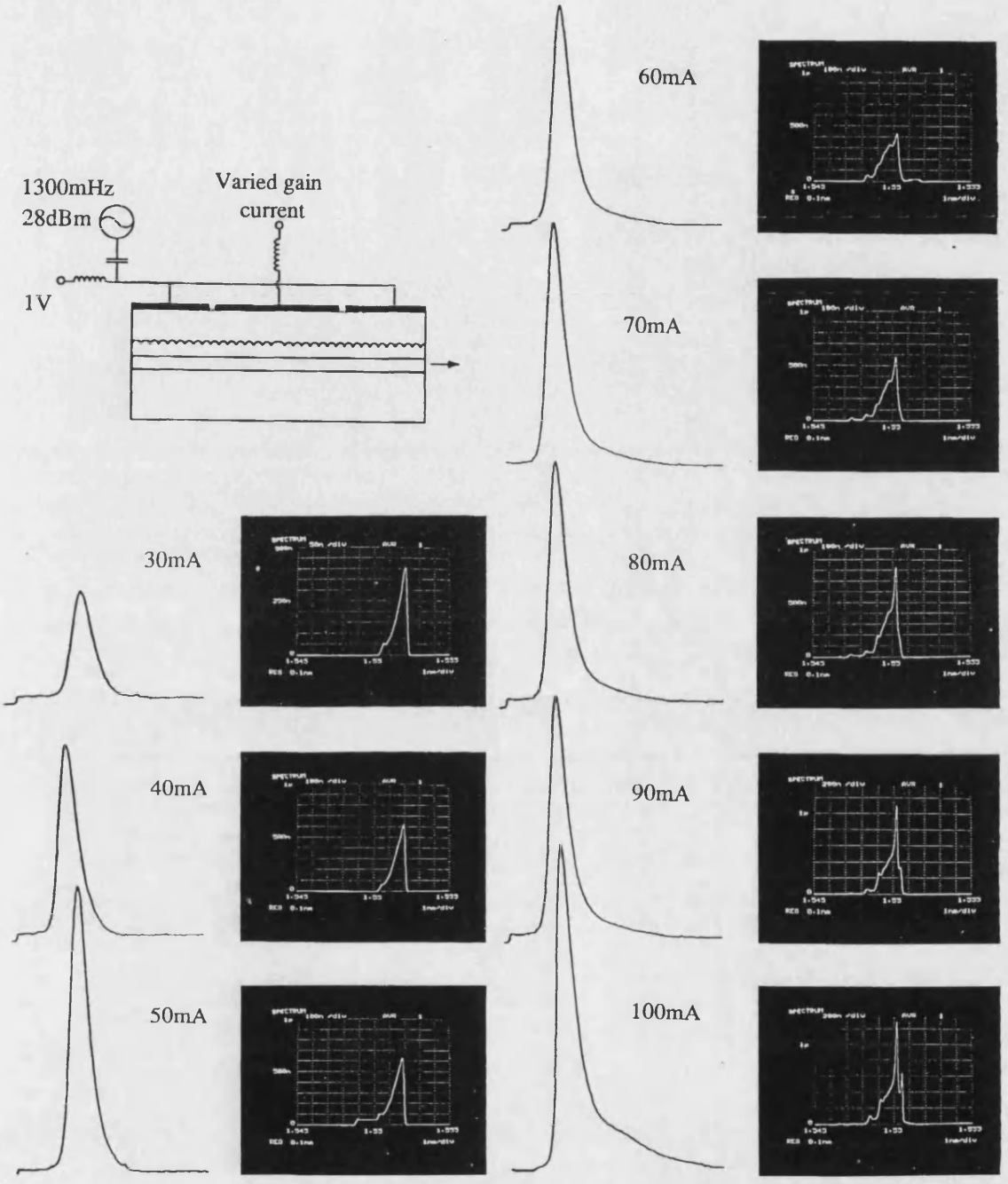

Figure 5.6: Temporal and spectral performance of a forced Q-switched bulk quarter wavelength phase shifted distributed feedback laser for varied gain section DC bias.

available low phase noise source. Values of 65fs are measured for the 50-500Hz range, and 35fs for the range 0.5-5kHz. Uncorrelated jitter is however identified as being significantly larger for Q-switched lasers, and is therefore quoted.

The dependence of pulse profiles on bias conditions is similar to gain-switching in that symmetric pulse profiles are readily achieved when the net cavity gain is low. Pulse profile degradation is not as rapid however as for gain-switching when the gain section bias is increased, and peak powers are considerably enhanced. While a tail at the rear of the pulse forms at the higher pumping conditions, this is readily removed by increasing the cavity saturable loss through either the DC voltage or microwave modulation power. Pulse durations decrease with the increased gain DC levels, although this plateaus out at around three times threshold. A linear increase in pulse energy with DC current does not therefore lead to a linear increase in peak power as a direct result of the gain saturation mechanisms outlined for gain-switching in chapter 4. Higher pulse energy and power levels are achieved as higher gain section currents are allowed through the loss modulation. Jitter initially decreases with increasing cavity gain as more spontaneous emission couples into the lasing modes. The jitter levels do however increase with DC bias after an optimum level is achieved. With high levels of gain being insufficiently depleted during the front pulse, long tails become associated with these pulses and interfere with subsequent pulses and lead to reduced stability at high bias conditions. An increase in absorption removes the tail, but also degrades the jitter performance. This occurs in a regime where pulse profiles are asymmetric with high energy tails and is therefore of little concern. Increased microwave levels allow faster rising edges and result in a higher spontaneous emission rate at pulse turn on. An optimum microwave level is noted however at 28dBm. At higher power

levels, too much absorption in the loss section for half the electrical period leads to degraded jitter performance. While pulse energies of up to 2pJ have been measured with pulse durations down to 28ps at 1300MHz, for the optimum 2.5ps timing jitter condition, 28ps duration, 1.5pJ energy pulses are measured as shown in figure 5.7.

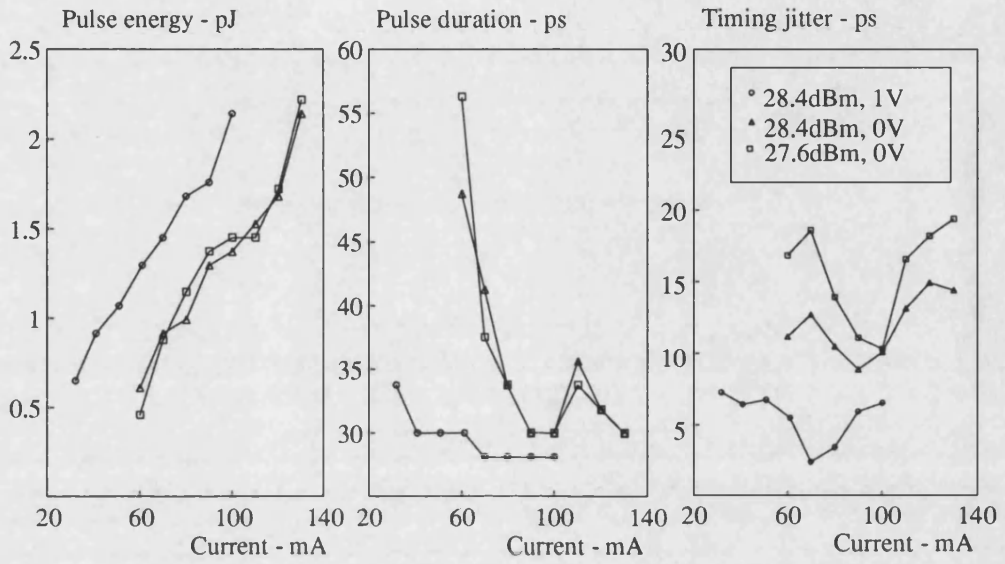

Figure 5.7 : Pulse duration, energy and jitter dependence on bias for a bulk distributed feedback laser.

5.6 Multimode Q-switching for Quantum Well InGaAsP Lasers.

The forced Q-switched performance of multiquantum well distributed feedback and Fabry-Perot lasers is considered to highlight the role of spontaneous coupling rates in jitter reduction. Five InGaAs wells with InGaAsP barriers form the active layers for the two lasers. The distributed feedback laser[5] has a central loss section of 200μm length in the 600μm cavity. Second order

gratings are used with a central $\lambda/4$ phase shift. Antireflection coatings of better than 0.1% are applied. The Fabry-Perot laser[6] contacts are configured to form a 100μm absorber at the output facet of a 400μm long cavity. No coatings are applied for the Fabry-Perot laser.

For optimum absorber conditions, the lasers are Q-switched for a range of gain DC bias currents. Measured jitter values are compared in figure 5.8. A subthreshold absorber DC forward bias of 0.5V with 28dBm microwave power at 1300MHz is used for both lasers.

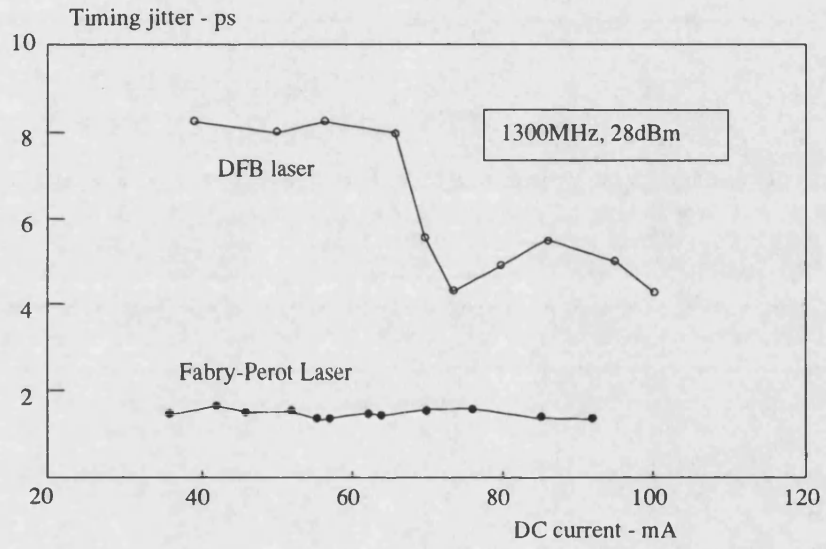

Figure 5.8 : Comparison of jitter performance of distributed feedback and Fabry-Perot lasers for varied gain section DC bias.

For otherwise optimised bias conditions, a reduction in timing jitter with increasing DC gain section bias is observed for the distributed feedback laser. Higher levels of spontaneous emission coupling into the lasing mode prior to pulse turn on is expected to account for the reduced jitter. The enhanced stability of Fabry-Perot lasers is similarly expected to result from more efficient

spontaneous emission coupling prior to pulse turn on. Here though the multimoded operation allows the reduced jitter.

Pulses with durations from 25-30ps are readily generated over a wide range of bias conditions with pulse energies from 1pJ to in excess of 2pJ. Measurements at 650MHz indicate a floor to the jitter at 1.9ps. Increasing the repetition rate to 1300MHz indicates a second floor at 1.4ps, almost irrespective of bias conditions, as long as the absorber section is not reverse biased. The dependence of timing jitter on modulation frequency is considered for the Fabry-Perot laser in figure 5.9.

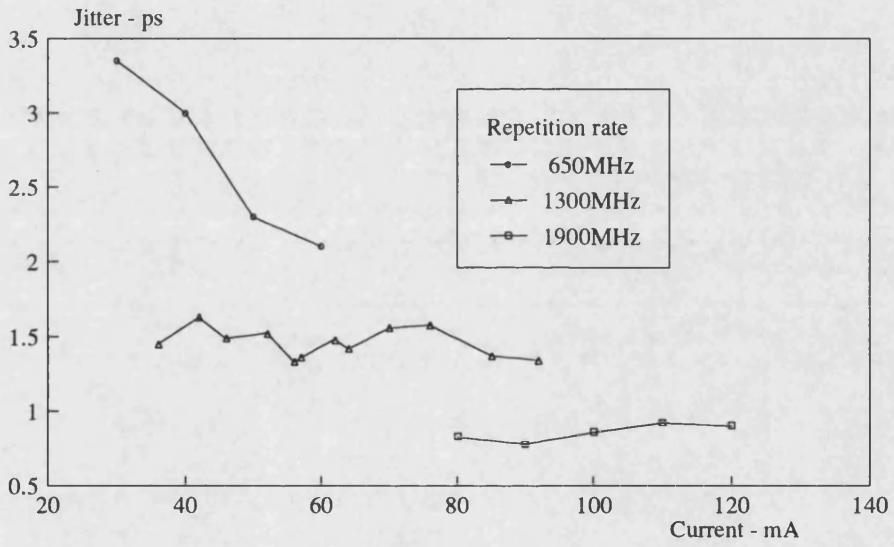

Figure 5.9 : Jitter as a function of gain section bias for Fabry-Perot lasers at three modulation frequencies showing reduced jitter at higher repetition rates. Data is given for tail-free operation.

Tail-free operation is maintained with 0.9ps timing jitter at a repetition rate of 1900MHz. An almost linear decrease in timing jitter with increasing repetition rate is noted for similar modulation power levels without significant pulse

energy deterioration. This is thought to be a direct consequence of the steepening electrical transient at optical turn-on. Lower gain biases are required at lower repetition rates to maintain tail-free pulses. With the noise floor at -132dBc/Hz at the second harmonic, a system limit of 0.2ps is estimated [9].

5.7 Bulk and Quantum Well Gallium Arsenide Lasers.

Fabry-Perot GaAs lasers of differing contact arrangements are assessed to optimise peak powers under forced Q-switched operation[1]. Comparisons are made between bulk active layer[7-9] and dual quantum well lasers[10-11] and between the forced Q-switching so far described in sections 3.5,5.5 and 5.6, and the self Q-switching described 3.5.

Initially a bulk active layer device[7] with an absorber length of 75μm in a 240μm cavity is assessed. Pulse profiles are recorded for varied bias conditions in figure 5.10 and compared with the profiles of an otherwise similar dual quantum well laser[10] in figure 5.10. The short durations and symmetry indicate significant reduction in gain nonlinearity for bulk GaAs lasers when compared with either bulk or multiquantum well InGaAsP and dual quantum well GaAs lasers. The onset of a satellite pulse at higher gain section DC bias conditions is an example of the reduced nonlinear gain suppression. Such subsequent pulsation might be avoided at higher modulation power levels and frequencies. Optical pulse energies and timing jitter deteriorate however with excess microwave power. Spectra are broadly chirped and multimode with a typical full width at half maximum of 3nm.

---

1 Lasers fabricated at University of Bath, Department of Electrical Engineering from material grown at University of Sheffield, III-V facility.

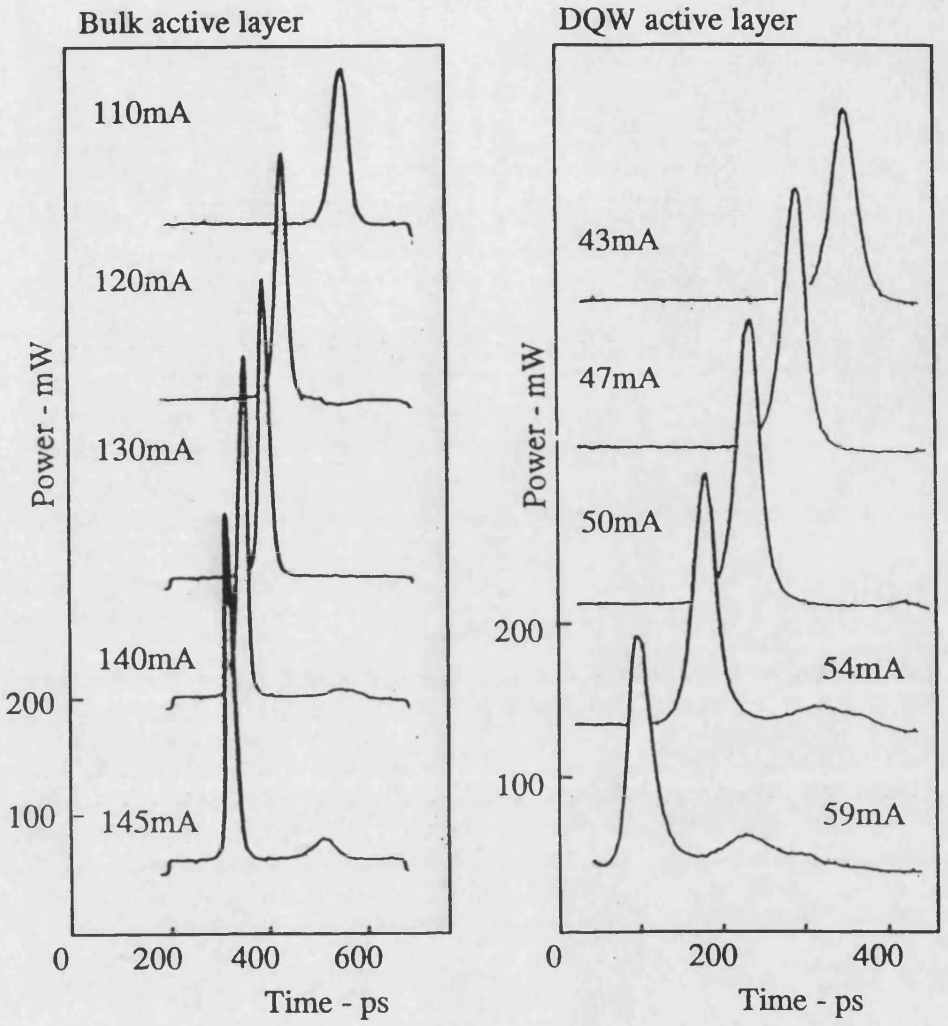

Figure 5.10 : Optical pulse profile variation with gain section DC bias for bulk and dual quantum well GaAs lasers. The time axis scale is different for the two sets of data.

A reduction of pulse duration with increased DC gain bias is in agreement with the trends for InGaAsP lasers, although the 20ps duration pulses are consistently shorter. The higher achievable gains before optical turn on and reduced photon dependent saturation effects in bulk lasers leads to faster turn on and hence gain depletion and pulse turn off. At higher gain currents satellite pulses result from excess gain or premature pulse turn on. Pulse energies of up to 7pJ are readily measured at 650 and 1300MHz. While timing jitter is limited to 5ps at 650MHz (figure 5.11) a reduction to 3ps is noted at 1300MHz modulation, as indicated in figure 5.12. The reduced gain suppression is expected to lead to larger variation in peak power. This increased amplitude noise is expected to lead to increased phase noise through cavity refractive index modulation.

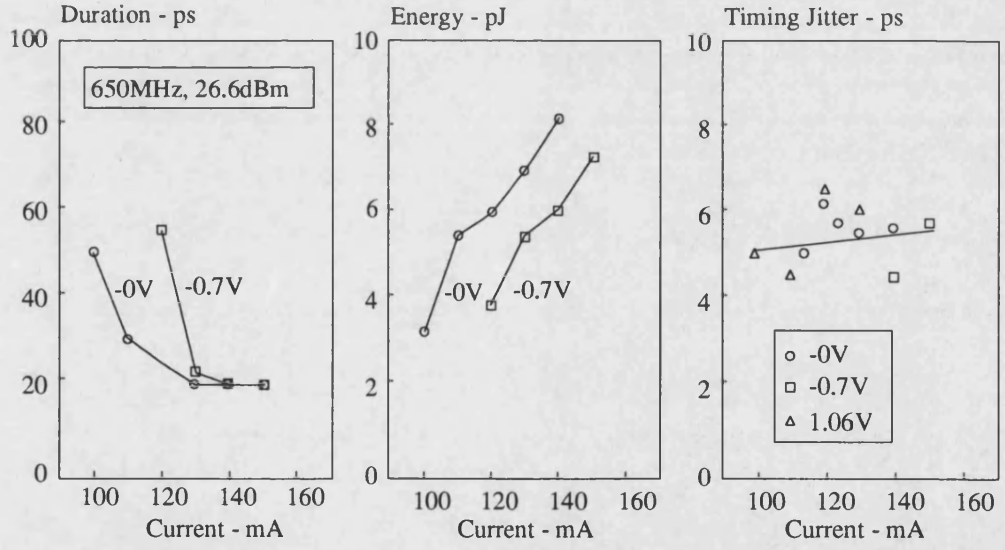

Figure 5.11 : Optical pulse parameters as a function of bias condition for bulk GaAs laser with overall length to absorber ratio of 5:1 for 650MHz modulation.

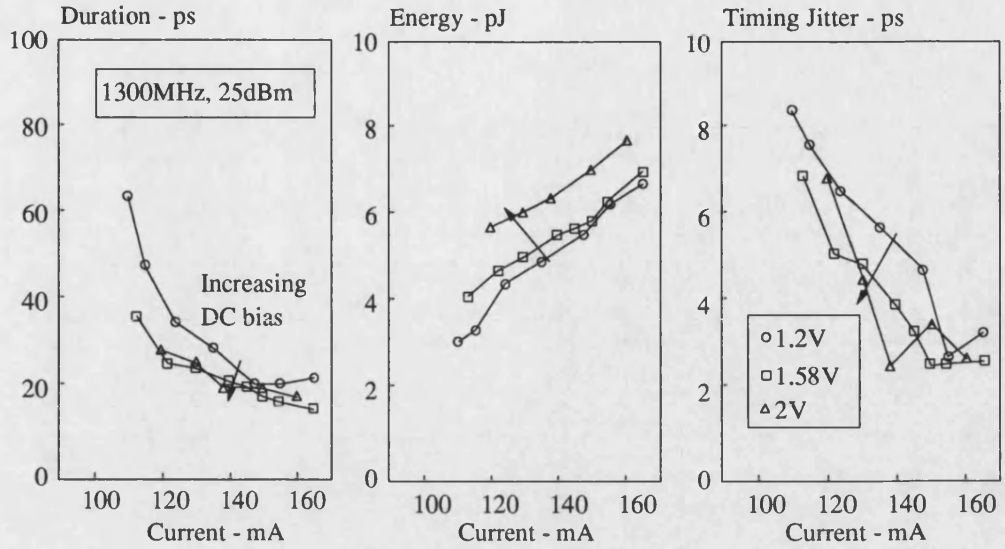

Figure 5.12 : Optical pulse parameters as a function of bias condition for bulk GaAs laser with overall length to absorber ratio of 5:1 for 1300MHz modulation.

Bulk GaAs lasers with the higher contact ratios of 7:1 and 9:1 tend to pulse at half the electrical repetition rate when modulated at 1300MHz. While 7pJ optimum pulse energies were invariant with contact configuration, pulse durations varied from 20ps to 36ps and 80ps at 650MHz. The intermediate length 200:40:200 device would readily gain-switch. There was also a tendency to Q-switch at 650MHz when modulated at 1300MHz. Such subharmonic modulation is well known in gain-switching [19]. At 650MHz modulation, applying 25dBm RF on 1.2V forward bias to the absorber while driving the gain sections with 210mA did allow the generation of 36ps pulses with 7.7pJ pulse energies. Higher gain section drive currents may have improved pulse energies significantly although junction heating prevented details assessment. The 720 μm bulk GaAs laser with the 80 μm central absorber gain-switched to produce

asymmetric 80ps duration, 7pJ energy pulses for a small range of bias conditions with 7ps timing jitter. The absorber area is too small to provide the required saturable absorption for Q-switching. Results are summarised in table 5.1.

	Contacts		Duration	Energy	Jitter	Rate
GaAs Laser	Ratio	μm	ps	pJ	ps	MHz
Bulk	5:1	260[*7]	20	7	5	650
			20	7	3	1300
	7:1	560[**8]	35	7	poor	660
	7:1	560[8]	36	7.7	5	650
	9:1	720[9]	80	7	7	650
Quantum well	3:1	240[10]	35	7.8	8	650
	5:1	240[11]	39	7.3	8.6	650

Table 5.1: Pulse parameters for Forced Q-switched GaAs lasers of differing contact arrangements for dual quantum well and bulk active layers.

[*] Device characterised in figures 5.9 and 5.10.

[**] Device is self Q-switching. i.e. No electrical modulation.

[7-11] Indicate the laser number as listed in appendix A.

Pulses trains generated under forced Q-switching are compared now with those generated under self Q-switching, where there is no longer a requirement for the electrical modulation to the absorber. Pulses with 35ps duration, 7pJ energy and a $sech^2$ profile are readily generated by reverse biasing the absorber with -7V [20]. Electrical pulses with 500mA peak current are applied to generate bursts of Q-switched pulses. Pulse jitter is too poor for spectral measurement

although assessment on a sampling oscilloscope shows jitter degradation towards the end of the optical pulse packet.

The optimised performance of dual quantum well GaAs lasers leads to pulses twice as long as those for bulk. Carrier transport across unoptimised confinement layers, as highlighted in chapter 4, can cause the excess gain suppression which may be responsible for long duration pulses and damped relaxation oscillations.

5.8 Spectral control.

By placing a forced Q-switched Fabry-Perot laser in a grating cavity whose length allows 1300MHz modulation (figure 5.13), good spectral control is achieved. The single longitudinal mode operation achieved is shown in figure 5.14. Pulses remained chirped as a result of the noncoated laser facet and insufficient wavelength selectivity in the cavity. A high degree of symmetry is achieved in the pulses considered. The spectra are given with linear and logarithmic axes to indicate the levels of side mode suppression. The pulses are however slightly broadened. A reduction in pulse energies for tail-free pulsation also leads also to a marked decrease in peak power.

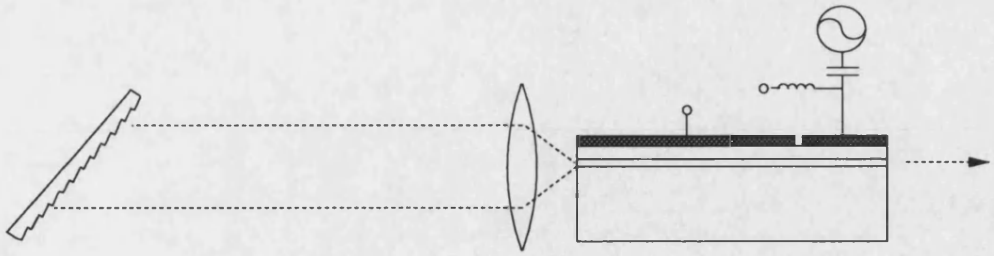

Figure 5.13 : Q-switching in a grating cavity.

Subsequent CW seeding experiments carried out at the University of St Andrews indicate that a low level of monomode continuous wave light injected into a gain-switched laser allows high spectral purity [21]. While these measurements were done at St Andrews in the authors absence, the relevance to this work is sufficient to warrant a brief discussion of the results.

By injecting CW light from a closely wavelength matched single longitudinal mode laser into a gain-switched Fabry-Perot laser, near transform-limited 47ps pulses with 6.6GHz spectral widths were generated. This corresponds to a 0.31 time-bandwidth product. A high degree of symmetry rarely seen in short pulsed diode lasers is observed. For a DC bias close to threshold, CW injection allows a jitter reduction from 22ps to 2.5ps. Subpicojoule pulse energies are noted for transform limited pulses however. In common with gain-switching and mode-locking schemes for transform limited pulse generation it is observed that extremely low levels of bias and modulation are required so as not to chirp the propagating pulses. The scheme has not allowed jitter improvements for Q-switched devices. Alternative feedback schemes for further jitter reduction are outlined in chapter 6.

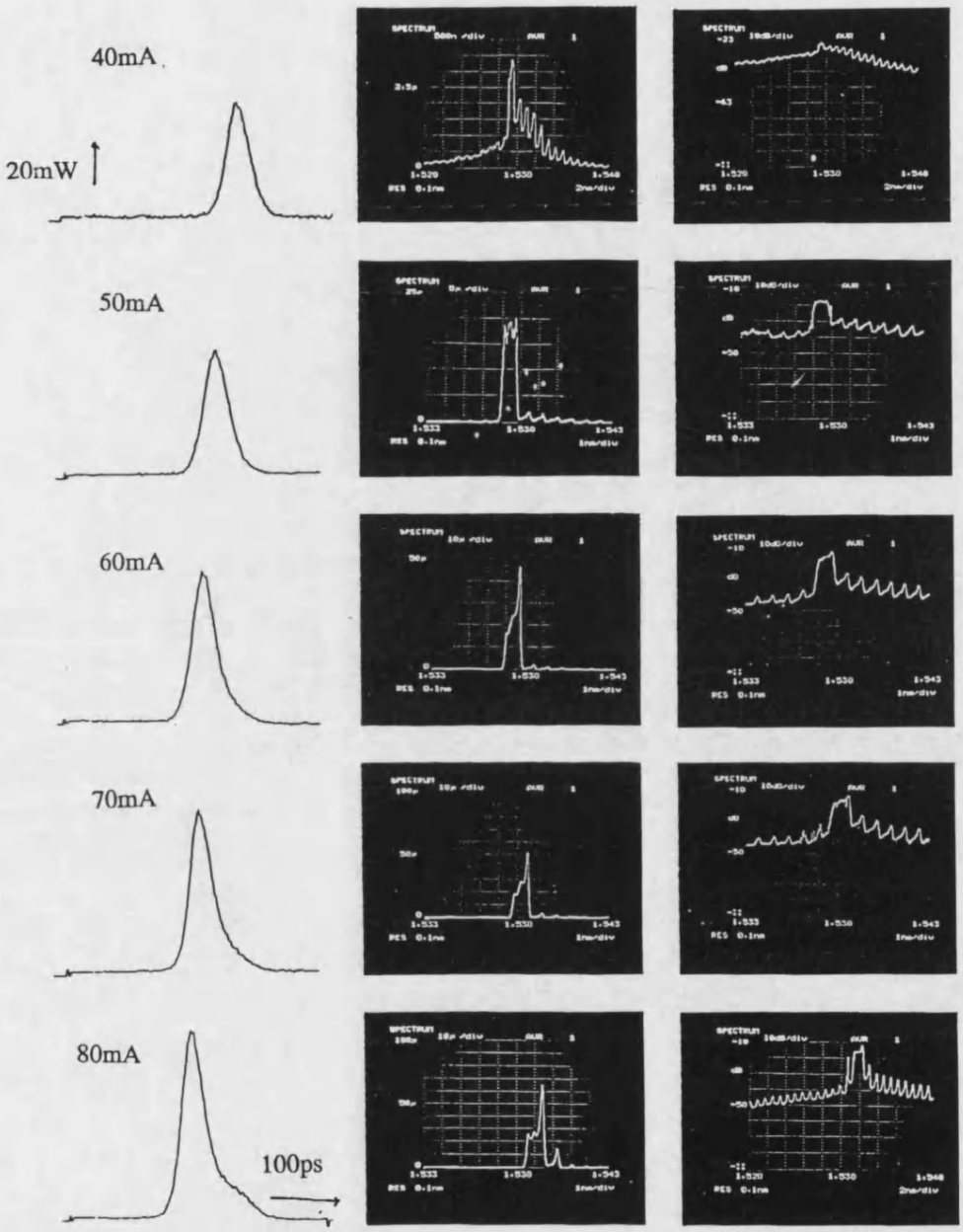

Figure 5.14: Self seeded forced Q-switching in a grating cavity. Pulse profile and spectral dependance on gain secion DC bias. 1300MHz, 30dBm microwave modulation on a -1.35V DC bias is applied to the absorber section.

5.9 Conclusions.

Forced Q-switched has been characterised in terms of pulse profile, spectral profile and stability for a wide range of laser designs. The gain section DC bias conditions have been increased to lead to enhanced powers, reduced stability, and ultimately to increased asymmetry. The increase in saturable absorption through the absorber section DC voltage has however shortened the pulse durations, and lead to an increase in the timing jitter. The device performance is summarised in terms of optimum values for pulse durations, peak optical powers and timing jitter in table 5.2.

Laser	Peak power	Duration	Jitter at 1.3GHz
InGaAsP bulk DFB[4]	60mW	33ps	2.5ps
InGaAsP MQW DFB[5]	60mW	30ps	4.5ps
InGaAsP MQW Fabry-Perot[6]	80mW	26ps	1.4ps
GaAs bulk Fabry-Perot[7]	350mW	20ps	3ps
GaAs DQW Fabry-Perot[10]	187mW	39ps	8.6ps

Table 5.2 : Summary of the optimum pulse peak powers, durations, and timing jitter for forced Q-switched operation at 1.3GHz. InGaAsP, GaAs, bulk and quantum well active layer lasers are compared.

Optimum timing jitter is noted for the InGaAsP multiquantum well Fabry-Perot laser. Enhanced coupling of the spontaneous emission into the lasing modes is expected to account for the improvement observed over the monomode distributed feedback lasers. An improvement in timing jitter with an increase in repetition rate is also measured, which may correspond to an increase in the rate of change of voltage experienced at the turn on time.

Seeding techniques are described which enhance the gain-switched operation of Fabry-Perot laser both in terms of spectral quality and in terms of the pulse train stability. Measurements indicate however that such techniques are of limited benefit for Q-switching. Injection levels sufficiently high to enhance the pulse train stability are observed to degrade the pulse profile. The pulse turn on time is advanced in the presence of a CW or picosecond pulse injection. This premature pulse turn on leads to reduced peak power pulses which do not sufficiently deplete the gain, and relaxation oscillations ensue.

This chapter has focussed on the high power forced Q-switched operation of diode lasers, and little comparison has been made with alternative picosecond pulse generation techniques. Chapter 6 now compares Q-switching with a wide variety of techniques and developes feedback techniques for stability enhancement.

5.10 References.

1. BÖTTCHER, E.H., and BIMBERG, D., "Detection of pulse to pulse timing jitter in periodically gain-switched semiconductor lasers", Applied Physics Letters, 54, 1971-1973, 1989.

2. BÖTTCHER, E.H., KETTERER, K. and BIMBERG, D., "Turn-on delay time fluctuations in gain-switched AlGaAs/GaAs multiple quantum well lasers", Journal of Applied Physics, 63, 2469-2471, 1988.

3. D'OTTAVI, A., MECOZZI, A., SPANO, P., and PIAZZOLLA, S., "Time jitter in multimode Fabry-Perot laser diodes", Applied Physics Letters, 53, 2362-2364, 1988.

4. SAPIA, A., SPANO, P., MIRASSO, C.R., COLET, P., and MIGUEL. M.S., "Pattern effects in time jitter of semiconductor lasers", Applied Physics Letters, 61, 1748-1750, 1992.

5. WEBER, A.G., RONGHAN, W., BÖTTCHER, E.H., SCHELL, M. and BIMBERG, D., "Measurement and simulation of the turn-on delay time jitter in gain-switched semiconductor lasers", IEEE Journal of Quantum Electronics, 28, 441-446, 1992.

6. JINNO, M., "Correlated and uncorrelated timing jitter in gain-switched laser diodes", IEEE Photonics Technology Letters, 5, 1140-1143, 1993.

7. PEPELJUGOSKI, P., CUTRER, D. and LAU, K., "3.4ps wide compressed optical pulses from electrically gain-switched vertical cavity surface emitting laser", Electronics Letters, 30, 491-492, 1994.

8. BURNS, D., FINCH, A., SLEAT, W. and SIBBETT, W., "Noise characterisation of a mode-locked InGaAsP semiconductor diode laser", IEEE Journal of Quantum Electronics, 26, 1860-1863, 1990.

9. LEEP, D.A. and HOLM, D.A., "Spectral measurement of timing jitter in gain-switched semiconductor lasers", Applied Physics Letters, 60, 2451-2453, 1992.

10. SCHELL, M. and coworkers currently use the spectral technique outlined in references [11-12] in agreement with references [6,7,9] as a result of measurement limiting trigger dependant timing jitter. Private communication.

11. VON DER LINDE, D., "Characterisation of the noise in continuously operating mode-locked lasers", Applied Physics B, 39, 201-217, 1986.

12. KLUGE, J., WIECHERT, D., and VON DER LINDE, D., "Fluctuations in synchronously mode-locked dye lasers", Optics Communications, 51, 271-277, 1984.

13. DELFYETT, P.J., HARTMAN, D.H. and AHMEDS, Z., "Optical clock distribution using a mode-locked semiconductor laser diode system", IEEE Journal Lightwave Technology, 9, 1646-1649, 1991.

14. RODWELL, M.J.W., BLOOM, D.M. and WEINGARTEN, K.J., "Subpicosecond laser timing stabilization", IEEE Journal of Quantum Electronics, 25, 817-827, 1989.

15. TAYLOR, A.J., WIESENFELD, J.M., EISENSTEIN, G. and TUCKER, R.S., "Timing jitter in mode-locked and gain-switched InGaAsP injection lasers", Applied Physics Letters, 49, 681-683, 1986.

16. PEPELJUGOSKI, P., LIN, J., GAMELIN, M., HONG, M. and LAU, K., "Ultralow timing jitter in electrically gain-switched vertical cavity surface emitting lasers", Applied Physics Letters, 62, 1588-1590, 1993.

17. WHITE, I.H., WILLIAMS, K.A., HUGHES, D.M., BURNS, D. and SIBBETT, W., "High power picosecond pulse generation in multicontact diode lasers using modified Q-switching techniques", proceedings CLEO Europe, Invited paper CTuL1, Amsterdam, 1994.

18. WILLIAMS, K.A., BURNS, D., WHITE, I.H., SIBBETT, W. and FICE, M.J., "Picosecond pulse generation with ultralow jitter in 1.5 μm multicontact MQW lasers using Q-switching", IEEE Photonics Technology Letters, 5, 867-869, 1993.

19. GALLAGHER, D.F.G., "Pulse position bistability in gain-switched diode lasers", PhD thesis, University of Cambridge, 1987.

20. WILLIAMS, K.A., SARMA, J., WHITE, I.H., PENTY, R.V., MIDDLEMAST, I., RYAN, T., LAUGHTON, F.R., and ROBERTS, J.S., "Q-switched bow-tie lasers for high energy picosecnd pulse generation", Electronics Letters, 30, 320-321, 1994.

21. HUGHES, D.M., BURNS, D., SIBBETT, W., WILLIAMS, K.A., WHITE, I.H., "Ultrashort pulse semiconductor lasers with improved timing jitter", proceedings CLEO, CWN4, Anaheim, 1994.

FEEDBACK TECHNIQUES FOR JITTER CONTROL

Feedback schemes enabling stable microwave oscillation in diode lasers are investigated for the generation of improved jitter picosecond pulsation. Multicontact and conventional single contact InGaAsP/InP lasers are considered in configurations which allow direct comparison with Q-switching, gain-switching and mode-locking for the first time. Optoelectronic, electrical, purely optical and hybrid optoelectronic schemes are considered in terms of the timing jitter content and pulse quality to determine the ultimate limits to timing jitter in diode lasers.

6.1 Outline.

A survey of work carried out for electrical and optical feedback techniques for picosecond pulsed diode lasers has been carried out, indicating enhancements in pulse train stability and pulse narrowing. Subsequent experimental work quantifies the improvements through jitter measurements for both novel and established techniques. Without the requirement for costly microwave modulation sources, the passive optical picosecond pulse generation techniques offer significant stability improvements over both passive and active monolithic Q-switching and mode-locking. Current interest in the role of feedback for stability improvement in diode lasers is addressed outlining recent work to stablise gain-switched and passively mode-locked pulse generation. Such work has been the motivation for improved stability passive Q-switching realised in the novel optoelectronic feedback subsequently described. Here multicontact InGaAsP lasers are demonstrated to self Q-switch using the

optoelectronic feedback technique at 1GHz with subpicosecond timing jitter. Alternative electrical schemes and optical schemes are addressed with their advantages leading to a direct comparison for the first time of optical, electrical and optoelectronic feedback schemes in terms of pulse duration, energy and stability. Further, comparisons are made with the direct modulation techniques (discussed in chapter 3) - gain-switching, forced Q-switching and active mode-locking. As a strong jitter dependence on repetition rate has already been observed in the chapter 5, it is instructive to compare the pulse performance at 1GHz for all schemes. Again, both distributed feedback lasers and Fabry-Perot lasers are compared, with multimoded operation allowing reduced jitter for the Fabry-Perot lasers. Significant improvements in the stability are found for the hybrid resonant electrical and optical feedback scheme when compared with passive mode-locking. Timing jitter is measured to be 240fs. External cavity active mode-locking however offered the lowest timing jitter, estimated to be below the measurement system limit of 160fs.

6.2 Feedback in Diode Lasers for Improved Stability.

From the conventional implementation of monitor photodiodes to regulate the optical power levels of continuous wave lasers [1] to linewidth reduction schemes [2-13], feedback techniques are widely implemented to improve laser stability. Experimental and theoretical investigations into linewidth and noise reduction through negative feedback schemes are well documented. Linewidth reduction is required primarily in communication systems for coherent modulation schemes such as phase shift keying [2]. Optical feedback has been used for linewidth reduction [2-3] although under these schemes temporal

variation with phase fluctuations in the reflected light is induced by mechanical vibration and thermal drift. Optoelectronic feedback schemes appear more favourable therefore as external cavities are no longer required. Such a feedback scheme for linewidth reduction is illustrated in figure 6.1. The optical output of the laser is spectrally filtered and monitored by the Germanium avalanche photodiode. The photocurrent provides an error signal, which after appropriate amplification, adjusts the laser drive current. A 100MHz bandwidth amplifier is used here in the 13ns feedback loop. Ohtsu and Kotajima have achieved linewidth reductions of fifteen times to 330kHz compared with a free-running distributed feedback lasers [6].

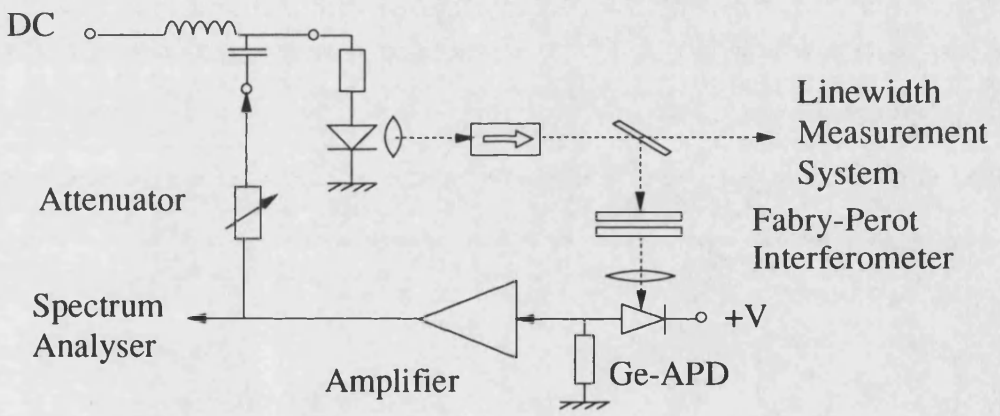

Figure 6.1 : Feedback scheme for linewidth reduction in a semiconductor laser, after Ohtsu and Kotajima [6].

Research interest is increasingly turning to feedback techniques for picosecond pulse applications as the limitations of the more established schemes become more apparent. An overview of feedback schemes is given to provide a context for the systematic comparison of novel and established feedback techniques for low jitter optical picosecond pulse generation. Feedback for

picosecond pulsation in semiconductor lasers may result from modulation the laser using either the forward voltage, the optical intensity, or a combination of the two. Schemes reported in the literature can therefore be subdivided into three main categories :

Optical	The optical pulse from a previous modulation cycle is reflected into the laser cavity to optically initiate pulse generation [14-18]
Electrical	The laser junction forward voltage fluctuation is amplified to modulate the same laser junction using a microwave directional coupler [14].
Opto-electronic	The optical signal incident on a photodetector is amplified to electrically modulate the laser [14,19-21].

Optical feedback requires either an external mirror [15], grating [16] or fibre loop [17] to feed back light into the cavity. Such self-seeded schemes do not involve laser facet coatings, therefore leading to two cavities as opposed to extending the laser cavity in external cavity mode-locking. The cavity provides a second round trip time synchronised to the modulation rate in order to optically assist subsequent pulse generation with stimulated emission. The reduced dependence on amplified spontaneous noise at turn on reduces timing jitter in the pulse train. Total jitter ultimately relies on the quality of electrical modulation, the stability of the cavity and reliance on spontaneous emission for pulse generation. A reduction in jitter with increased feedback is ultimately limited by pulse profile deterioration as pulse turn off is prevented.

Electrical feedback schemes have received little attention and are considered in some detail in section 6.4. While stable pulsation is observed in a

wide ranging study on feedback schemes in GaAs lasers in 1970 [14], a lack of optimised lasers and appropriate diagnostic facilities limits the comparative value of the measurements.

Optoelectronic feedback has received more current experimental interest. Schemes address stability improvements that can be made to the conventional schemes of self-pulsing [19], gain-switching [20] and passive mode-locking [21]. For the gain-switched case, picosecond pulsation is readily controlled by feeding back information about the optical pulse train incident on a photodetector. The amplified photocurrent directly modulates the laser. After a number of modulation periods the signal will stabilise to generate a microwave signal defined by the frequency response of the feedback loop. Pulse widths decrease from 60ps to 35ps as the repetition rate is tuned from 230-500MHz under the regeneratively gain-switched scheme. The original self-pulsing scheme employing the same optoelectronic feedback however allows the generation of 20ps pulses at 1GHz, decreasing in width to 10ps as the repetition rate increases to 5GHz.

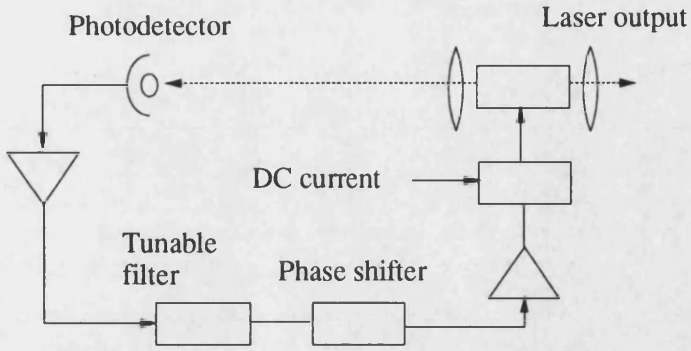

Figure 6.2 : Feedback scheme for stable picosecond pulse generation in self-pulsing and regeneratively gain-switched semiconductor lasers. After Yan and coworkers [20].

While phase noise is known to be reduced for external cavity actively mode-locked lasers where timing jitter of 240fs has been measured (150Hz-500MHz), monolithic schemes show a degraded 600fs jitter [22]. For passively mode-locked schemes the jitter deteriorates further to 12.2ps and 12.5ps for external cavity and monolithic schemes in the 150kHz-50MHz bands. Schemes which enhance the stability of monolithic mode-locked diode lasers are therefore of interest. Stable picosecond pulse generation at 46.8GHz in passively mode-locked lasers is achieved by Georges and coworkers using a combination of a phase-locked optoelectronic loop and optical feedback [21]. The optical signal is initially mixed down to 6.8GHz for amplification and phase noise assessment. The 6.8GHz signal is then mixed down to baseband to act as a loop error signal to compensate with the DC level.

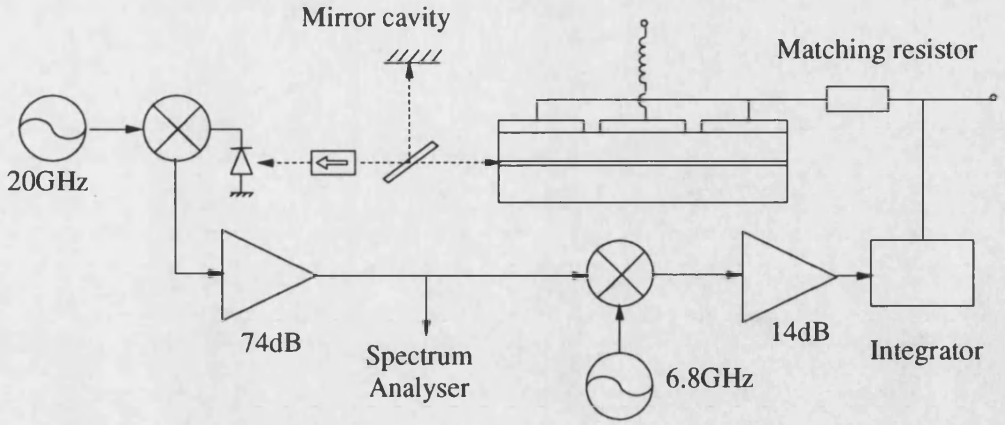

Figure 6.3 : Phase noise reduction in a passively mode-locked laser through feedback. After Georges and coworkers [13].

6.3 Optoelectronic Feedback.

Using a novel optoelectronic feedback scheme as illustrated for a three contact laser in figure 6.4, the uncorrelated jitter is now shown to be reduced dramatically for self Q-switched lasers. Here, rather than using photodiode detection, shot noise from a DC-biased gain section is coupled into the feedback loop through a microwave tee. This causes repetitive pulse generation at frequencies determined predominantly by the electrical bandwidth of the feedback loop. With no microwave source or critical narrow-band filtering in the feedback loop system, costs are kept to a minimum. The signal is amplified with Minicircuits ZHL42 and Motorola CA5915 integrated circuit amplifiers, and injected into a subthreshold biased absorber section.

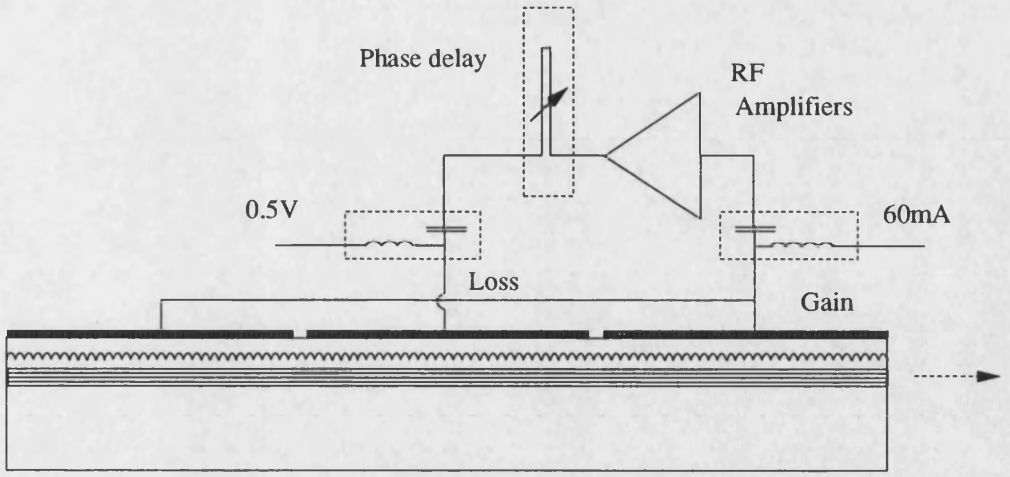

Figure 6.4 : Schematic to show the implementation of optoelectronic feedback on a single chip for a multicontact laser diode.

Using quantum well InGaAsP/InP lasers[5,6] with the same structure and contact configurations described previously for forced Q-switching (section 5.6), stable self Q-switching at 1GHz is demonstrated without a separate electrical oscillator. The distributed feedback[5] laser with three 200 μm contacts is biased to allow a central absorbing region surrounded by regions of gain. Implementing the optoelectronic feedback scheme with appropriate phase correction and between 40-50dB of amplifier gain, leads to a reduction in jitter to be observed in the microwave spectrum. The noise sidebands accompanying the first and fifth harmonics are used in the measurement of the phase noise and the calculation of jitter. The jitter performance is monitored as a function of feedback loop delay time in figure 6.5. Uncorrelated jitter is reduced from 6ps to 2.5ps for the appropriate returned electrical phase. This is half the uncorrelated jitter measured under the electrically modulated forced Q-switching scheme outlined in section 5.6. The phase of the feedback electrical signal is important, having a tolerance of 2-3° as shown in figure 6.5. Error bars indicate the ±1.5dB error

associated with noise sideband measurement using a spectrum analyser. Pulse to pulse amplitude fluctuation is observed as subharmonic modulation in the pulse microwave spectrum at some phase shifts outside the low jitter regime. Fibre-coupled pulse energies of 1pJ are readily measured, and are noted to be independent of the feedback loop length. The microwave power fed back into the absorber is measured to be 24dBm for optimum operation, corresponding to the power levels for forced Q-switching. For an increased amplification in the loop there is, however, a uniform increase in noise across the frequency spectrum indicating the existence of higher levels of amplitude noise. Such increases in amplitude noise with feedback loop gain are also reported for continuous wave feedback linewidth reduction schemes [12].

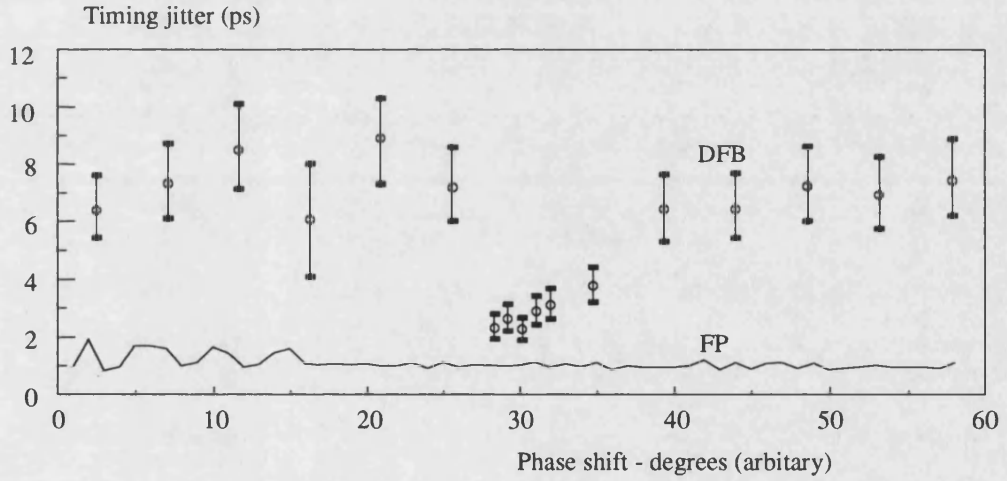

Figure 6.5 : Uncorrelated timing jitter in multimode[6] and single mode[5] self-Q-switched laser with optoelectronic feedback.

Feedback also leads to a reduction in the uncorrelated jitter observed for diode lasers in quantum well Fabry-Perot cavity configuration[6]. The contacts are split to allow 300μm gain and 100μm absorber sections. For the same

optimum bias conditions, pulsing is observed at the loop dependent 1GHz repetition rate with pulse energies of 1pJ. While jitter is reduced from 1.3ps for forced Q-switching (section 5.6) to 1ps with optoelectronic feedback (as illustrated in figure 6.5), the appropriate phase shift allowed a further reduction to as low as 0.8ps. The repetition rate for the scheme decreases with increasing phase shift at the rate 0.3 MHz/degree, and allows low jitter pulsation over a wide range of electrical phase shifts in the Fabry-Perot laser. At around 180° phase shift subharmonic modulation is observed along with a jump to a higher repetition rate. Further improvements regarding the long term repetition rate stability are expected with the inclusion of narrow band filters and low noise amplifiers in the feedback loop.

6.4 Resonant Electrical Feedback.

As optoelectronic feedback is compared with Q-switching, resonant electrical feedback in a single contact laser is now compared to gain-switching. Measurements are carried out on multiquantum well multiple phase shifted distributed feedback[2] (used in section 4.5) and multiquantum well Fabry-Perot[12] InGaAsP lasers. The experimental arrangement is shown schematically in figure 6.6. Using a directional coupler (Minicircuits ZFDC-10-2) junction noise is coupled into a loop with a variable delay line (Narda 3753B). A low cost cellular telephone band-pass filter provides frequency discrimination. The Toko 302HN-071B filter has a 20MHz -1dB nominal bandwidth centred at 1015Mz. A Minicircuits (ZHL42) amplifier and variable Tekscan MA-50 attenuator allows the gain to be varied to give reinjected RF levels from 15-25dBm at the fundamental frequency.

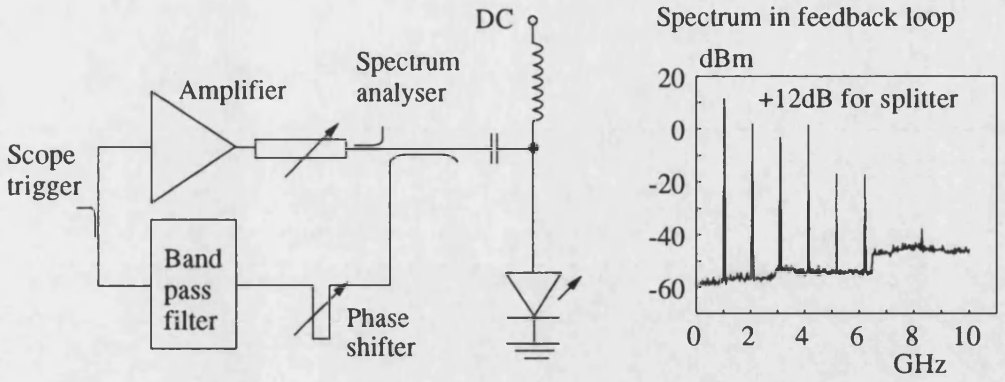

Figure 6.6 : Resonant electrical feedback in a single contact diode laser for picosecond pulse generation at Gigahertz repetition rates.

The microwave spectrum at the 10dB coupler given in the system schematic indicates the frequency components present in the loop and does not change significantly with optimum operating conditions. While the broadband comb in the loop might explain the lower uncorrelated jitter, the harmonics are observed to be 10dB below the modulation frequency. The modulation level dependence of jitter is plotted in figure 6.7 for gain-switching and resonant feedback to emphasise the improvement is not merely due to an optimising of the injected power level. Indeed, significant jitter improvements are observed for the distributed feedback laser[2]. While results are reproducible, jitter measurements appear susceptible to ambient temperature fluctuations.

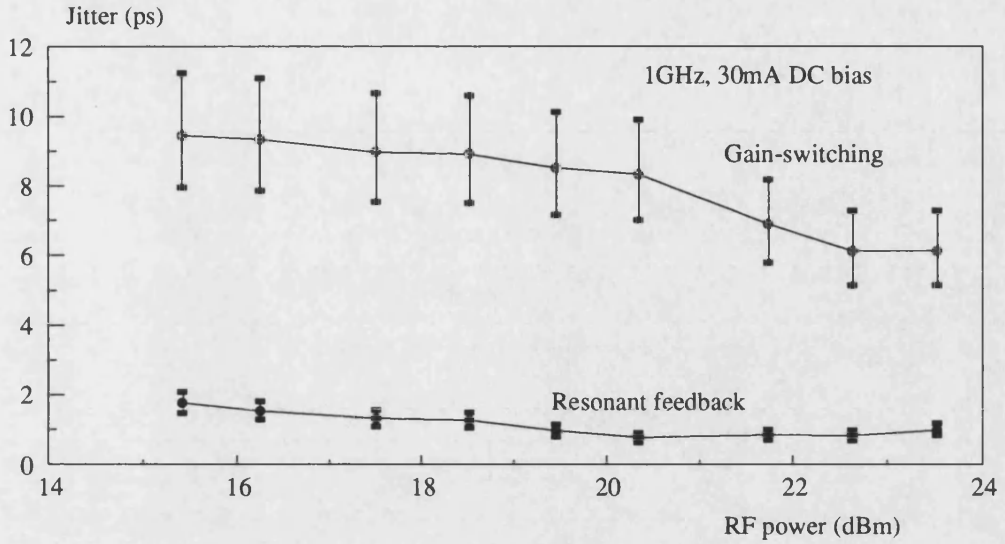

Figure 6.7: Timing jitter in a single contact distributed feedback laser[2] under gain-switching and resonant electrical feedback. The plotting of uncorrelated jitter against modulation power indicates that reduced jitter does not result from optimised power levels in the case of feedback.

For optimum feedback conditions the jitter is assessed for varied DC bias conditions in the distributed feedback laser in figure 6.8. The high values of uncorrelated jitter at low bias are a direct result of insufficient amplified spontaneous emission. With increasing DC bias the pulse turn-off characteristic deteriorates until a long tail builds up. This interferes with turn on in subsequent pulses through amplitude noise manifested as pulse profile variation. Pulse profiles are assessed with a 32GHz detector (HP3440D) and 50GHz sampling oscilloscope (HP54124T). An amplified lightwave convertor (HP11982A) and spectrum analyser (HP8593A) enabled jitter assessment. Dependence of jitter and profiles on bias current are illustrated in figure 6.8. The reduction of jitter and increasing amount of energy in the tail with increasing current is

characteristic of gain-switching. Jitter improvements from the optimum 6ps for gain-switching to 0.8ps for resonant feedback are noted by comparing figures 6.7 and 6.8.

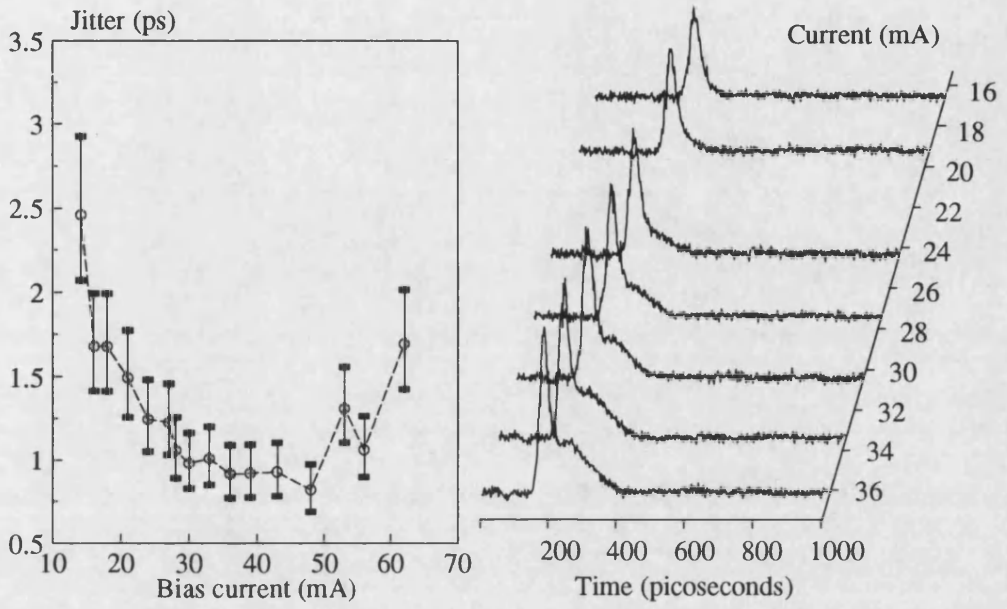

Figure 6.8 : Timing jitter and pulse profiles in distributed feedback lasers for varied DC bias.

The Fabry-Perot laser[12] also shows an improvement using the scheme. However, poorer pulse profiles were observed, when compared to gain-switched Fabry-Perot lasers. The back of the pulse shows an exponential fall off at the higher bias conditions. Without any filter in the feedback loop, self-pulsation occurs at 3GHz with 4ps timing jitter. The lack of frequency discrimination in the feedback loop results in the amplification of broadband noise responsible for much of the jitter. The inclusion of the narrow band filter reduces jitter to 0.8ps with a bias dependence as outlined for the Fabry-Perot laser in figure 6.9. Jitter levels are not significantly better than observed for

distributed feedback lasers however, indicating that a limit is being reached. A reduction in pulse duration as compared to gain-switching is noted for all DC bias levels considered.

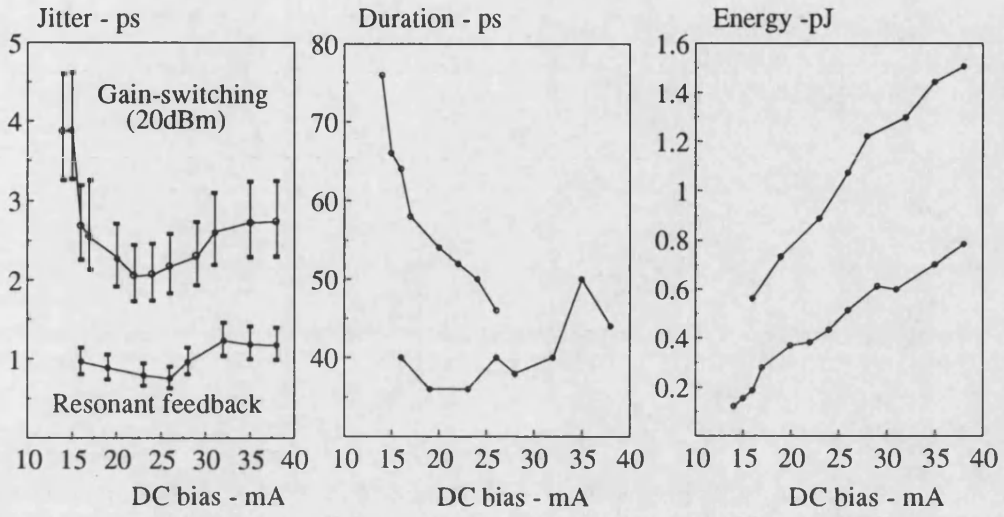

Figure 6.9 : Timing jitter, pulse durations and pulse energies in InGaAsP Fabry-Perot lasers[12] for varied DC bias conditions. Gain-switching and resonant electrical feedback are compared.

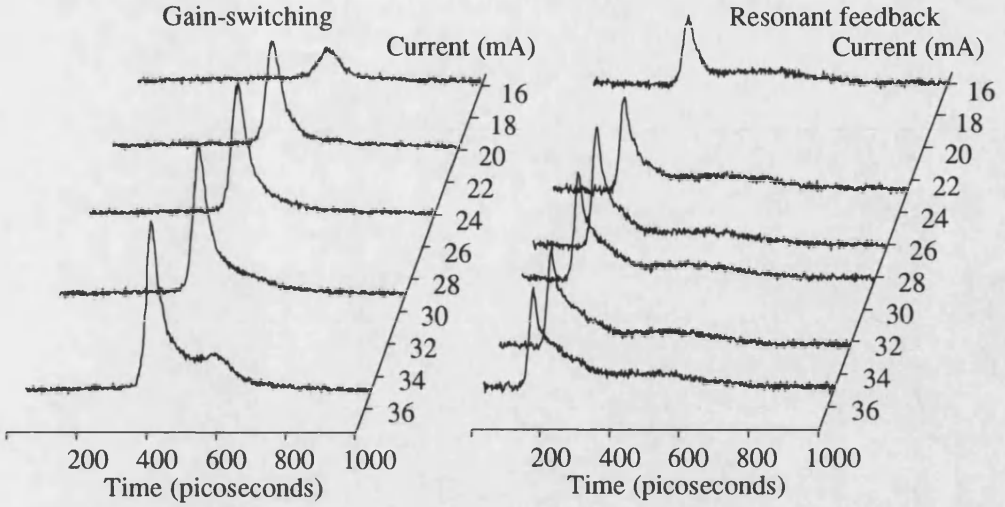

Figure 6.10 : Pulse profile dependence on bias conditions in a Fabry-Perot laser under both gain-switching and resonant feedback.

6.5 Optical Feedback.

Optical feedback is known to improve timing jitter in gain-switched lasers [16], and it is therefore of interest to consider resonant feedback in conjunction with optical feedback for further jitter reduction. The role of optical feedback is first assessed for a gain-switched bulk InGaAsP Fabry-Perot laser[13] in a mirror cavity with the cavity length set to the modulation period. The Fabry Perot laser in the resonant electrical feedback experiments of section 6.4 was mounted such that the rear facet was not accessible. The device was therefore replaced with a device with as similar structure as possible (see appendix A, laser number 13). No coatings are applied to the first laser. Light on the cavity facet is focussed to a spot at the mirror with a x40 magnification, 0.65 numerical aperture microscope

objective, while light at the output facet is coupled to lensed fibre. Hewlett Packard lightwave converters allow assessment of the optical pulse train. Care is taken to avoid reflections from optical connectors.

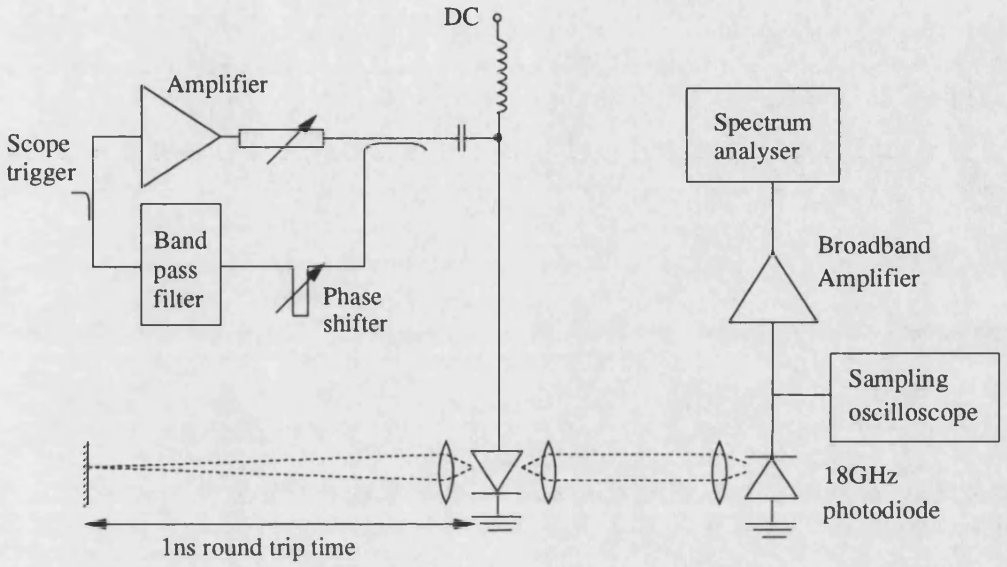

Figure 6.11 : Scheme for hybrid optical feedback for further jitter reduction in single contact lasers. Lasers with both 33% and 3% facet reflectivities are measured.

Implementing the feedback loop as optimised and illustrated in figure 6.6 allows self-pulsation at the external cavity round trip frequency. Uncorrelated timing jitter of 1.11ps is noted for the subthreshold 20mA DC bias condition. Increasing the electrical modulation slightly relative to the cavity round trip frequency leads to a phase noise reduction. For pulsation with solely resonant electrical feedback phase noise is not critically dependent on the feedback loop length and therefore electrical modulation frequency. Broadband timing jitter was calculated to be 1.08ps. At higher DC bias conditions, self-pulsing becomes

increasingly unstable and cavity dependant. Enhanced levels of amplitude noise are noted for the measurements involving optical feedback indicating significant fluctuations in the pulse profile.

Advantages are however more evident for gain-switched operation where a halving of the timing jitter is noted for subthreshold operation with the introduction of feedback. Figure 6.11 outlines the trends for gain-switching with 20dBm, 1GHz modulation. The reducing jitter with increasing DC bias and therefore increasing levels of amplified spontaneous emission is as expected for the gain-switched laser. Jitter does however degrade as the pulse profile degrades for the case under feedback.

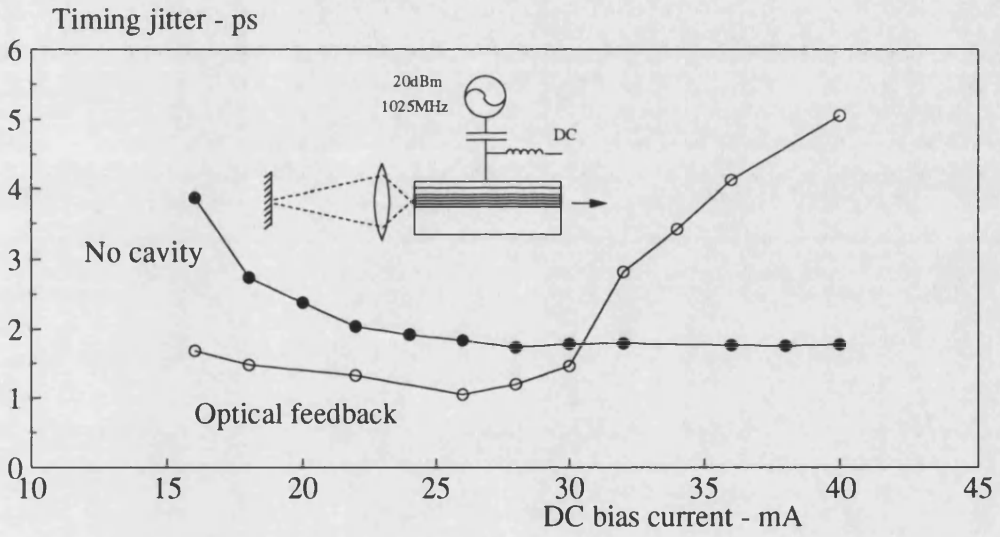

Figure 6.12 : Jitter reduction in single contact gain-switched lasers through self-seeding in an external mirror cavity. No facet coatings are applied to the laser.

The resonant feedback scheme does not benefit from optical self-seeding, indicating that insufficient light is reinjected into the laser cavity. Two options exist to enhance the role of self-seeding in pulse stabilisation. The pulse could be compressed in a dispersive cavity to form shorter duration higher power pulses. A grating cavity as implemented by Huhse and coworkers [16] leads to 210fs timing jitter. An alternative solution involving antireflection coating of the laser is considered here.

Further jitter reductions are possible using a Fabry-Perot laser with 3% reflectivity on one facet[14] [24]. While the previous optical feedback scheme considered is analogous to self-seeded gain-switching, the reduced reflectivity makes mode-locking a more relevant control now. The lack of an absorber section requires that active mode-locking is used. The laser threshold current of 70mA reduces to 40mA when aligned within a 1ns long mirror cavity. Bulk optics are now used to couple the optical pulse train to the 18GHz InGaAs PIN photodetector. A fibre cavity would allow a much less complex system [25]. Preamplification to the spectrum analyser is provided by a 4GHz bandwidth Minicircuits ZHL-42 amplifier.

Once initiated, mode-locked pulses do not rely on the build up of spontaneous emission and are expected to have minimal uncorrelated jitter and broadband phase noise. Measurements confirm for optimum pulse profiles that wideband noise is below the 160fs measurement system noise floor. The hybrid feedback scheme however allows uncorrelated timing jitter to be reduced to 250fs. Pulse durations of down to 50ps are an improvement over mode-locking, while subpicojoule pulse energies are the same for the two schemes. Pulse profiles are similar for both mode-locking and hybrid optical feedback, with the onset of a tail at 55mA.

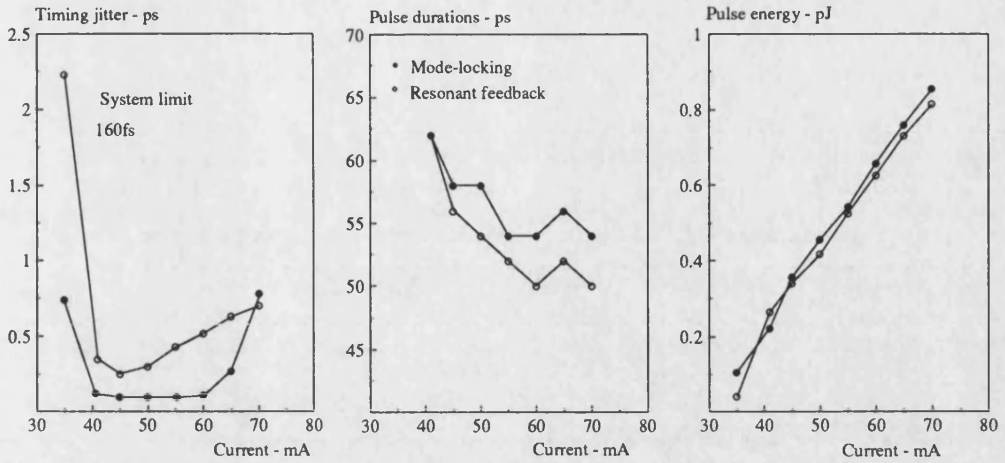

Figure 6.13 : Timing jitter, pulse duration and energy for hybrid optical feedback and mode-locking for varied current levels.

6.6. Conclusions.

Feedback has been demonstrated to reduce the uncorrelated timing jitter in picosecond pulsed lasers for a variety of optical cavities and microwave frequency drive circuit combinations. Without the requirement for costly microwave modulation sources, the passive optical picosecond pulse generation techniques offer significant stability improvements over both passive and active monolithic Q-switching and mode-locking. Current interest in the role of feedback for stability improvement in diode lasers is addressed outlining recent work to stablise gain-switched and passively mode-locked pulse generation. Table 6.1 summarises the optimum values of timing jitter for the feedback schemes considered.

Laser	Feedback scheme	Jitter	Control scheme	Jitter
Distributed	Optoelectronic	2.5ps	Q-switching	5-6ps
feedback	Electrical	0.8ps	Gain-switching	6-10ps
Fabry-Perot	Optoelectronic	0.8ps	Q-switching	1.3ps
	Electrical	0.8ps	Gain-switching	2ps
	+ self-seeding	1.1ps	+ self-seeding	1.1ps
	+ optical feedback	0.25ps	Mode-locking	<0.16ps

Table 6.1 : A comparison of optimum uncorrelated jitter in picosecond pulsed InGaAsP lasers.

6.6 References.

1. SENIOR, J., Optical Fibre Communications, Englewood Clifts, NJ : Prentice-Hall, 1985.

2. KIKUCHI, K., OKOSHI, T., NAGAMATSU, M., and HENMI, H., "Bit error rate degradation due to spectral spread of transmitter and local oscillator", Electronics Letters, 19, 417-418, 1983.

3. SAITO, S., and YAMAMOTO, Y., "Direct observation of Lorentzian lineshape of semiconductor laser and linewidth reduction with external grating feedback", Electronics Letters, 17, 325-327, 1981.

4. FAVRE, F., LE GUEN, D., and SIMON , J.C., "Optical feedback effects upon laser diode oscillation field spectrum", IEEE Journal of Quantum Electronics, 18, 16712-1717, 1982.

5. SAITO, S., "FM noise and linewidth reduction of a 1.5μm laser by electrical feedback", Japanese Journal of Applied Physics, 24, L256-L258, 1985.

6. OHTSU, M., and KOTAJIMA, "Linewidth reduction of a semiconductor laser by electrical feedback", IEEE Journal of Quantum Electronics, 21, 1905-1912, 1985.

7. YAMAMOTO, Y., NILSON, O., and SHIGERU, S., "Theory of a negative frequency feedback semiconductor laser", IEEE Journal of Quantum Electronics, 21, 1919-1928, 1985.

8. GLANCE, B., "Performance of AFC for phase noise reduction of optical sources", Electronics Letters, 21, 994-996, 1985.

9. OHTSU, M., and KOTAJIMA, S., "Linewidth reduction of a semiconductor laser by electrical feedback", IEEE Journal of Quantum Electronics, , 1905-1911, 1985.

10. YAMAMOTO, Y., NILSSON, O., and SAITO, S., "Theory of a negative feedback semiconductor laser", IEEE Journal of Quantum Electronics, 21, 1919-1928, 1985.

11. SHARAF, K., and IBRAHIM, M.M., "The effect of electronic feedback on semiconductor lasers", IEEE Journal of Quantum Electronics, 26, 1347-1352, 1990.

12. LI, L., "AM noise enhancement in a semiconductor laser with electrical feedback", IEEE Journal of Quantum Electronics, 27, 174-177, 1991.

13. LI, L., "The optimal loop gain design for the spectral linewidth reduction in an electrical feedback semiconductor laser", IEEE Journal Quantum Electronics, 27, 1975-1980, 1991.

14. PAOLI, T.L., and RIPPER, J.E., "Frequency stabilization and narrowing of optical pulses from CW GaAs injection lasers", IEEE Journal of Quantum Electronics, 6, 335-339, 1970.

15. SOLGAARD, O., and LAU, K.Y., "Optical feedback stabilization of the intensity oscillations in ultrahigh-frequency passively mode-locked monolithic quantum well lasers", IEEE Photonics Technology Letters, 5, 1264-1267, 1993.

16. HUHSE, D., SCHELL, M., UTZ, W., KÄSSNER, J., and BIMBERG, D., "Generation of low jitter (210fs) single mode pulses from a 1.3μm Fabry-Perot laser diode by self-seeding", proceedings ECOC, poster paper Tu.P.24, Florence, 1994.

17. HUHSE, D., SCHELL, M., KAESSNER, J., and BIMBERG, D., "Generation of electrically wavelength tuneable ($\Delta\lambda$=40nm) single mode laser pulses from a 1.3 μm Fabry-Perot laser by self-seeding in a fibre-optic configuration", Electronics Letters, 30, 157-158, 1994.

18. DEBEAU, J., BARRY, L.P., and BOITTIN, R., "Tunable, transform limited pulse generation at 5GHz by self-injection locking of a gain switched FP laser", proceedings ECOC, paper WeP8.5, Montreux, 1993.

19. LAU, K.Y., and YARIV, A., "Self sustained picosecond pulse generation in a GaAlAs laser at an electrically tuneable repetition rate by optoelectronic feedback", Applied Physics Letters, 45, 124-126, 1984.

20. YAN, C., REDDY, K.P.J., JAIN, R.K., and MCINERNEY, J.G., "Picosecond pulse generation in CW semiconductor lasers using a novel regenerative gain-switching technique", IEEE Photonics Technology Letters, 5, 494-497, 1993.

21. GEORGES, J.B., BUCKMAN, L., VASSILOVSKI, D., PARK, J., KIANG, M.-H., SOLGAARD, O., and LAU, K.L., "Stable picosecond pulse generation at 46GHz by modelocking of a semiconductor laser operating in an optoelectronic phaselocked loop", Electronics Letters, 30, 69-71, 1994.

22. DERICKSON, D.J., HELKEY, R.J., MAR A., KARIN, J.R., WASSERBAUER, J.G., BOWERS, J.E., "Short pulse generation using multisegment mode-locked semiconductor lasers", IEEE Journal of Quantum Electronics, 28, 2186-2203, 1992.

23. CONSTABLE, J.A., PhD thesis, University of Bath, 1993.

24. ZHU, B., NYAIRO, K.O., and WHITE, I.H., "Dual-wavelength picosecond optical pulse generation using an actively mode-locked multichannel grating cavity laser", IEEE Photonics Technology Letters, 3, 348-351, 1994.

25. IZADPANAH, H., "Generation of self-sustained optical pulses from transients in external cavity semiconductor lasers", Electronics Letters, 24, 137-138, 1988.

HIGH POWER PICOSECOND PULSED BOW-TIE LASERS

A novel double tapered waveguide structure is used to allow enhanced power picosecond pulsation in a multicontact Bow-Tie laser. Monolithic Q-switching and passive mode-locking lead to record pulse powers and energies in a single transverse mode.

7.1 Outline.

Tapered waveguides allow the optical mode to expand during propagation along the cavity length. The reduced optical intensity therefore experiences a reduced nonlinear gain suppression. The advantages of the enhanced optical power in broad area lasers and mode control associated with narrow ridge waveguide lasers are therefore combined for high power tapered lasers. The Bow-Tie laser incorporates a narrow central waveguide for mode control and two tapered waveguide sections to avoid optically induced facet damage.

High power tapered waveguide lasers are introduced through a discussion of state of the art single pass travelling wave tapered optical amplifiers. The integration of preamplifiers and master oscillators with tapered waveguide postamplifiers is addressed. An overview of state of the art picosecond pulsed tapered waveguide laser systems is given. It is noted that work to date has focussed on the use of tapered structures as single pass postamplifiers for mode-locked laser systems.

The novel Bow-Tie laser is introduced as a high power semiconductor laser to be used as a monolithic picosecond pulse source. Compared with

straight guide lasers, the novel double tapered Bow-Tie laser is shown to offer an order of magnitude increase in power and energy under Q-switched operation. Enhanced power mode-locked operation is also described.

7.2 Tapered-Waveguide Amplifiers and Lasers.

The development of tapered-waveguide lasers results from demonstrations of single pass semiconductor tapered amplifiers [1-12]. The tapered amplifier maximises its efficiency by expanding the gain volume along the amplifier length in order to maintain a near uniform power density and hence reduced gain saturation [2]. Since the amplified beam is diverging the extent of the spatial overlap of the reflected backward travelling wave and the forward input wave is reduced relative to nontapered structures. Walpole and coworkers consider tapered-waveguide structures for lasers by allowing a 30% reflectivity at the narrow facet of 2mm long device. Powers of up to 2W are measured in a near-diffraction-limited (0.23°) lobe [13]. Straight waveguide distributed Bragg reflector lasers are also integrated with the tapered amplifiers by Mehuys and coworkers leading to single mode powers of 1.3W pulsed from an monolithic-active-grating master-oscillator power-amplifier device [14]. Continuous wave powers have subsequently increased to 2W [15] and more recently 3W [16]. External cavity tapered lasers are also demonstrated as high power, (1W), diffraction limited sources with a 50nm wavelength tunability [17].

The short pulsed operation of tapered-waveguide laser systems focuses on mode-locked operation in the 1-5GHz range [18-21]. Cavity design involving a mode-locked source as the master-oscillator and a

tapered-waveguide amplifier as the power-amplifier leads to actively mode-locked pulse trains with pulses as short as 4.2 ps with powers as high as 28W [18-19]. Passively mode-locked 4.1ps duration 5W peak power pulses are also demonstrated using a tapered-waveguide postamplifier configuration [20].

A single chip picosecond pulse source is demonstrated with a grating cavity [21]. In a direct comparison of straight with tapered-waveguide, Helkey demonstrates 4.2ps pulses with 1W power at 5GHz repetition rate for the tapered source. This indicates an energy enhancement of 2.3 over the straight waveguide control. It is monolithic picosecond pulse sources that are to be the focus of this work.

7.3 Q-switched Bow-Tie Lasers.

A schematic for the Bow-Tie laser used in the Q-switching experiments is given in figure 7.1. A bulk active layer is used for the GaAs/AlGaAs lasers considered [22]. A weak rib waveguide is formed by ion etching the tapers from 5 μm in the centre to 26 μm facets[15]. The adiabatic taper has a 6 degree half angle. The electrically isolated 90 μm long central waveguide region acts both as a transverse mode filter and saturable absorber under Q-switched operation. The electrical isolation between the contacts is 1-2 kΩ, and so intercontact leakage is expected to be small. The facets are uncoated, although power enhancements are anticipated through high reflectivity and low reflectivity coating of the rear and front facets respectively. Initial comparisons between tapered and nontapered multicontact lasers of otherwise identical dimensions indicate an order of magnitude increase in power and energy [22].

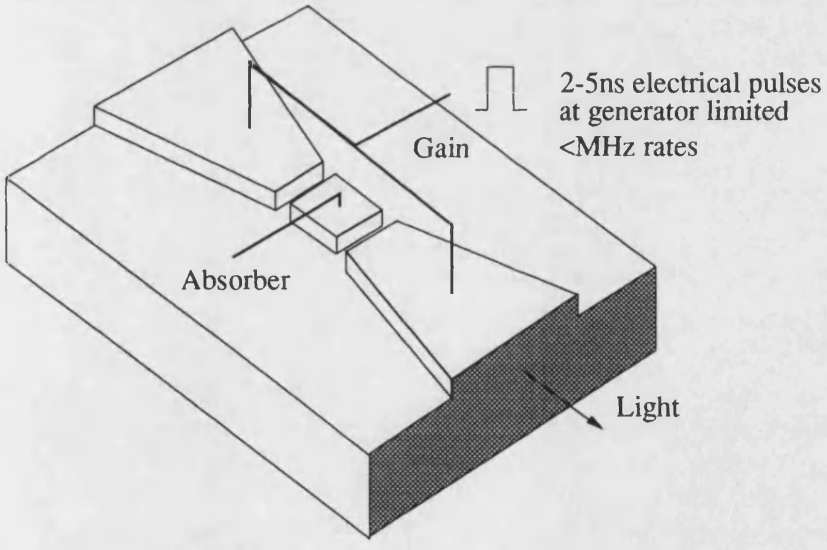

Figure 7.1 : Schematic for a double tapered waveguide Bow-tie laser with patterned p-side electrodes for picosecond pulsed operation.

For Q-switched operation, 25V, 2-5ns duration pulses are applied to the tapered gain sections. Step recovery diodes are used to allow subnanosecond rise and fall times. Impedance matching with a 47Ω surface mount resistor allows 500mA currents corresponding to three to five times the threshold current. A reverse bias is applied to the central nontapered section to enhance the carrier density in the gain sections prior to pulse turn on, shape the optical pulse and prevent subsequent pulsation after the Q-switched pulse. The experimental arrangement is given in figure 7.2.

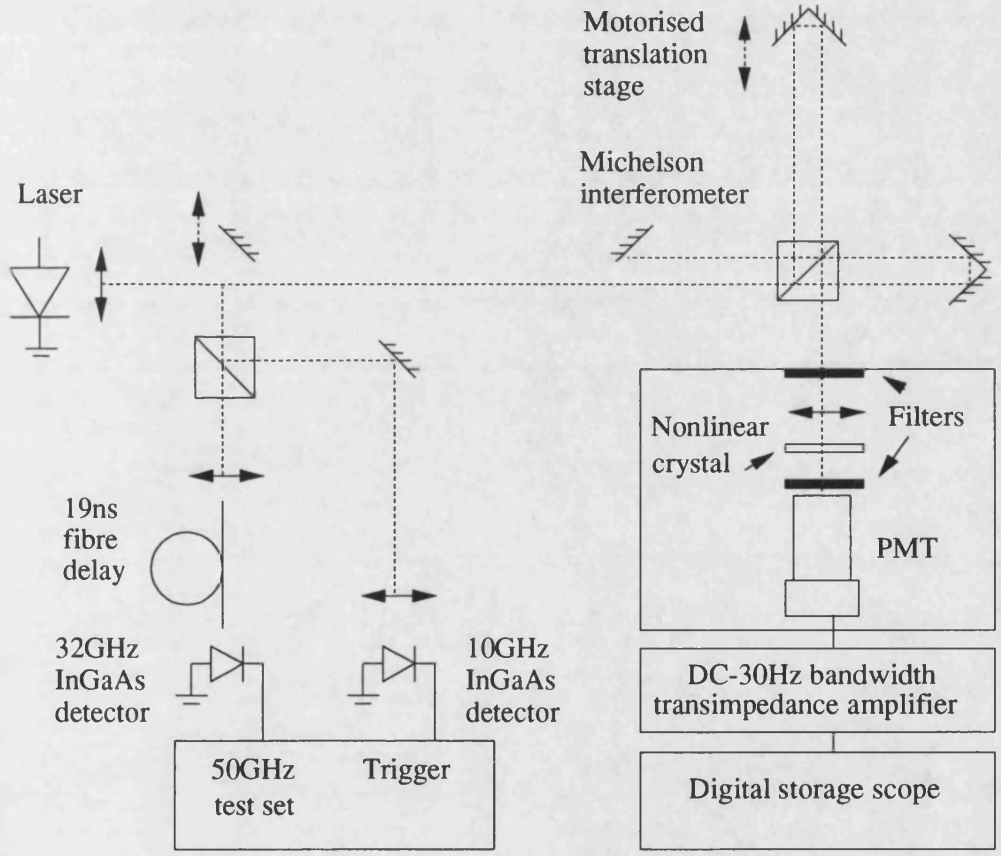

Figure 7.2 : Experimental arrangement for the assessment of picosecond pulsed Bow-tie lasers.

As the HP214B pulse generator has a 100ps timing jitter, the oscilloscope was triggered by the optical pulse. By splitting the optical beam, a 10GHz InGaAs photodetector is used as the trigger. A 19ns fibre delay preceding the 32GHz InGaAs signal photodetector allows sufficient pretrigger for the 50GHz oscilloscope to view the pulse used for triggering. A system limited 2ps timing jitter is observed for the photodetector measurement arrangement. Figure 7.3 shows the resolution limited oscilloscope trace for a 5.6W peak power, 21ps duration pulse. Tail free operation is achieved by shortening the gain section electrical drive for the given reverse bias.

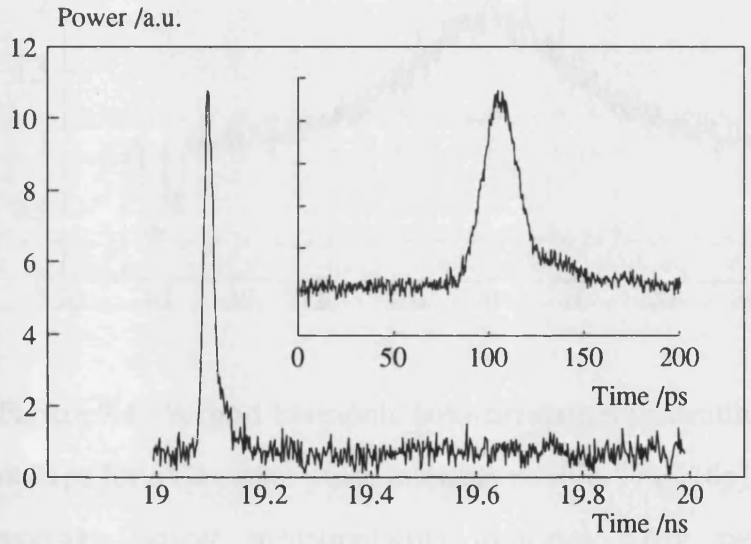

Figure 7.3 : Q-switched pulse profile measured with a 32GHz photodetector and 50GHz sampling oscilloscope. Tail-free pulsation is noted. Inset is an expanded trace to indicate profile detail. Laser number [15].

Pulse duration measurements are made by second harmonic autocorrelation as outlined in chapter 3. The oscilloscope trace suggests an

approximately Gaussian intensity profile, and a pulse energy of 116pJ is estimated from average power measurements. The oscilloscope trace allows the assumption that most of the power is in the 21ps duration pulse and that the pulse power is 5.6W. Q-switching results from nontapered bulk GaAs/AlGaAs lasers detailed in chapter 5 indicate pulse energies of up to 7pJ with peak powers of 350mW.

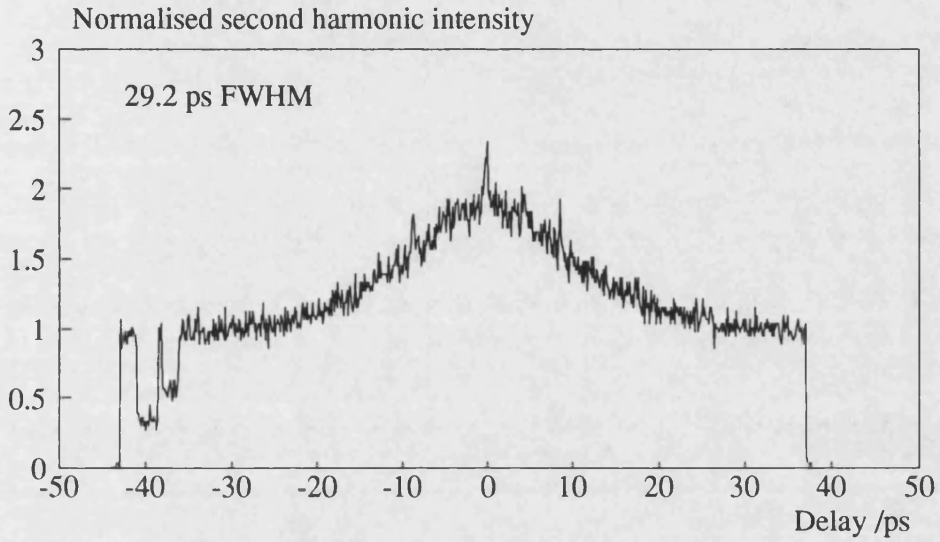

Figure 7.4 : Second harmonic autocorrelation indicating a pulse duration of 21ps for a Gaussian pulse intensity profile. The 116pJ pulse energy from average power measurements indicates 5.6W peak power. Laser number[15].

The transverse mode structure is monitored through the near field pattern. Figure 7.5 shows a single lobed pattern with a 17 μm full width at half maximum. The measurement is made by imaging the intensity profile at the laser facet onto a linearised infrared camera with a microscope objective. The

pattern is recorded with a digital storage oscilloscope. The near field width is calibrated by illuminating the laser chip of known width, and imaging the chip on the camera.

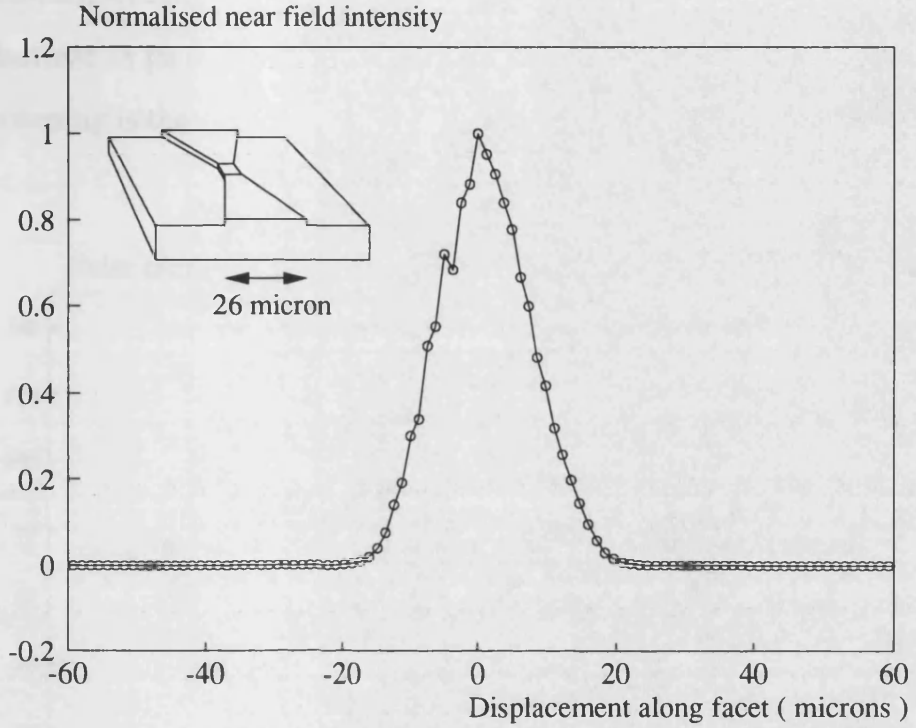

Figure 7.5 : The near field intensity pattern under Q-switched operation indicates a single spatial mode filling approximately two thirds of the 6° tapered waveguide. Laser number[15].

The effect of the saturable absorption allowed by reverse biasing the central waveguide section can be monitored by considering the output pulse profile as a function of absorber reverse bias. As the reverse bias is increased, the turn on delay time increases due to enhanced cavity losses. Longer duration electrical pulses are required to acheive enhanced population inversion required to bleach the absorber. In figure 7.6, the electrical pulse

duration of the gain section bias is optimised for each bias condition to enable high power tail free pulsation. Pulse width measurement is made by second harmonic autocorrelation. As the reverse bias is increased, and the sweep out time and optical losses are increased, the carrier density prior to pulse turn on is enhanced, leading in turn to a faster depletion and shorter duration pulses. The shortest 13 ps duration pulses are achieved for a reverse bias of -3.5V. A rebroadening is then noted as the optical losses become too high.

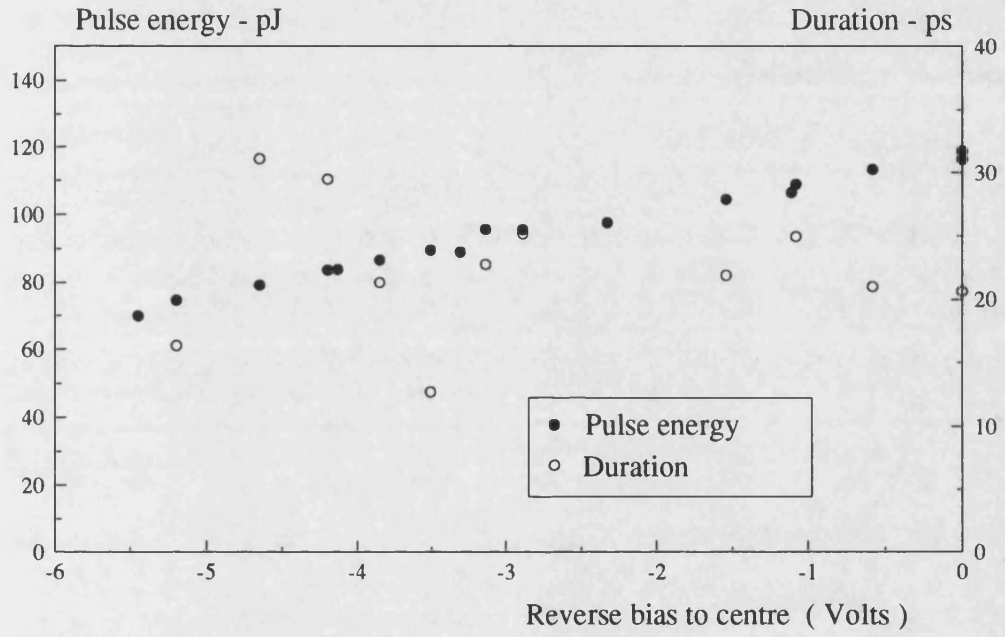

Figure 7.6 : Pulse energy and duration dependence on reverse bias. For a constant 500mA gain section bias, pulses as short as 13ps are measured at a absorber bias of -3.5V. A reduction in pulse energy is noted for tail free pulsation.

While the design of Bow-Tie lasers is best considered through detailed modelling [23-24], the complexity of the problem requires much experimental

data. Insight into optimum design is made through the comparison of lasers with varied taper angles, cavity lengths, absorber dimensions and bias schemes.

The central waveguide width and taper angle defines the proportion of the laser filled by the mode. Table 7.3 describes the optimum Q-switched operation for 500mA gain section bias. The half width of the near field is approximately half the waveguide width at the facet for the 3° half angle. Self-focussing is however noted for the wider 10° bow-tie leading to a nonoptimum use of the waveguide and multi-transverse-mode operation for long pulsed operation.

Half angle of taper	Absorber length	Facet width	Near field FWHM	Peak power (Q-switched)
3°	75 μm	15 μm	6 μm	5W[16]
6°6°	75 μm	26 μm	17 μm	6.9W[15]
10°	100 μm	22 μm	11 μm	3.3W[17]
	75 μm	40 μm	4 μm	3.2W[18]

Table 7.3 : Dependence of near field width and peak Q-switched power on taper angle for 300 μm long Bow-Tie lasers.

High frequency 1GHz modulation for forced Q-switched operation allows 41ps duration 1W peak power optical pulses. While the modulation is pulsed at a low duty cycle, heating at the junction limits the achievable powers and energies [25]. A patterned submount for p-side down mounting should allow more efficient cooling while allowing isolated electrical connection.

7.4 Monolithic Passively Mode-Locked Bow-Tie Lasers.

High power pulsed and CW mode-locking is achieved in InGaAs/GaAs multiquantum well Bow-Tie lasers. Stable generation of 750fs pulses with average powers of up to 35mW at frequencies of 132GHz are achieved. Both bulk active layer AlGaAs/GaAs [26] and quantum well InGaAs/GaAs [27] bow-tie lasers ar shown to mode-lock. For the AlGaAs/GaAs lasers average powers of up to 50mW have been achieved under pulsed conditions. Modulation was however sinusoidal with an estimated modulation depth of 95%. At a repetition rate of 100GHz, a time bandwidth product of 0.9 was estimated from both grating spectrometer and first order interferometric spectral measurement. Single contact InGaAs/GaAs tapered waveguide lasers are shown to mode-lock [28]. It is the enhanced mode-locked operation of the quantum well lasers that is to be considered in detail now.

Preliminary work by Summers and coworkers [27] on the InGaAs/GaAs laser has indicated continuous wave mode-locked operation with a time bandwidth product of 0.61. While average powers of around 17mW are readily generated for mode-locked pulse trains under a pulsed electrical modulation, increased electrical bias to the taper regions allows average powers of up to 35mW. As heat sinking has yet to be optimised, CW powers fall to 13.3mW. Mode-locked operation is maintained through varying the negative or subthreshold bias voltage to the centre absorbing section. Temporal characterisation is made with a first order cross-correlation technique [28]. Second harmonic intensity correlation is however a more widely accepted technique for pulse characterisation, as the measurement is not as dependent on the coherence of the pulse train. The completeness of mode-locking also

becomes apparent through the background to peak ratio in the second order autocorrelation. This is discussed in appendix B.

Second harmonic generation autocorrelation is used for a 400 μm device with a 3° taper angle and 70 μm long central absorber section, whose threshold current is 180mA[19]. 700 fs pulse widths are estimated assuming a Gaussian pulse shape. The ratios in the autocorrelation trace indicate only partial mode-locking confirmed by the observation on a sampling oscilloscope of self-pulsations at the start of the electrical pulse. This and previous measurements [27] indicate that complete mode-locking may result under CW operation. A grating spectrometer is used with a linearised infrared camera to measure the 971GHz spectral full width at half maximum. Assuming here that the pulse duration is 700fs, a moderately chirped time-bandwidth product of 0.68 results.

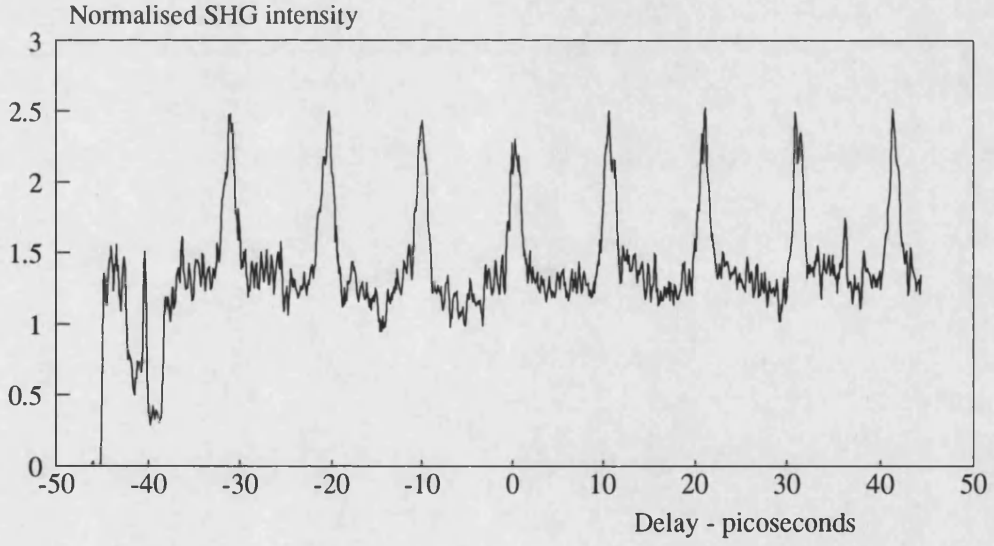

Figure 7.7 : Second harmonic autocorrelation trace indicating mode-locking in a InGaAs/GaAs multiquantum well Bow-Tie laser. The tapered gain sections are biased at 273mA and the central absorber is

biased at 0.42V[19].

With a centrally placed absorber, the cavity is well designed for colliding pulse mode-locked operation. Such operation is observed through half round trip features in the autocorrelation traces and alternate mode suppression in the optical spectra. The autocorrelation in figure 7.8 indicates optimised conditions for colliding pulse mode-locking operation.

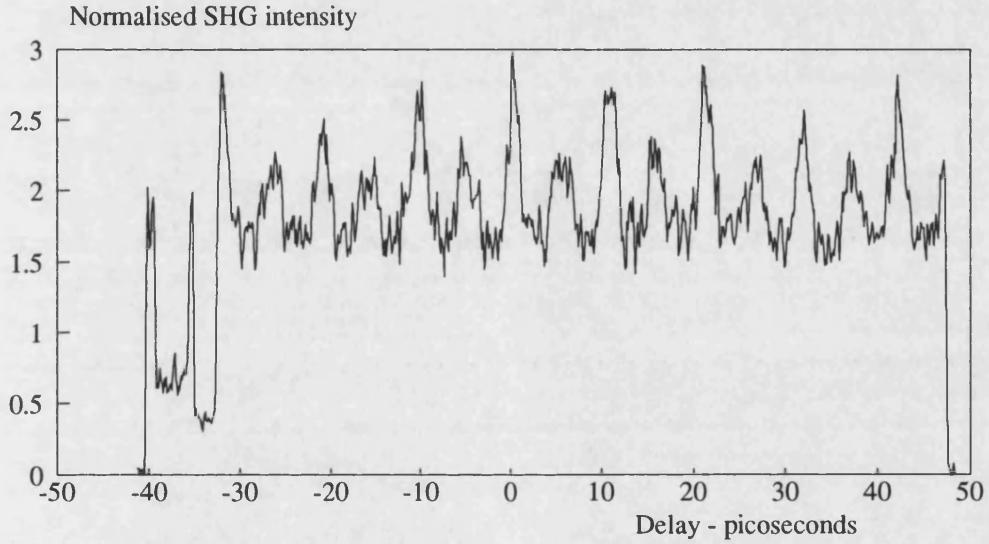

Figure 7.8 : Second harmonic autocorrelation trace indicating colliding pulse mode-locking in a InGaAs/GaAs multiquantum well Bow-Tie laser. The tapered gain sections are biased at 273mA and the central absorber is biased at 0.07V[19].

No pulse narrowing is apparent and contrast ratios differ for pulsations at the round trip and half round trip spacing. This is likely to result from a noncentrally located absorber section. The autocorrelations are made for variable delays of ±30ps and so self-pulsations with durations of greater than 60ps become evident through an apparent shift in the background level across the trace. Depending on the proportion of energy in the self-pulsations, the background level could vary between one and two. A discussion of the contributions to the autocorrelation traces in the appendix highlights that at least 66% of the energy is phase-locked.

7.5 References.

1. MEHUYS, WELCH, D.F., and GOLDBERG, L., "2.0W CW diffraction limited tapered amplifier with diode injection", Electronics Letters, 28, 1944-1946, 1992.

2. JACOB, J.H., ROKNI, M., KLINKOWSTEIN, SINGER, S., "Expanding beam concept for building very large excimer laser amplifers", Applied Physics Letters, 48, 318-320, 1986.

3. WALPOLE, J.N., KINZTER, E.S., CHINN, S.R., WANG, C.A., and MISSAGGIA, L.J., "High-power strained layer InGaAs/AlGaAs tapered travelling wave amplifier", Applied Physics Letters, 61, 740-742, 1992.

4. GOLDBERG L., MEHUYS, D., and HALL, D.C., "3.3W CW diffraction limited broad area semiconductor amplifier", Electronics Letters, 28, 1082-1084, 1992.

5. GOLDBERG, L., MEHUYS, D., "21W broad area near-diffraction limited semiconductor amplifier", Applied Physics Letters, 61, 633-635, 1992.

6. KINZTER, E., WALPOLE, J.M. CHINN, S., WANG, C., and MISSAGIA, L., "High power strained layer amplifiers and lasers with tapered gain regions", IEEE Photonics Technology Letters, 5, 605-608, 1993.

7. MEHUYS, D,M GOLDBERG, L., and, WELCH, D.F., "5.25W CW near diffraction limited tapered stripe semiconductor optical amplifier", IEEE Photonics Technology Letters, 5, 1179-1182, 1993.

8. MEHUYS, D., GOLDBERG, L., WAARTS, R., WELCH, D.F., "4.5W CW near diffraction limited tapered stripe semiconductor optical amplifier", Electronics Letters, 29, 219-221, 1993.

9. YEH, P.S., WU, I.-F., JIANG, S., DAGENAIS, M., "High power high gain monolithically integrated preamplifier/power amplifier", Electronics Letters, 29, 1981-1983, 1993.

10. BENDELLI, G., KOMORI, K., ARAI, S., and SUEMATSU, "A new structure for high power TW-SLA", IEEE Photonics Technology Letters, 3, 42-44, 1991.

11. BENDELLI, G., KOMORI, K., and ARAI, S., "Gain saturation and propagation characteristics of index guided tapered waveguide travelling wave semiconductor laser amplifiers", IEEE Journal of Quantum Electronics, 28, 447-458, 1992.

12. LANG, R.J., HARDY, A., PARKE, R., MEHUYS, D., DZURKO, K., O'BRIEN, S., WELCH, D.F., and SCIFRES, D.R., "Numerical modelling of semiconductor laser amplifiers", proceedings CLEO, paper CTuI2, 1993.

13. WALPOLE, J.N., KINZTER, E.S., CHINN, S.R., LIVAS, J.C., WANG, C.A., MISSAGGIA, L.J., WOODHOUSE, J.D., "High power monolithic tapered semiconductor oscillators", proceedings CLEO, invited paper CMA1, 1994.

14. MEHUYS, D., WELCH, D.F., PARKE, R., WAARTS, R.G., HARDY, A., and SCIFRES, D., "High power diffraction-limited emission from a monolithically integrated active grating master oscillator power amplifier", Electronics Letters, 27, 492-494, 1991.

15. PARKE, R., WELCH, D.F., HARDY, A., LANG, R.J., MEHUYS, D., O'BRIEN, S., DZURKO, K.M., and SCIFRES, D.R., "2.0W cw diffraction-limited operation of a monolithically integrated master oscillator power amplifiers", IEEE Photonics Technology Letters, 5, 297-300, 1993.

16. WELCH, D.F., PARKE, R., O'BRIEN, S., DZURKO, K., MEHUYS, D., LANG, R., and OSINSKI, J., "High power, diffraction limited laser diodes", proceedings LEOS, Invited paper SCL1.2, 1994.

17. MEHUYS, D., WELCH, D.F., and SCIFRES, D.R., "High power diffraction limited external cavity tunable diode lasers", proceedings LEOS, paper SCL7.3, 1993.

18. GOLDBERG, L., MEHUYS, D., and WELCH, D., "High power mode-locked compound laser using a tapered semiconductor amplifier", IEEE Photonics Technology Letters, 6, 1070-1072, 1994.

19. MAR, A., HELKEY, R., BOWERS, J.E., MEHUYS, D., and WELCH, D., "Mode-locked operation of a master oscillator power amplifier", IEEE Photonics Technology Letters, 6, 1067-1069, 1994.

20. MAR, A., HELKEY, R., BOWERS, J., MEHUYS, D., and WELCH, D., "Mode-locked operation of a master oscillator power amplifier", proceedings LEOS, paper MSFL4.2, 1993.

21. HELKEY, R., "Mode locked semiconductor lasers", proceedings LEOS, Invited paper MSFL3.2., 1993.

22. WILLIAMS, K.A., SARMA, J., WHITE, I.H., PENTY, R.V., MIDDLEMAST, I., RYAN, T., LAUGHTON, F.R., and ROBERTS, J.S., "Q-switched bow-tie lasers for high energy picosecond pulse generation", Electronics Letters, 30, 320-321, 1994. The structure is given as an example in figure 2.1.

23. AGRAWAL, G.P., "Fast-Fourier-transform based beam-propagation model for stripe geometry semiconductor lasers : inclusion of axial effects", Journal of Applied Physics, 56, 3100-3109, 1984.

24. LANG, R.J., HARDY, A., PARKE, R., MEHUYS, D., O'BRIEN, S., MAJOR, J., and WELCH, D., "Numerical analysis of flared semiconductor laser amplifiers", IEEE Journal of Quantum Electronics, 29, 2044-2051, 1993.

25. WHITE, I.H., WILLIAMS, I.H., HUGHES, D.M., BURNS, D., and SIBBETT, W., "High power picosecond pulse generation in multicontact diode lasers using modified Q-switching techniques", proceedings CLEO Europe, Invited paper CTuL1, Amsterdam, 1994.

26. WILLIAMS, K.A., WHITE, I.H., LAUGHTON, F.R., SARMA, J., PENTY, R.V., MIDDLEMAST, I., RYAN, T., and ROBERTS, J.S., "Passive mode-locking of Bow-Tie lasers", proceedings CLEO Europe, paper CTuL2, Amsterdam, 1994.

27. SUMMERS, H.D., WHITE, I.H., LAUGHTON, F.R., RALSTON, J.D., PENTY, R.V., WILLIAMS, K.A., SARMA, J., MIDDLEMAST, I., and RYAN, T., "Passive mode-locking in p-doped MQW bow-tie lasers", proceedings CLEO, Baltimore, 1995.

28. CHOI, K.N., and TAYLOR, H.F., "Novel cross-correlation technique for characterisation of subpicosecond pulses from mode-locked semiconductor lasers", Applied Physics Letters, 62, 1875-1877, 1993.

CONCLUSIONS

Overview.

Q-switched semiconductor diode lasers are described in terms of their operational characteristics and in the context of the wide variety of available techniques for picosecond pulsed diode lasers. Through a discussion of the requirements of picosecond pulse laser systems and applications, critical pulse parameters are highlighted in the introductory *chapter 1*. Pulse profiles, durations and stability can be resolution and bit rate limiting in signal processing and communications applications. Beam profile, peak power and divergence are performance limiting in sensing and ranging applications. The spectral chirp defines the fibre propagation characteristics of the generated pulses. It is noted that while pulse parameters may in some modes of operation need stringent control, not all are simultaneously important, allowing for a wide range of potential schemes for picosecond pulse generation in diode lasers.

Physical processes key to the picosecond pulsed operation of diode lasers is discussed in *chapter 2*. Bulk and quantum well structures are compared in terms of the density of states functions to highlight the sublinear gain carrier density relationship. While it was established that a linear gain approximation could be made for bulk lasers operating close to transparency, it was also apparent that the approximation was not acceptable for the large changes of carrier density experienced under Q-switched operation. The sublinearity is exacerbated for quantum well lasers as a direct result of the characteristic step-like density of states function. Because of this sublinearity, enhancements to the differential gain observed at transparency do not translate to improved

picosecond Q-switched operation of quantum well lasers relative to bulk lasers as noted in *chapter 5*. Indeed further nonlinearities resulting from carrier transport (*chapter 4*) to and from the wells leads to a degraded picosecond pulsed performance in many of the lasers considered.

Comparisons are also made between lasers fabricated in the InGaAsP and AlGaAs material systems. The narrower band gap of the InGaAsP lasers leads to significant levels of Auger recombination. The increased levels of nonradiative recombination impair the picosecond pulsed performance, limiting peak powers. The nonlinear gain suppression term is also introduced to account for spectral and spatial hole-burning. Increased suppression in InGaAsP lasers broadens both gain-switched and Q-switched pulse durations. *Chapter 3* summarises the established techniques for picosecond pulse generation in diode lasers. State of the art approaches for gain-switching, Q-switching and mode-locking are reviewed. Passive and active schemes are considered. The role of saturable absorbers in Q-switching and mode-locking is discussed and the use of multicontact structures for improved control of picosecond pulsed diode lasers is considered. *Chapters 1 to 3* are intended to describe the motivation behind the work, to review the physics key to the picosecond pulsed operation of diode lasers, and finally to establish the current status of research into picosecond pulsed semiconductor lasers. A general discussion of measurement techniques and their limitations is also included.

The subsequent four chapters include experimental and theoretical work which build on this to develop picosecond sources optimised for current and future applications. At the outset, *chapters 4 and 5* highlight the limitations of quantum well lasers under gain-switched and Q-switched operation. *Chapter 4* is a general review of nonlinear gain suppression mechanisms through a

systematic comparison of laser structures. The structures considered isolate carrier transport and spatial hole-burning effects from spectral hole burning and carrier heating. The spectral and temporal profiles are simulated with good agreement for the first time to take into account the carrier transport effects. Time constants for the carrier diffusion across the separate confinement layers to the wells, and for the thermionic emission from the wells to the barriers are evaluated to be 40ps and 80ps respectively from the theory experiment comparison. Pulse profile distortion as a result of nonlinear gain suppression at high injection and under high field conditions is also characterised, indicating limits to peak achievable powers for gain-switched InGaAsP lasers to around 20mW. The role of longitudinal mode spatial hole burning is also experimentally and theoretically explored. The modelling is based on empirical relations describing the interplay of carrier densities at the end of the laser with the suppressed carrier density in the centre and the optical intensity. While the relations are approximations for the small signal operation, and are shown in *chapter 4* to hold for gain-switched operation, the modelling is carried out predominantly to confirm the carrier transport model for a second laser structure. It does however become apparent that such gain suppressing mechanisms only limit device performance through a pulse broadening and profile asymmetry and are therefore highly undesirable. The slow fall time off the optical pulses is likely to degrade error rates in communications applications, and limit the resolution in sampling applications. Asymmetry in the optical spectra is observed to be characteristic of the nonlinear gain suppression. To enhance the peak optical powers, a saturable absorbing section is included in the Q-switched lasers of *chapter 5*. Peak powers of up to 100mW for InGaAsP lasers are measured. GaAs lasers are also assessed, with peak pulse powers of

up to 350mW.

Chapters 5 and 6 consider the stability of picosecond pulsed diode lasers through a detailed assessment of timing jitter. The stability of forced Q-switched multicontact InGaAsP/InP and GaAs/AlGaAs is discussed for the first time. Operating ranges over which tail free pulsation is maintained are highlighted. Timing jitter down to 900fs for lasers operating at 2GHz is measured and further reductions are anticipated at higher modulation rates. Continuous wave injection and self seeding techniques are highlighted for the additional control over spectral purity and temporal stability in gain-switched and Q-switched lasers. The stability of gain-switching, Q-switching and mode-locking are compared for lasers of similar structure for the first time in *chapter 6*. Feedback techniques are introduced to enhance the stability at reduced system cost. The novel optoelectronic feedback scheme allows timing jitter of 800fs at 1GHz repetition rates - a significant reduction over the 1.3ps timing jitter achieved for forced Q-switching at the same repetition rate. While reduced timing jitter is observed at elevated bias conditions, a trade off between pulse profile asymmetry and stability is ultimately observed. Fluctuations in the pulse profile, characterised by amplitude noise, is observed to couple through to phase noise and enhance timing instabilities through a modulation of the cavity refractive index. Gain suppression evident in InGaAsP lasers appears to dampen such coupling however, leading to reduced jitter relative to AlGaAs lasers. The summary of the feedback techniques in table 6.1 highlights the limits to timing jitter in picosecond pulsed lasers. The Fabry-Perot lasers are pulsed using a variety of feedback schemes with a timing jitter of the order of 1ps. It is only under mode-locked conditions that the jitter is reduced to the system limit (160fs). It is however demonstrated that mode-locked operation without a stable

microwave source can be achieved with the hybrid optical feedback scheme to allow 240fs timing jitter, with the same pulse durations and energies as observed for mode-locking. A discrimination between self-seeding and the extended cavity operation observed for antireflection coated lasers is observed. While no jitter reduction is noted for self-seeding a noncoated laser, considerable stability enhancement is observed for the AR coated laser.

Chapter 7 considers further enhancements to Q-switched pulse powers and energies through the use of a novel tapered waveguide multicontact Bow-Tie laser. Q-switched powers are an order of magnitude greater than equivalent nontapered lasers. Record pulse energies of over 100pJ are readily achieved in a single spatial mode, with powers of up to 7W. The mode-locked operation of Bow-tie lasers is also considered. For the first time, passive monolithic mode-locking is achieved within a tapered waveguide structure, enabling the generation of 700fs pulses at a repetition rate of 94GHz with average powers of 17mW. Further work to enhance the Q-switched optical power focuses now on the use of tapers in arrays and postamplification.

Developments.

The work as a whole has initiated significant industrial and academic interest in areas as diverse as electrooptic sampling for high speed optical analogue to digital conversion, millimetre-wave generation for astronomy and the mobile communications market, and nonlinear frequency conversion. For the techniques and laser designs described so far in this thesis to adequately fulfil their roles in these exciting applications, further optimisation is still required.

While considerable enhancements to the optical peak powers have been achieved for Q-switched Bow-Tie lasers, limits are not fully understood. It is observed experimentally in *chapter 7* that the optical mode does not completely fill the waveguide, leading to considerable inefficiency. It is for this reason that a two dimensional time resolved model has been developed at Bath University, and is currently being implemented to describe the experimentally characterised gain-switched dynamics of Bow-Tie lasers for varied waveguide design [1]. Good agreement between experiment and theory has been achieved for optical gain-switched pulse powers, profiles, and near field distributions. Transverse mode spatial hole burning is expected to limit the peak achievable powers in the broader devices, as highlighted in the instantaneous spatially resolved carrier density and intensity profiles given in figure 8.1. Here the intensity and carrier density profiles for a 4° and a 7° half angle Bow-Tie laser are compared to highlight the strong self focussing experienced for the broader device. Optimisation of the current injection is to be investigated to enhance the optical overlap with the injected carriers. Such a model should ultimately be extended to Q-switched operation.

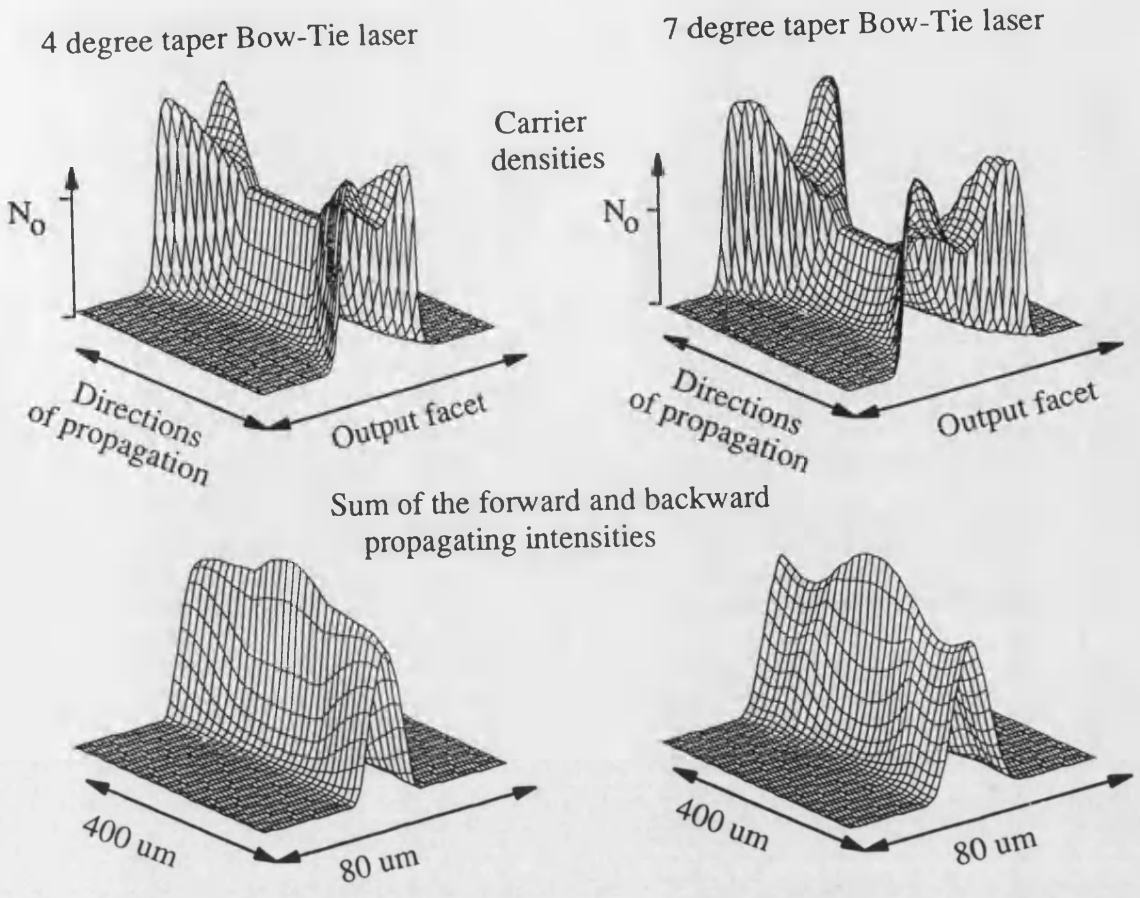

Figure 8.1 : Simulation of transverse mode spatial hole burning in a gain-switched Bow-Tie laser, using a model currently being developed at Bath University.

Alternative schemes for power enhancement have considered the use of multistripe Bow-Tie arrays. An example structure is given in figure 8.2. The work has so far demonstrated sufficiently close coupling and uniformity of mode intensity to generate 13ps duration Q-switched pulses [2]. Powers have so far been limited to 10W, as a result of low electrical isolation between saturable

absorbing and gain sections, and unoptimised electrical pulse generators. The work has however shown an order of magnitude reduction in the achieved Q-switched pulse duration when compared to the previous work on arrays.

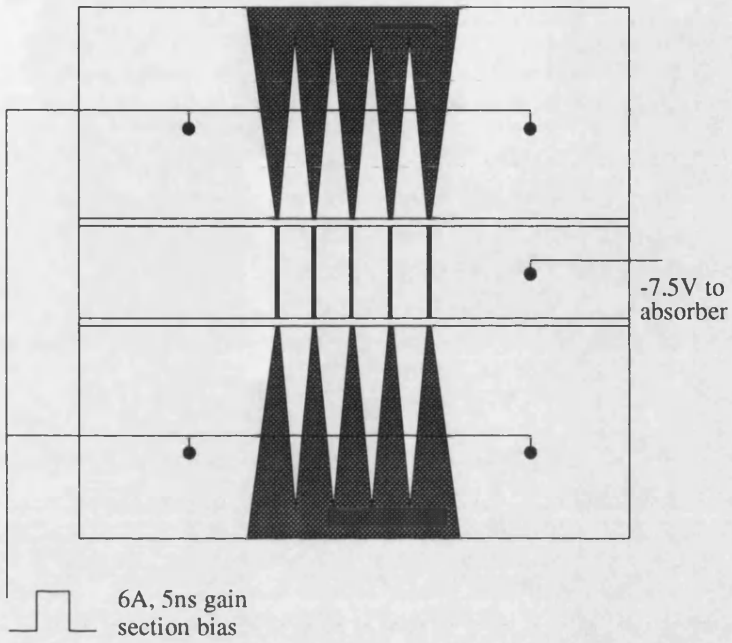

Figure 8.2 : An array of Bow-Tie lasers for enhanced power picosecond pulse generation.

The use of tapered amplifiers has also been explored for further pulse power enhancement [3]. A schematic diagram for the experimental arrangement is given in figure 8.3. While preliminary measurements were made with a nonoptimally AR coated amplifier, 9dB of net gain enabled the generation of 45W peak power optical Q-switched pulses. Order of magnitude improvements are expected for improved amplifier facet coatings. Tapered amplifers are also expected to allow enhanced mode-locked powers for pumping terrahertz switches in millimeter wave generation.

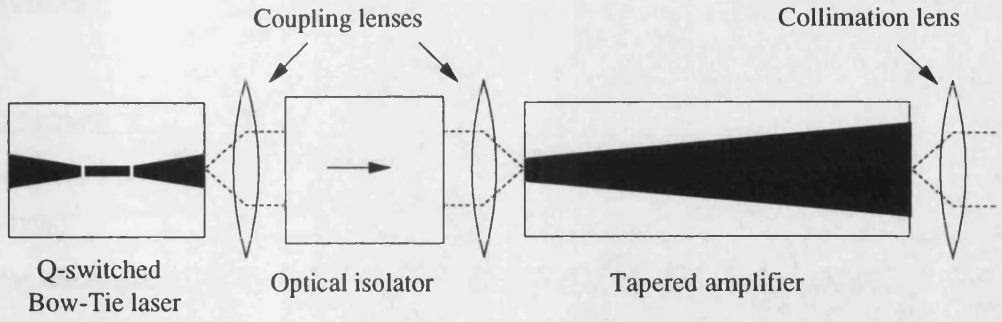

Figure 8.3 : Postamplification with a flared waveguide amplifier for enhanced power picosecond pulse generation.

While work has so far focussed predominantly on 880nm AlGaAs Bow-Tie lasers, interest in other wavelengths has lead to the investigation of Q-switched operation of 750nm wavelength Bow-Tie lasers. Requirements for Q-switched pulse generation at higher repetition rates has lead to the use of a pulsed radio frequency modulation for the saturable absorbing section. Using moderate currents of up to 500mA to the gain sections, and modulation powers of 32dBm, bursts of 4W peak power, 30ps duration Q-switched pulses have already been generated in trains at 700MHz. The product of the pulse power and duration gives a pulse energy of 120pJ. The work aims to develop a high energy (nanojoule) Q-switched diode laser pump for frequency tripled ultraviolet light generation.

References.

1. WILLIAMS, K.A., WHITE, I.H., LAUGHTON, F.R., JIANG, Z., and PENTY, R.V., "Gain-switched dynamics of tapered waveguide Bow-Tie lasers", submitted for publication at CLEO 1996.

The time resolved two dimensional model was originally written by Ziping Jiang, now at the Department of Electrical Engineering at the Chinese University of Hong Kong.

2. WILLIAMS, K.A., KITCHER, D.J., LAUGHTON, F.R., WHITE, I.H., and PENTY, R.V., "Picosecond Q-switched Bow-Tie Laser array", submitted for publication at IQEC 1996.

The development of Bow-Tie arrays has been a result of the efforts of Dan Kitcher at the School of Physics at the University of Bath.

3. ZHU, B., WHITE, I.H., WILLIAMS, K.A., LAUGHTON, F.R., and PENTY, R.V., "High peak power picosecond optical pulse generation from Q-switched Bow-Tie laser with a tapered travelling wave amplifier", submitted for publication, IEEE Photonics Technology Letters.

The work on the postamplification of Q-switched Bow-Tie lasers has been carried out by Benyuan Zhu at the School of Physics at the University of Bath.

APPENDIX A

This appendix summarises the laser diodes used throughout the text, cross referencing lasers with both experimental work and wafer details.

Summary of Diode Lasers and Wafers.

The lasers are ordered in table 9.1 as they are encountered in the text of chapters 4-7. Only a brief description of the layers is given as many of the lasers are from the same wafers. Available data for the wafers are given in table 9.2.

Included in the lists are many lasers where the p-side metallisation has been segmented to create a saturable absorbing centre [4-11,15-19]. Excluding the two contact Fabry-Perot laser [5], the lasers are symmetrically segmented such that an electrically isolated saturable absorber section is created. The lengths of each of the three resulting electrodes are given. For the five Bow-Tie lasers [15-19], the waveguide is straight in the central section and then flares out in the two end sections to the specified aperture width at both facets. Included in the tables is a cross reference guide to the chapter sections where the lasers are investigated along with a cross reference with the letters [A-J] for the wafer details tabulated in table 9.2. While data for the InGaAsP/InP lasers operating at 1.5μm are limited, the layer structures for the all the supplied wafers are given in tables 9.3, 9.4 and figure 9.1.

Number	Laser design	Section
1. LW5386	Bulk InGaAsP active layer [A]	§4.4
	Two λ/8 phase shifts in DFB grating	
	Wavelength 1536nm, threshold current 26mA.	
2. LW6484	Five InGaAs quantum well active layer [B]	§4.5
	2λ/8 phase shifts in DFB grating	§6.4
	Threshold current 23mA.	
	Device length 350μm	
3. LW6480	Five InGaAs quantum well active layer [B]	§4.6
	λ/4 phase shift in DFB grating	
	Threshold current 16mA.	
	Device length 380μm	
4. DF755	Bulk InGaAsP active layer [C]	§5.5
	λ/4 phase shift in DFB grating	
	Wavelength 1533nm.	
	Threshold current 40mA.	
5. DF1094	Six InGaAs quantum well active layer [D]	§5.6
	Fabry-Perot cavity.	§5.8
	Multicontact with one 300 and one 100 micron electrode	§6.3
	Wavelength 1.52μm, threshold current 22mA	
6. DF886	Six InGaAs quantum well active layer [D]	§5.6
	λ/4 phase shift in DFB grating	§6.3
	Multicontact with three 200 micron long electrodes, the two ends are connected together off-chip.	
	Wavelength 1.505μm, threshold current 32mA	
7. UB507J	Bulk GaAs active layer [E]	§5.7
	Fabry-Perot cavity.	
	Multicontact with 85, 75, 85 micron long electrodes. The two ends are connected together off-chip. The waveguide is 7μm wide.	
	Wavelength 880nm.	
8. UB485D	Bulk GaAs active layer [E]	§5.7
	Fabry-Perot cavity.	
	Multicontact with 235, 75, 235 micron long electrodes. The two ends are connected together off-chip. The waveguide is 7μm wide.	
	Wavelength 880nm.	
9. UB521I	Bulk GaAs active layer [E]	§5.7
	Fabry-Perot cavity.	
	Multicontact with 315, 75, 315 micron long electrodes. The two ends are connected together off-chip. The waveguide is 7μm wide.	
	Wavelength 880nm.	

10. S30C	Dual quantum well GaAs active layer [F] Fabry-Perot cavity. Multicontact with 75, 75, 75 micron long electrodes. The two ends are connected together off-chip. The waveguide is 7μm wide. Wavelength 850nm.	§5.7
11. S33C	Dual quantum well GaAs active layer [F] Fabry-Perot cavity. Multicontact with 75, 75, 75 micron long electrodes. The two ends are connected together off-chip. The waveguide is 7μm wide. Wavelength 850nm.	§5.7
12. LW5853	Multiquantum well InGaAs/InGaAsP active layer [G] Fabry-Perot cavity. Threshold current 30mA, device length 400μm	§6.4
13. WG3	Bulk InGaAsP active layer. [H] Fabry-Perot cavity. 400μm long.	§6.5
14. MGC4	Bulk InGaAsP active layer. [I] Fabry-Perot cavity with one facet AR coated to 3% reflectivity. The second facet is cleaved to give 30% reflectivity. Threshold current 70mA.	§6.5
15. BT120A	Bulk GaAs active layer. [E] Fabry-Perot Bow-Tie cavity. Multicontact with 100, 75, 100μm long electrodes. The end contacts are joined together off-chip. The waveguide is 5μm wide at the centre and flares symmetrically and linearly to 15μm at the facets. Threshold current 82mA	§7.3
16. BT123A	Bulk GaAs active layer. [E] Fabry-Perot Bow-Tie cavity. Multicontact with 100, 75, 100μm long electrodes. The end contacts are joined together off-chip. The waveguide is 5μm wide at the centre and flares symmetrically and linearly to 26μm at the facets. Threshold current 101mA	§7.3
17. BT125A	Bulk GaAs active layer. [E] Fabry-Perot Bow-Tie cavity. Multicontact with 100, 75, 100μm long electrodes. The end contacts are joined together off-chip. The waveguide is 5μm wide at the centre and flares symmetrically and linearly to 40μm at the facets. Threshold current 129mA	§7.3
18. BT163A	Bulk GaAs active layer. [E] Fabry-Perot Bow-Tie cavity. Multicontact with 90, 100, 90μm long electrodes. The end contacts	§7.3

	are joined together off-chip. The waveguide is 5μm wide at the centre and flares symmetrically and linearly to 22μm at the facets. Threshold current 135mA	
19. BT82D70	Three quantum well InGaAs active layer.[J] Fabry-Perot Bow-Tie cavity. Multicontact with 160, 70, 160 micron long electrodes. The end contacts are joined together off-chip. The waveguide is 5μm wide at the centre and flares symmetrically and linearly to the facets. Threshold current 180mA	§7.4

Table 9.1 : Lasers used in the experimental work. The number in the left hand column is used to identify the laser when it is first encountered in the text. The second code is also serial number specific to the laser which is included for completeness, although it offers no additional information. The right hand column highlights the sections of the thesis where experimental results are described. The letters [A-J] indicate the wafer as described in table 9.2.

Number	Wafer details	Lasers
A. BB607	Bulk active layer InGaAsP/InP Wavelength 1.5μm. Laser supplied by BNR Europe Limited	1
B. A2322	Five InGaAs quantum wells in the active layer. Wavelength 1.5μm. InGaAsP barriers at 1.15μm. Upper and lower waveguides are both 0.2μm in thickness. Lasers supplied by BNR Europe Limited	2,3
C. BB65312A	Bulk active layer InGaAsP/InP Wavelength 1.5μm Laser supplied by BNR Europe Limited	4
D. C957/3	Six quantum wells in the active layer. 75Å InGaAs quantum wells with 100Å InGaAsP barriers. Upper and lower waveguides are 0.21μm and 0.24 μm in thickness respectively. Wavelength Lasers supplied by BNR Europe Limited	5,6
E. QT476	Bulk active layer GaAs, details given in table 9.3. Wavelength 880nm. Wafer supplied by University of Sheffield	7-9 15-18
F. QT550	Dual quantum well GaAs active layer. Wavelength 850nm. Details given in table 9.4. Wafer supplied by University of Sheffield	10,11
G. A2249/G2	Multiquantum well active layer InGaAsP/InP. Wavelength 1.5μm Laser supplied by BNR Europe Limited	12
H.	Bulk active layer InGaAsP/InP Wavelength 1.5μm Laser supplied by BNR Europe Limited	13
I.	Bulk active layer InGaAsP/InP Wavelength 1.5μm One stripe from a multichannel grating cavity laser. Zhu et al, IEEE Photonics Technology Letters, 3, 348, 1994.	14
J. D70	Three InGaAs quantum wells. Wavelength 1.02μm Details given in figure 9.1 Wafer supplied by Fraunhofer Institute	19

Table 9.2 : Wafers from which lasers were fabricated. The number in the left hand column is used to identify the wafer when it is first encountered in the text. The second code is also serial number specific to the wafer which is included for completeness, although it offers no additional information. The right hand column indicates the lasers which were fabricated from the wafer.

	Material	Doping	Thickness
Capping layer	GaAs	$5x10^{18}cm^{-3}$ Zn	0.3μm
	$Al_{0.36}Ga_{0.64}As$	$7.5x10^{17}cm^{-3}$ C	1.6μm
	$Al_{0.36}Ga_{0.64}As$		0.4μm
Active layer	GaAs		0.17μm
	$Al_{0.36}Ga_{0.64}As$	$7.5x10^{17}cm^{-3}$ Si	2.0μm
	GaAs	$1.2x10^{18}cm^{-3}$ Si	1.0μm
n+ substrate	GaAs		

Table 9.3 : Layers for bulk GaAs/AlGaAs wafer QT746.[E]

	Material	Doping	Thickness
Capping layer	GaAs	$5x10^{18}cm^{-3}$ Zn	0.3μm
	$Al_{0.6}Ga_{0.4}As$]	$1.6x10^{18}cm^{-3}$ C	1.6μm
	$Al_{0.6}Ga_{0.4}As$		
Active layer	103Å GaAs wells, 100Å $Al_{0.6}Ga_{0.4}As$ barriers		
	$Al_{0.25}Ga_{0.75}As$		0.2μm
	$Al_{0.6}Ga_{0.4}As$	$1.1x10^{18}cm^{-3}$ Si	1.6μm
	GaAs	$5x10^{17}cm^{-3}$ Si	1.0μm
n+ substrate	GaAs - vertical freeze grown (100) 3° to (110)		

Table 9.4 : Layers for dual quantum well GaAs/AlGaAs wafer QT550.[F]

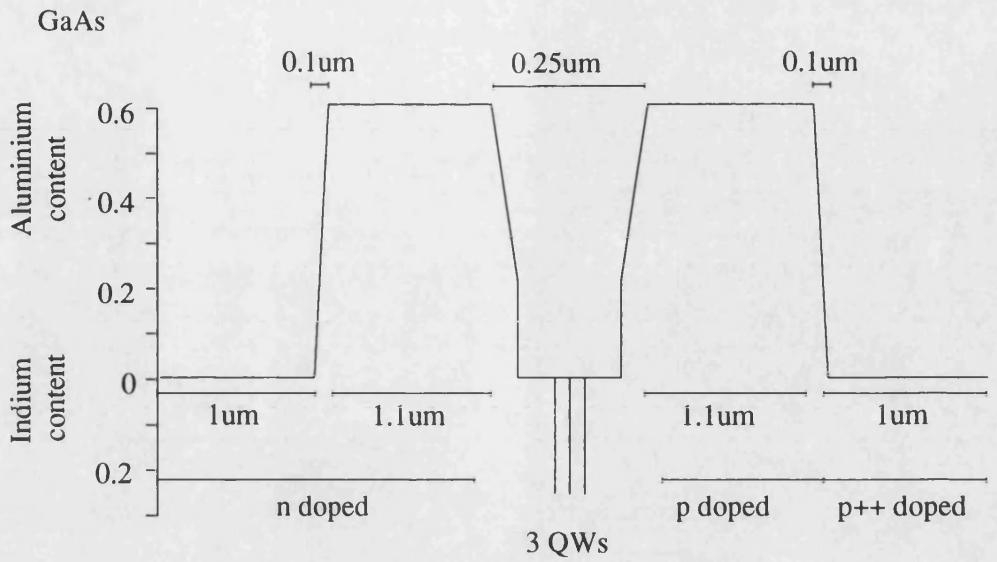

Figure 9.1 : A schematic of the layer structure of Fraunhofer wafer D70.[J]

APPENDIX B

Autocorrelation functions with both coherent and incoherent contributions are analysed specifically to interpret the autocorrelation trace in chapter 7. Expressions for the contrast ratios are generalised for unequal intensities in the two arms of the autocorrelator.

Outline.

The second order autocorrelation measurement recombines the two fields $E_1(t)$ and $E_2(t+\tau)$ at a frequency doubling crystal. The delay τ is varied to give the pulse overlap function and therefore information on the duration or partial information on the shape of the incident pulses. For the autocorrelations considered in this work a background level is measured which results the sum of the independently detected fields. The peak of the function results from the mixed fields.

For the analysis of the autocorrelation trace in figure 7.7, analytic expressions are required for the peak to background ratios for coherent and incoherent pulse trains. From this information, contributions to the second harmonic intensity from mode-locked pulse trains may be isolated from a non phase-locked background. An estimate of the proportion of coherent mode-locked energy in the Bow-Tie laser emission is made at 66%.

Autocorrelation Function for Coherent Pulse Trains.

The recombined fields $E(t)$ are defined by the pulse envelope $\xi(t)$, optical frequency ω and the time dependent optical phase $\phi(t)$.

$$E(t) = \xi(t)\cos(\omega t + \phi(t)) \qquad 10.1$$

The two overlapping fields are summed and squared twice to give the second harmonic intensity. The second harmonic intensity is given as a function of overlap through the delay τ. The sum is normalised to the sum of the squares of the intensities for the nonoverlapping condition.

$$g_B^2(\tau) = \frac{\int_{-\infty}^{+\infty}\{E_1(t)+E_2(t+\tau)\}^4 dt}{\int_{-\infty}^{+\infty}\{E_1^4(t)+E_2^4(t)\}dt} \qquad 10.2$$

$$= \frac{\int_{-\infty}^{+\infty}\{E_1^4(t)+4E_1^3(t)E_2(t+\tau)+6E_1^2(t)E_2^2(t+\tau)+4E_1(t)E_2^3(t+\tau)+E_2^4(t+\tau)\}dt}{\int_{-\infty}^{+\infty}\{E_1^4(t)+E_2^4(t+\tau)\}dt} \qquad 10.3$$

As measurements made in chapter 7 consider a 'slow' autocorrelation, the phase terms in equation 9.1 must be time averaged. Equation 9.1 is now substituted into 9.3. An integration is performed over 2π to determine a phase independent expression for the second harmonic intensity. Assuming the modes to be phase locked allows ϕ to be time invariant. As $\int_0^{2\pi}\cos(\omega t)d\omega t = 0$ and $\int_0^{2\pi}\cos^3(\omega t)d\omega t = 0$, the phase terms in the second and fourth numerator terms in 9.3 become zero. Integration is performed for the phase in the third term of the numerator to allow 9.3 to be expressed in terms of pulse envelopes $\xi(t)$:

$$\frac{1}{4\pi^2}\int_0^{2\pi}\int_0^{2\pi}\cos^2(\omega t).\cos^2(\omega t+\phi)d\omega t d\phi \quad = \quad \frac{1}{4\pi^2}\int_0^{2\pi}\int_0^{2\pi}\left(\frac{1}{8}\cos(2\phi)+\frac{1}{4}\right)d\omega t d\phi$$

$$= \quad \frac{1}{4\pi^2}\int_0^{2\pi}2\pi\left(\frac{\sin(2\phi)}{16}+\frac{1}{4}\right)d\phi \quad = \quad \frac{1}{4}$$

The phase contributions for terms $E_1^4(t)$ and $E_2^4(t+\tau)$ are similarly evaluated.

$$\frac{1}{2\pi}\int_0^{2\pi}\cos^4(\omega t)d\omega t \quad = \quad \frac{3}{8}$$

Substituting the above factors for the phase terms into equations 9.1 and 9.3 gives the 'slow' or phase-independent autocorrelation function :

$$G_B^2(\tau) \quad = \quad 1 \quad + \quad 4\,\frac{\int_{-\infty}^{+\infty}\{\xi_1^2(t)\xi_2^2(t+\tau)\}dt}{\int_{-\infty}^{+\infty}\xi_1^4(t)dt+\int_{-\infty}^{+\infty}\xi_2^4(t+\tau)dt} \qquad 10.4$$

The peak to background contrast ratio for the autocorrelation function in 9.4 may now be determined from the levels at $\tau = 0$ and $\tau \to \infty$, i.e. for complete and no pulse overlap. The second harmonic intensities resulting independently from each arm of the autocorrelator are conveniently defined by A and B :

$$A \quad = \quad \int_{-\infty}^{\infty}\xi_1^4(t)dt \qquad B \quad = \quad \int_{-\infty}^{\infty}\xi_2^4(t+\tau)dt \quad = \quad \int_{-\infty}^{\infty}\xi_2^4(t)dt$$

This enables the peak to background level to be measured in terms of known second harmonic intensities. A peak to background ratio of 3:1 results for A=B as noted in chapter 3. The peak to background ratio does however decrease with increasing asymmetry (defined by $k = A/B$) in the autocorrelator [2].

$$\frac{G_B^2(\tau=0)}{G_B^2(\tau\to\infty)} \quad = \quad \frac{A+B+4\sqrt{AB}}{A+B} \quad = \quad \frac{A(1+k)+4A\sqrt{k}}{A(1+k)} \qquad 10.5$$

Autocorrelation Function for Incoherent Pulse Trains.

Pulses generated under gain-switching and Q-switching do not retain the pulse to pulse coherence observed for mode-locked operation [3]. As the modes are no longer phase-locked, the expressions for the fields must explicitly account for the multimode nature. Assuming the m modes separated by $\delta\omega$ have equal pulse envelope functions $\xi(t)$ but random phases ϕ_m, the fields can be approximated.

$$E(t) = \xi(t)\cos(\omega t + \phi(t))\Sigma_m \cos(m\delta\omega t + \phi_m) \qquad 10.6$$

Ito and coworkers have simulated the autocorrelation function given by the substitution of equation 9.6 into 9.2 [4]. The random phase relation between the modes modifies the contrast ratio.

$$\frac{G_B^2(\tau=0)}{G_B^2(\tau\to\infty)} = \frac{A+B+2\sqrt{AB}}{A+B} = \frac{A(1+k)+2A\sqrt{k}}{A(1+k)} \qquad 10.7$$

Coherence is however observed for complete pulse overlap at $\tau = 0$. The coherence spike peaks at three times the background level, and has a width dependent on the coherence time. Coherence spikes are also observed at separations of the round trip time as reflected fields in the laser cavity sum in phase. Such coherence spikes are observed in the autocorrelation function for the Q-switched Bow-Tie laser in figure 7.4.

Autocorrelation Function for Mixed Signals.

The autocorrelation function in figure 7.7 has been shown in a simplified schematic above. As the signal is not entirely mode-locked, the background level does not equal the sum *A+B*, and the peak does not equal *3(A+B)*. It is to be shown that the measured background and peak levels are consistent with there being a low level signal incoherent both with the mode-locked pulses and itself.

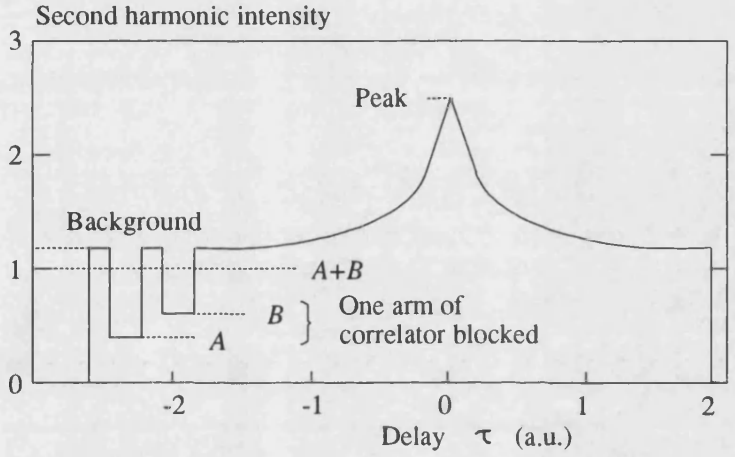

Figure 10.1 : Schematic autocorrelation function with the intensity normalised to the sum of the two input levels *A+B*.

Q-switched pulses were observed at the start of the electrical pulse on a 32GHz bandwidth photodiode with a sampling oscilloscope. As the second harmonic generation process is assumed to be instantaneous, it can further be assumed that mode-locked and Q-switched pulses do not mix for the delays considered. Autocorrelation over the increased range of -150ps < τ < 150ps indicates that the duration of these Q-switched pulses is of the order of 100ps and therefore significantly broader than the 700fs mode-locked pulses. For the

purposes of this calculation the non-mode-locked components are therefore assumed to be incoherent and continuous in time.

The contributions to the second harmonic intensity A may be divided into the mode-locked m, and the non-phase-locked components q. Introducing a ratio of second harmonic intensities in the two arms, k, allows A and B to be defined in terms of coherent and incoherent components:

$$B = Ak = (m+q)k \qquad 10.8$$

Further, the levels m and q are assumed not to mix and are therefore added together. The background level has contributions from both nonmixed mode-locked pulses m and mk and from the mixed incoherent q.

$$G_B^2(\tau \to \infty) = m(1+k)+q(1+k)+2q\sqrt{k} \qquad 10.9$$

Values for A, B and the background are used now to estimate k, m and q. The level in the low power input of the autocorrelator is $m+q = 0.35$. The level in the high power input of the autocorrelator is $(m+q)k = 0.65$. The background level defined in equation 9.9 is 1.2. Therefore m and q are estimated at m=0.272 and q=0.074. This in turn implies that 66% of the energy is coherent and mode-locked.

The peak level for the autocorrelation can be estimated from equation 9.5. The peak to background ratio for the mode-locked component is 2.91:1. This is expected to be slightly lower than 3:1 as a result of the nonequal powers in the two arms of the autocorrelator. Considering only the mode-locked components, the expected peak level above the background level ($4m\sqrt{k}$) is estimated at 1.48, in agreement with that experimentally measured.

References.

1. SALA, K.L., KENNEY-WALLACE, G.A., and HALL, G.E., "CW autocorrelation measurements of picosecond laser pulses", IEEE Journal of Quantum Electronics, 16, 990-996, 1980.

2. POPOV, Y.M., editor, Proceedings of the Lebedev Physical Institute, Academy of Sciences of the USSR, volume 185, page 20, Nova Science Publishers, 1987.

3. CURTIS, J.P., and CARROLL, J.E., "Autocorrelation systems for the measurement of picosecond pulses from injection lasers", International Journal of Electronics, 60, 87-111, 1986.

4. ITO, H., YOKOYAMA, H., MURATA, S., and INABA, H., Generation of picosecond optical pulses with highly RF modulated AlGaAs DH laser", IEEE Journal of Quantum Electronics, 17, 663-670, 1981.